2008-02-01

The Molecular Mechanisms of Activity-Dependent Wingless (Wg)/Wnt Signaling at a Drosophila Glutamatergic Synapse: a Dissertation

Bulent Ataman
University of Massachusetts Medical School

A Dissertation Presented

By

Bulent Ataman

Submitted to the Faculty of the

University of Massachusetts Graduate School of Biomedical Sciences, Worcester

in partial fulfillment of the requirements for the degree of

DOCTOR OF PHILOSOPHY

February 2008

Program in Neuroscience

The Molecular Mechanisms of Activity-Dependent Wingless (Wg)/ Wnt Signaling

At a *Drosophila* Glutamatergic Synapse

A Dissertation Presented

By

Bulent Ataman

Approved as to style and content by:

_____
Vivian Budnik, PhD. Thesis Advisor

_____
Marc Freeman, PhD., Chair of Committee

_____
Rolf O. Karlstrom, PhD., External Member of Committee

_____
Scott Waddell, PhD., Member of Committee

_____
Patrick Emery, PhD., Member of Committee

_____
Stephen Doxsey, PhD., Member of Committee

_____
Anthony Carruthers, Ph.D.,
Dean of the Graduate School of Biomedical Sciences

Ph.D. Program in Neuroscience
February 20, 2008

DEDICATION

Dedicated to my beloved family:

Nuran (mother) & Yucel (father) & Berna (sister) Ataman, Nurettin Sipahioglu (grandfather), Zeliha Ataman (grandmother) and Burcu Guner-Ataman (my wife).

FOREWORD

Studies detailed in this dissertation have been carried out in Dr. Vivian Budnik's lab in the Neurobiology department at UMASS Medical School. This dissertation consists of five chapters in which chapters II, III and IV have been individually published in peer-review journals. I have a separate acknowledgement section at the end of the fifth chapter to acknowledge my collaborators and their respective contributions for each chapter in detail.

Foremost, I would like to express my deep gratitude to my advisor Dr. Vivian Budnik for her continued encouragement, motivation and invaluable suggestions. She shared with me a lot of her expertise and research insights and became my role model for successful researcher in the Neuroscience field. Apart from being an excellent mentor, she has also been a great friend for me. I would also like to thank the members of my committee, Dr. Scott Waddell, Dr. Patrick Emery, Dr. Rolf Karlstrom, Dr. Stephen Doxsey and my chair, Dr. Marc Freeman. I would like extend my gratitudes to all the past and present members of the Budnik lab for creating a productive and friendly work environment. In particular, I would like to thank Dr. James Ashley and Dr.Dennis Mathew for being excellent friends and perfect collaborators throughout the graduate school.

I would like to thank the faculty of the Neurobiology Department here at UMASS Medical School, particularly Dr. David Weaver, who has been a great resource during and after our transition from UMASS Amherst campus to UMASS Worcester campus.

I would also like to thank all my friends from various places, too many to list here, who supported me and enriched my life in so many ways. Finally, I would like to dedicate this work to my family in Turkey and here, who have been extremely supportive and helpful over the years.

ABSTRACT

Synaptic plasticity, the ability of synapses to change in strength, underlies complex brain functions such as learning and memory, yet little is known about the precise molecular mechanisms and downstream signaling pathways involved. The major goal of my doctoral thesis was to understand these molecular mechanisms and cellular processes underlying synaptic plasticity using the *Drosophila* larval neuromuscular junction (NMJ) as a model system.

My work centered on a signaling pathway, the Wg/Wnt signaling pathway, which was found to be crucial for activity-driven synapse formation. The Wg/Wnt family of secreted proteins, besides its well-characterized roles in embryonic patterning, cell growth and cancer, is beginning to be recognized as a pivotal player during synaptic differentiation and plasticity in the brain. At the *Drosophila* NMJ, the Wnt-1 homolog Wingless (Wg) is secreted from presynaptic terminals and binds to Frizzled-2 (DFz2) receptors in the postsynaptic muscle. Perturbations in Wg signaling lead to poorly differentiated NMJs, containing synaptic sites that lack both neurotransmitter release sites and postsynaptic structures. In collaboration with other members of the Budnik lab, I set out to unravel the mechanisms by which Wg regulates synapse differentiation. We identified a novel transduction pathway that provides communication between the postsynaptic membrane and the nucleus, and which is responsible for proper synapse development. In this novel Frizzled Nuclear Import (FNI) pathway, the DFz2 receptor is internalized and transported towards the nucleus. The C-terminus of DFz2 is subsequently cleaved and imported into the postsynaptic nucleus for potential

(Abstract continued)

transcriptional regulation of synapse development (Mathews, Ataman, et al. Science (2005) 310:1344).

My studies also centered on the genetic analysis of Glutamate Receptor (GluR) Interacting Protein (dGRIP), which in mammals has been suggested to regulate the localization of GluRs and more recently, synapse development. I generated mutations in the gene, transgenic strains carrying a dGRIP-RNAi and fluorescently tagged dGRIP, and antibodies against the protein. Remarkably, I found *dgrip* mutants had synaptic phenotypes that closely resembled those in mutations altering the FNI pathway. Through the genetic analysis of *dgrip* and components of the FNI pathway, immunoprecipitation studies, electron microscopy, *in vivo* trafficking assays, time-lapse imaging, and yeast two-hybrid assays, I demonstrated that dGRIP had a hitherto unknown role as an essential component of the FNI pathway. dGRIP was found in trafficking vesicles that contain internalized DFz2. Further, DFz2 and dGRIP likely interact directly. Through the use of pulse chase experiments I found that dGRIP is required for the transport of DFz2 from the synapse to the nucleus. These studies thus provided a molecular mechanism by which the Wnt receptor, DFz2, is trafficked from the postsynaptic membrane to the nucleus during synapse development and implicated dGRIP as an essential component of the FNI pathway (Ataman et al. PNAS (2006) 103:7841).

In the final part of my dissertation, I concentrated on understanding the mechanisms by which neuronal activity regulates synapse formation, and the role of the

(Abstract continued)

Wnt pathway in this process. I found that acute changes in patterned activity lead to rapid modifications in synaptic structure and function, resulting in the formation of undifferentiated synaptic sites and to the potentiation of spontaneous neurotransmitter release. I also found that these rapid modifications required a bidirectional Wg transduction pathway. Evoked activity induced Wg release from synaptic sites, which stimulated both the postsynaptic FNI pathway, as well as an alternative presynaptic Wg pathway involving GSK-3ß/Shaggy. I suggest that the concurrent activation of these alternative pathways by the same ligand is employed as a mechanism for the simultaneous and coordinated assembly of the pre- and postsynaptic apparatus during activity-dependent synapse remodeling (Ataman et al. Neuron (2008) in press).

In summary, my thesis work identified and characterized a previously unrecognized synaptic Wg/Wnt transduction pathway. Further, it established a mechanistic link between activity-dependent synaptic plasticity and bidirectional Wg/Wnt signaling. These findings provide novel mechanistic insight into synaptic plasticity.

TABLE OF CONTENTS

LIST OF FIGURES

LIST OF FIGURES (continued)

LIST OF THE FREQUENTLY USED ABBREVIATIONS

BMP – Bone Morphogenetic Protein

ChR2 – Channelrhodopsin-2 transgene

CNS – Central Nervous System

DFz2 – *Drosophila* Wnt/Wg receptor Frizzled-2

DLG – Discs-large

EJP – Excitatory Junctional Potential

mEJP – miniature Excitatory Junctional Potential

FNI – Frizzled Nuclear Import pathway

GFP – Green Fluorescent Protein

GluR – Glutamate Receptor

GRIP – Glutamate-Receptor-Interacting Protein

dGRIP – *Drosophila* homolog of GRIP

LTP – Long Term Potentiation

NMJ – Neuromuscular Junction

PDZ – Postsynaptic Density-95/Discs-large/Zona Occludens

PKA – Protein Kinase A

PKC – Protein Kinase C

aPKC – Atypical Protein Kinase C

PNS – Peripheral Nervous System

PTP – Post Tetanic Potentiation

Sgg – Shaggy, *Drosophila* homolog of GSK3-β

LIST OF THE FREQUENTLY USED ABBREVIATIONS (continued)

SSR – Subsynaptic Reticulum

RFP – Red Fluorescent Protein

RNAi – RNA Interference

TGF-β – Transforming Growth Factor β

Wg – Wingless

CHAPTER 1

Introduction

The *raison d'être* of neuroscience is to understand the biological mechanisms underlying behavioral processes such as perception, learning and memory. All of these complex processes are principally the consequence of the most complicated cell network in the human body, the nervous system. The brain, the central component of the nervous system, contains about 10^{11} individual nerve cells and each of them can make up to 10,000 synaptic connections. These elaborate networks of circuits not only direct a multitude of innate and stereotypical behaviors, but also are sufficiently flexible to respond and adapt to novel situations. There is a general consensus that at least some of the key processes underlying the flexibility of the nervous system rely on the ability of synapses to change – a process termed synaptic plasticity. The major goal of this thesis research is to elucidate some of the genetic and molecular mechanisms underlying synaptic plasticity.

The concept of a "plastic" nervous system dates back to the early 1900s when Santiago Ramón y Cajal, the father of modern neuroscience, suggested that the nervous system is not simply hard-wired, but that there are dynamic structural changes in the neuronal connections of the peripheral nervous system (PNS) and the central nervous system (CNS) (Ramón y Cajal, 1904). Cajal's studies mostly focused on the "regenerative plasticity" of injured spinal cord and cerebral cortex neurons. However his findings opened a new era in neuroscience and led researchers to explore synaptic plasticity phenomena in other contexts of nervous system development (DeFelipe, 2002; Stahnisch and Nitsch, 2002).

In 1949, Canadian psychologist Donald Hebb postulated a plasticity hypothesis in which correlated activity between a presynaptic cell (or a group of cells) and a postsynaptic cell (or a group of cells) leads to an increase in synaptic strength or "efficacy" through some structural growth processes or a metabolic change in one or both cells (Hebb, 1949). Hebb developed his theory purely on a theoretical basis to explain the formation and/or stabilization of specific neuronal activity patterns in the brain, which presumably represent specific types of behaviors. Hebb's postulate, supported by many subsequent studies particularly emphasized the role of "structural plasticity" in behavioral processes in which, neural activity patterns in the brain such as acquisition of new information (learning) or storage of acquired information (memory) are created through structural modifications in the corresponding synaptic circuits (Chklovskii et al., 2002; Stepanyants et al., 2002). Although the proposed role of structural plasticity in behavioral processes seems to be irrelevant for some types of brain functions, Hebb's postulate that *"cells that fire together, wire together"* has become an inspiration and foundation for many neuroscience studies in different *in vitro* and *in vivo* plasticity models (Seung, 2000).

The prime illustration of Hebbian plasticity is found in the phenomenon of long-term potentiation (LTP), the most commonly used cellular plasticity model. LTP is an electrophysiological increase in synaptic efficacy and can be elicited in cultured neurons, brain slices and in intact animals (Bliss and Lomo, 1973). LTP is evoked through a brief, repetitive high frequency stimulation of a presynaptic cell, which induces a long-lasting (ranging from several hours to several weeks

depending on the preparation and pattern of stimulation) potentiation of the synaptic response by the postsynaptic neurons (Bennett, 2000; Bliss and Lomo, 1973). The functional enhancement in synaptic strength during LTP is also accompanied by rapid modifications in synaptic structure, which has been particularly well-studied in postsynaptic dendrites (Engert and Bonhoeffer, 1999; Maletic-Savatic et al., 1999; Nagerl et al., 2004; Toni et al., 1999). The so called late-LTP, which is induced by multiple trains of high frequency stimulation, has been widely used as a cellular model for long-term memory because of its equivalent characteristics, such as its induction properties, its long-term maintenance and its requirement for new protein synthesis (Malenka and Nicoll, 1999). The significance of LTP in behavioral learning and memory of living animals has been highlighted in many studies. For instance, pharmacological or genetic blockade of NMDA-type glutamate receptor activation, a crucial step in LTP induction, has been shown to cause spatial memory defects in rats that had been pretrained in the Morris water maze (McHugh et al., 1996; Morris et al., 1986). Conversely, mice overexpressing the NMDA subunit NR2 in the hippocampus show improved spatial learning and enhanced LTP (Tang et al., 2001). Further, a recent study demonstrated that a one-trial inhibitory avoidance learning paradigm in rats can actually elicit identical glutamate receptor phosphorylation events and the potentiation of synaptic transmission in a spatially-restricted manner, as the induction of LTP through high-frequency stimulation of the CA1 region of the hippocampus (Whitlock et al., 2006). LTP studies have also significantly contributed to our knowledge of the molecular

components and their mode of action in neuronal plasticity. In fact, many of the molecules identified as important for LTP have also been shown to be involved in behavioral processes (Malenka and Nicoll, 1999). The list of major signaling molecules include prominent kinases such as Ca^{2+}/Calmodulin dependent kinase II (CamKII), protein kinase C (PKC), cyclic adenosine 3′,5′-monophosphate (cAMP)-dependent protein kinase (PKA), mitogen-activated protein kinase (MAPK), neurotransmitter receptors such as NMDA and AMPA type glutamate receptors, transcription factors such as cAMP response element binding protein (CREB) and many other kinases, cell adhesion molecules, scaffolding molecules and secreted factors (Bennett, 2000; Malenka and Nicoll, 1999; Sweatt, 1999). These findings provide significant evidence that LTP and behavioral plasticity share common signaling components and mechanisms in which activity-driven modifications alters synaptic efficacy, in part through structural alterations at synapses.

Another leading plasticity model has been developed through the pioneering studies of Eric Kandel's group on the sea snail *Aplysia* (Kandel, 2001). The nervous system of this marine invertebrate is comprised of small number (20,000) of extraordinarily big (up to 1mm diameter) and distinctively pigmented nerve cells (Eric R. Kandel, 2000). *Aplysia* exhibits a simple "gill and siphon withdrawal reflex (GSWR) " behavior when it encounters a noxious stimulus and the neuronal circuitry underlying this behavior has been fully mapped (Bailey et al., 2004). Using the GSWR as a behavioral readout, researchers have characterized a number of crucial synaptic phenomena such

as facilitation, sensitization and habituation. In particular, repetitive stimulation of the GSWR circuitry with spaced patterns, either by simply squirting water onto the mantle of an intact snail or by applying the neurotransmitter serotonin to a reconstituted cell culture system, induces long-term potentiation of synaptic transmission and the growth of sensory terminals in a process that requires new protein synthesis (Castellucci et al., 1986; Montarolo et al., 1986). Further, these stimulation paradigms have been shown to initiate a transduction cascade involving the downregulation of *Aplysia* cell adhesion molecule (ApCam) and activation of PKA, MAPK and ultimately CREB-1 in the nucleus where transcription of synapse specific target genes was enhanced (Kandel, 2001). In parallel with these findings, long-term olfactory memory in *Drosophila* has been shown to require patterned training paradigms and new protein synthesis downstream of the activation of the transcription factor dCREB (Tully et al., 1994; Yin et al., 1994; Yu et al., 2006). All of these plasticity studies using fruit fly, sea snail and vertebrate model systems point to highly conserved physiological mechanisms and signaling molecules that operate downstream of patterned synaptic activity and that consequently govern the behaviors of the organism.

Synaptic plasticity is not only observed in the adult nervous system for behavioral processes. Indeed, immature synaptic circuits in the developing nervous system undergo continuous reorganization and fine-tuning, mostly directed by spontaneous and sensory-evoked patterns of neuronal activity. For example, normal stereotypic formation of eye-specific layers in the mammalian lateral geniculate nucleus (LGN) is guided by spontaneous retinal activity

(Huberman, 2007). In addition, eye-specific patches (also known as ocular dominance (OD) columns) in the developing visual cortex requires afferent inputs from the eyes as well as spontaneous retinal activity (Del Rio and Feller, 2006). Similarly, refinement and maintenance of retinotectal maps, the topographic projections from the retina to its midbrain targets in developing fish and frogs are regulated by correlated patterns of afferent activity in an NMDA-dependent manner (Debski and Cline, 2002). Further, temporal synaptic activity during vertebrate NMJ development regulates “synapse elimination”, a process in which polyneuronal innervation of the postsynaptic target muscle is converted to single axon innervation (Wyatt and Balice-Gordon, 2003). These studies demonstrate that correlated activity is the master modulator of synaptic structure and function, both during the refinement of synaptic circuits in immature nervous systems and later during adult behavior. Moreover, they highlight the well-conserved intrinsic capacity of neurons to respond equivalently to corresponding activity patterns in different spatio-temporal contexts throughout the life of an organism.

Although, there is a large body of literature on activity-dependent synaptic plasticity and there are plenty of identified molecules involved, we still know very little about the precise mechanisms and the operation of downstream signaling pathways underlying this truly complex phenomenon. In addition, the majority of the previous studies have been carried out *in vitro* due to the complexity and the inaccessibility of the mammalian nervous system. Hence, their validity in an intact nervous system often remains to be determined. During my thesis research I used the *Drosophila* larval neuromuscular synapses as a model system to

investigate the cellular mechanisms of synaptic plasticity and its downstream signaling pathways. Considering its genetic amenability, the availability of advanced cellular and biochemical tools and many other advantages that makes it one of the most elegant *in vivo* model systems, *Drosophila* seems to be an ideal system to uncover mechanistic aspects of synapse plasticity.

The Drosophila Larval Neuromuscular Junction (NMJ) as a Model System for the study of Synaptic Plasticity:

The body wall muscles and neuromuscular junctions of *Drosophila* larvae have been an excellent and popular model system for more than 30 years to address many fundamental questions in neurobiology including the mechanisms of neurotransmitter release, synapse physiology, ion channel localization and function, pre- and postsynaptic protein organization, synapse formation and structural as well as functional plasticity (Ruiz-Canada and Budnik, 2006). The great advantage of the larval NMJ emanates from its simple and easily accessible synapses in an intact animal combined with the vast array of genetic and cellular tools in the fly. In addition, many studies have established that synaptic mechanisms and components identified at the larval NMJ are highly conserved from simple metazoans to more complex organisms such as mouse and humans (Ruiz-Canada and Budnik, 2006).

One of the great benefits of *Drosophila* as a model system is its short life cycle, in which a fertilized egg develops into an adult fly in about 10 days. Fruit fly eggs complete their embryonic development and hatch into a worm-like larva in

20-22 hr post-fertilization at 25˚C (Michael Ashburner, 2005). The newly hatched larvae continuously feed and grow for a total of three instars (L1, L2, and L3), molting the cuticle between instars, as the larva dramatically increases in body size within a relatively short time period (~ 96 hr). Fruit fly larvae have a very thin and transparent cuticle surrounding the larval body and thus synaptic structures and their fluorescently tagged molecular components can be readily visualized in live or fixed preparations through a variety of microscopy techniques.

The body-wall muscles of the larva consist of 30 skeletal, supercontractile muscle fibers per hemisegment that are segmentally repeated in abdominal segments A1 through A7 (Crossley, 1978), see Fig.1-1). These muscles are highly stereotypic and they can be uniquely and easily identified in terms of their shape, size and position at the body wall. Each muscle of the body wall is innervated by a characteristic complement of motorneurons that project axons from the ventral ganglion. Each class of motorneuron gives rise to terminals with different structural properties (Gorczyca et al., 1993; Johansen et al., 1989).

Larval NMJs are typically characterized by the branched synaptic terminals containing varicosities, also known as synaptic “boutons” (Fig. 1- 2A and B). All muscle cells of the body wall are innervated by type I boutons, which can be subdivided into type Ib (big) and type Is (small) boutons depending on their ultrastructural and electrophysiological properties (Gramates and Budnik, 1999). These boutons release glutamate, the primary excitatory transmitter at the larval NMJ (Jan and Jan, 1976). Additionally, subsets of muscles are innervated by peptidergic and/or octopaminergic motorneurons (type II and III boutons),

which are thought to modulate the glutamatergic response (Anderson et al., 1988; Gorczyca et al., 1993; Monastirioti et al., 1995; Zhong and Pena, 1995). For my analyses, I mostly focused on muscles 6 & 7 on segment A3 of 3rd instar larvae (Fig. 1-1, red dotted box at left) which are exclusively innervated by type Ib and Is boutons (Fig. 1-2B) and that exhibit highly stereotypic innervation, morphology and bouton number.

Ultrastructural analyses of type I bouton cross-sections showed that the presynaptic compartment contains synaptic vesicles, mitochondria and neurotransmitter release sites, or active zones. At these active zones observed at the presynaptic membrane there are electron-dense T-bar shaped structures surrounded by vesicle clusters, the readily releasable synaptic pool (Atwood et al., 1993; Jia et al., 1993a). At the postsynaptic region, synaptic boutons are surrounded by multiple layers of a membranous network, called the subsynaptic reticulum (SSR) (Fig. 1-3A and C). The exact physiological significance of SSR is poorly understood, but several functions have been proposed, including being the site of glutamate uptake (Faeder and Salpeter, 1970), a synaptic scaffolding matrix where cell adhesion molecules, ion channels and neurotransmitter receptors as well as postsynaptic density proteins are precisely anchored for efficient synaptic transmission and signaling (Ataman et al., 2006b). There is also evidence that the SSR may be a site for local translation of glutamate receptors (GluRs) (Sigrist et al., 2000).

An important characteristic that makes larval NMJs an exceptional synapse plasticity model is that they are continuously changing. Muscle patterning and axon guidance for *Drosophila* larvae are completed by the end of embryonic development. However, during larval development the body size of the larvae substantially grows from ~ 0.5 mm to ~ 5 mm in roughly 4 days. This growth does not represent a change in the number of muscle cells, but rather in a remarkable increase in the size of individual muscle cells by approximately 100-fold in surface area (Gorczyca et al., 1993; Keshishian and Chiba, 1993; Keshishian et al., 1993; Schuster et al., 1996b). This profound growth of the postsynaptic target cell is accompanied by a coordinated increase in the synaptic input, both structurally and functionally, to maintain synaptic efficacy. In particular, synaptic efficacy is sustained by both increasing the number of synaptic boutons and enhancing the physiological properties of individual boutons, such as increasing presynaptic active zone number, postsynaptic density volume and glutamate receptor area (Griffith and Budnik, 2006). Therefore, these rapidly growing muscles can be stimulated efficiently by continuously strengthening synapses in correlation with muscle growth. Successful regulation of synaptic growth and efficacy requires the coordinated operation of both the presynaptic motor neuron and the postsynaptic muscle cell (Atwood et al., 1993; Guan et al., 1996; Keshishian et al., 1996). For example, the second wave of GluR synthesis and postsynaptic GluR clustering does not occur without innervation, indicating the requirement of synaptic activity for NMJ development (Broadie and Bate, 1993). Conversely, active zones are not

properly organized at the presynaptic terminal without the presence of a corresponding postsynaptic muscle cell, indicating a retrograde signaling pathway that responds to presynaptic activity (Prokop et al., 1996).

Previous studies using short-term or long-term manipulations in electrical activity, as well as in behavioral conditions, have demonstrated the presence of activity-dependent structural and functional plasticity at the larval NMJ (Schuster, 2006). In an earlier study, hyperactive K^+ channel mutants *eag (ether-a-go-go)* and *Sh (shaker)* were shown to have increased number of branches and boutons as well as synaptic branch complexity (Budnik et al., 1990). Consistently, this morphological enhancement was rescued back to normal levels by introducing *no action potential* (nap^{ts}), a mutation which induces reduced excitability by downregulating the number of presynaptic Na^+ channels (Budnik et al., 1990). Later, similar activity-dependent morphological enhancements were independently reported using presynaptic expression of a Shaker dominant-negative transgene suggesting the requirement of activity in the presynaptic compartment (Mosca et al., 2005). These studies used genetic manipulations to alter electrical activity in a chronic manner throughout larval development. Other studies have altered larval locomotor behavior to modify synaptic activity in an acute manner (Sigrist et al., 2003; Sigrist et al., 2000; Steinert et al., 2006). These studies simply used the fact that when larva are starved on a hard agar plate instead of placing them on a standard growth medium containing rich and slurry food, they usually display much higher locomotor activity (i.e., they show enhanced crawling behavior), perhaps in search of food. Transferring larva from

culture to agar plates for short time periods potentiated synaptic transmission, in a reversible manner (Sigrist et al., 2003). This functional enhancement also resulted in an increase in postsynaptic translation aggregates, which were previously shown to contain glutamate receptor mRNAs (Sigrist et al., 2000). Utilizing a similar assay, a recent study examined the ultrastructure and electrophysiology of NMJs from the population of larva that showed high locomotor activity and compared them to those that showed low locomotor activity (Steinert et al., 2006). These systematic analyses revealed that high crawling activity induced potentiation of synaptic transmission and the strengthening of NMJ synapses. This functional enhancement was attributed to an increase in quantal size, as the synaptic terminals of larvae with high crawling activity were found to contain significantly larger vesicles. The size and content of synaptic vesicles are decisive factors in synaptic transmission, and therefore this finding suggests an alternative mechanism for the regulation of synaptic strength. Further dissection of the cellular components involved in activity-driven formation and recruitment of large synaptic vesicles has identified PKA and actin-dependent mechanisms (Steinert et al., 2006), which are also known to be critical for LTP induction in mammalian system (Malenka and Nicoll, 1999). Live imaging of NMJs in this locomotor assay have showed no activity-dependent morphological changes at synapses (Steinert et al., 2006). However, this study only used a postsynaptic marker for live imaging. Thus, any potential presynaptic change would have been missed. A recent study in *Drosophila* embryos showed that NMJ synapses exhibit a dramatic potentiation of miniature event release

frequency after high frequency stimulation (High Frequency-induced Miniature Release; HFMR), but similarly this study did not report any structural synaptic modifications associated with HFMR (Yoshihara et al., 2005).

Another form of activity-dependent potentiation elicited at larval NMJs is called “Post - Tetanic Potentiation” (PTP), which lasts on a time scale of several minutes (Beaumont et al., 2002; Zhong and Wu, 1991). The phenomenon of PTP is reminiscent of LTP observed in the vertebrate synapses and it can similarly be induced upon high frequency stimulation. In addition, some of the signaling components of *Drosophila* adult learning and memory, which were previously shown to regulate the larval NMJ development (Griffith and Budnik, 2006), are also required for normal PTP induction. These molecules include the well-studied cAMP pathway (Zhong et al., 1992), the cell adhesion molecule Integrin (Rohrbough et al., 2000) and the fruit fly homolog of 14-3-3, Leonardo (Broadie et al., 1997) supporting the idea that acute synaptic plasticity mechanisms at the NMJ might also be applicable to the behavioral processes in the adult brain.

The current evidence clearly indicates that short-term or long-term activity-driven synaptic modifications are observed at the larval NMJs and that these plasticity phenomena mostly utilize similar mechanisms and molecules as in higher organisms. However, the question of what are the exact molecular mechanisms and signaling pathways underlying continuous change at the larval NMJ are largely unresolved.

Signaling across the synapse: Anterograde and Retrograde Signals

When the immense complexity of synaptic circuits is considered, whether during short-term or long-term plasticity, it is very clear that the coordinated formation and operation of a continuously changing synapse requires signaling molecules that are able to have both spatial and temporal effects, and which coordinate changes between the pre- and postsynaptic compartments. It is becoming increasingly clear that secreted signaling molecules, utilized in early pattern formation of the embryo, function later in nervous system development and plasticity (Packard et al., 2003). These factors usually coordinate the communication between adjacent cells during cell-fate specification in early development. In the context of synapses, the same classes of molecules secreted from pre- and/or postsynaptic cells interact with the corresponding membrane receptors at the pre- and/or postsynaptic membrane. The activation of these receptors initiates transduction pathways, which in many instances regulate gene expression in the target cell. Prime examples of these molecules are members of the transforming growth factor- β (TGF-β) pathway and Wnt/ Wingless (Wg) pathways. These two pathways have been extensively studied in embryonic development and are recently beginning to be recognized as synaptic factors (Packard et al., 2003; Speese and Budnik, 2007).

The TGF-β pathway at the larval NMJ has been suggested to operate in a retrograde manner. In this pathway, the TGF-β member Glass Bottom Boat (Gbb), which is secreted by postsynaptic muscles, interacts with the type II bone morphogenetic protein (BMP) receptor Wishful Thinking (Wit), and with either of

the Type I BMP receptors Thick vein (Tkv) or Saxophone (Sax) (Aberle et al., 2002; Marques et al., 2002; Marques et al., 2003). Activation of the receptor complex leads to the phosphorylation of the *Drosophila* R-smad homolog Mad, which in turn associates with the Smad-4 Medea. Ultimately the Mad/Medea complex is imported into the nucleus where it regulates transcription. This pathway is believed to provide information to the motorneurons about changes in muscle size, triggering a parallel increase in the size of the presynaptic arbor (Marques, 2005).

In my studies, I focused on the synaptic role of another prominent secreted factor, Wingless (Wg/Wnt-1), a member of the Wnt family of glycoproteins. Wg is expressed and secreted by presynaptic motor neurons (Packard et al., 2002). The Wg receptor, DFrizzled-2 (DFz2), is localized both pre- and postsynaptically. The role of Wg during larval NMJ development was investigated using a temperature sensitive *wg* allele (wg^{ts}) in which, at the restrictive temperature, Wg protein cannot be properly processed and exit the ER, and thus cannot be secreted (van den Heuvel et al., 1993). Reducing Wg signaling during the last day of larval development using heat-pulsed wg^{ts} mutants led to a dramatic synaptic growth defect. The remarkable reduction in bouton number in wg^{ts} larva was completely rescued to wild-type levels by presynaptic, but not by postsynaptic expression of a Wg transgene, corroborating the crucial role of presynaptically secreted Wg. In addition, presynaptic expression of Wg alone causes a significant increase in the total number of boutons. These results suggest that synaptic growth is governed by Wg

signaling, as reducing Wg levels hampered synaptic growth and increasing Wg levels enhanced synaptic growth (Packard et al., 2002).

The perturbations in Wg signaling not only affected overall synaptic growth but also caused striking defects in synaptic architecture (Packard et al., 2002). Ultrastructural analyses of wg^{ts} synapses revealed a population of severely defective boutons that were filled with synaptic vesicles but lacked presynaptic active zones, mitochondria and postsynaptic SSR. Consistent with the ultrastructural defects, postsynaptic GluRs and the postsynaptic protein Discs-Large (DLG) are reduced and abnormally localized. Similar morphological and ultrastructural defects were also observed in *dfz2* alleles. These results suggest that a signal transduction cascade initiated by Wg coordinates key steps in target-dependent synapse formation and maturation (Packard et al., 2002). Several Wg/Wnt transduction mechanism have been described in other tissues and systems (Ciani and Salinas, 2005; DasGupta et al., 2005). In epithelial tissues Wg and its DFz receptors are known to operate through a canonical pathway in which Wg binding to DFz prevents the phosphorylation of the *Drosophila* ß-catenin homolog, Armadillo (Arm) by GSK-3ß/Shaggy, thus averting its degradation by the proteasome. Arm then forms a complex with LFT/TCF (Lymphoid enhancer factor / T cell-specific transcription factor) family of transcription factors and is imported into the nucleus where it regulates transcription of target genes (Ciani and Salinas, 2005). Although this canonical pathway appears to operate during cell-fate specification in epithelial differentiation, other non-canonical pathways have also been described (Speese

and Budnik, 2007). For example, in the planar cell polarity (PCP) pathway, Fz signals through G-proteins to activate Disheveled and its downstream effectors Rho GTPases, which in turn regulate the cytoskeleton. Similar mechanisms have been also implicated in dendritic growth and branching in the mammalian brain. The Wnt/calcium pathway is another non-canonical pathway in which Wnt signaling releases Ca^{2+} from intracellular stores and activates downstream proteins such as PKC and CaMKII, which turn on transcriptional programs that regulate cell fate and cell movement in vertebrate embryos (Ciani and Salinas, 2005; Speese and Budnik, 2007).

In the presynaptic compartment of NMJs, GSK-3ß/Shaggy (Sgg) was localized in synaptic boutons and mutations in both *sgg* and *wg* had microtubule cytoskeleton defects (Franco et al., 2004; Packard et al., 2002). This suggests that a divergent canonical Wg pathway, activated by an autocrine signal in the presynaptic cell, might be in charge of organizing microtubule dynamics through Sgg. However, in the postsynaptic cell, the mechanism of Wg transduction was not known. The major components of the canonical Wnt pathway, such as Disheveled and Armadillo, seem to be absent from larval NMJs and when mutations in these genes were examined, they showed either no synaptic phenotype or mild defects, which did not resemble the phenotypes in *wg* mutants (Mathew et al., 2005; Packard et al., 2002). These findings led us to investigate the possibility that there was an alternative Wg transduction pathway operating at the NMJ.

In the second chapter of my thesis, I will present findings from a project led primarily by Dennis Mathew, a former graduate student, and myself, and which identified and characterized yet another non-canonical Wg transduction pathway, the Frizzled Nuclear Import (FNI) pathway. This is a previously unrecognized pathway in which DFz2 is transported from the postsynaptic membrane to the nucleus, where the C-terminus of DFz2 is cleaved and imported into the nucleus. This work was published in Science (2005) 310:1344.

In the third chapter of my thesis, I will present evidence for a mechanism required for the nuclear trafficking of DFz2, from the postsynaptic membrane to the nucleus, through interactions with the 7 PDZ protein dGRIP. Previous studies showed that the vertebrate GRIP (Glutamate Receptor Interacting Protein) is involved in scaffolding and trafficking of many crucial synaptic proteins including AMPA-type glutamate receptors, Ephrin ligands and receptors and Liprin-α in the mammalian brain (Kim and Sheng, 2004). In the process of searching for molecular components of the FNI pathway, I identified the scaffolding protein dGRIP as a crucial interacting partner of DFz2. These studies were published in PNAS (2006) 103:7841.

In the fourth chapter of this thesis, I will present my recent studies that describe acute activity-dependent structural and functional changes uncovered at the NMJ and the role of bidirectional Wg signaling in this process. Although previous findings had demonstrated a role for chronic activity in structural changes at the NMJ, the relevance of acute changes in activity in this process was not known. In addition, although a role for Wg signaling during

synaptogenesis was clear, whether there was a relationship between activity dependent changes and Wg signaling had not been addressed. Here, I will show evidence that patterned stimulation induced rapid activity-dependent changes in synaptic structure and function and describe a molecular mechanism in which, simultaneous activation of Wg signaling in pre- and postsynaptic compartments coordinates these modifications. As of the writing of this thesis the work described in this chapter is in press in Neuron.

In conclusion, the work detailed in this thesis highlights a novel Wg transduction mechanism and its critical signaling component dGRIP in postsynaptic cell as well as a bidirectional Wg pathway that operates downstream of synaptic activity and that induces rapid structural and functional modifications at the larval NMJ synapses.

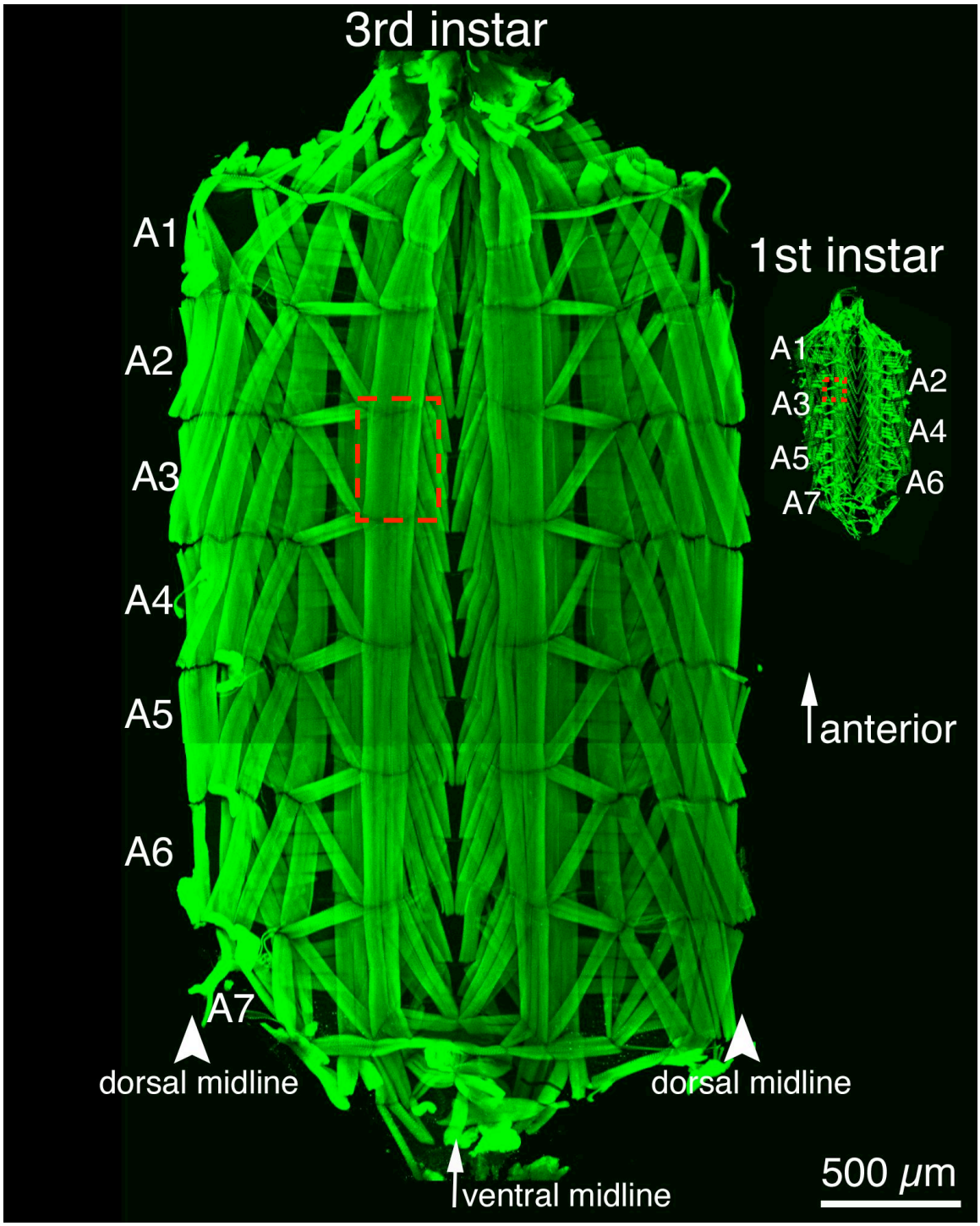
3rd instar
A1
A2
A3
A4
A5
A6
A7
dorsal midline
dorsal midline
ventral midline
1st instar
A1
A2
A3
A4
A5
A6
A7
anterior
500 μm

Figure 1-1

Figure 1-1. (Modified from (Budnik and Ruiz-Canada, 2006)) Body wall muscles of 1st instar (right) and 3rd instar larva (left). Filleted preparations of larval body wall muscles were visualized with FITC-conjugated phalloidin (green) staining. Red dotted boxes indicate Muscle 6&7 of abdominal segment 3 (A3). Note the remarkable size difference of the same muscle set between 1st instar and 3rd instar larva.

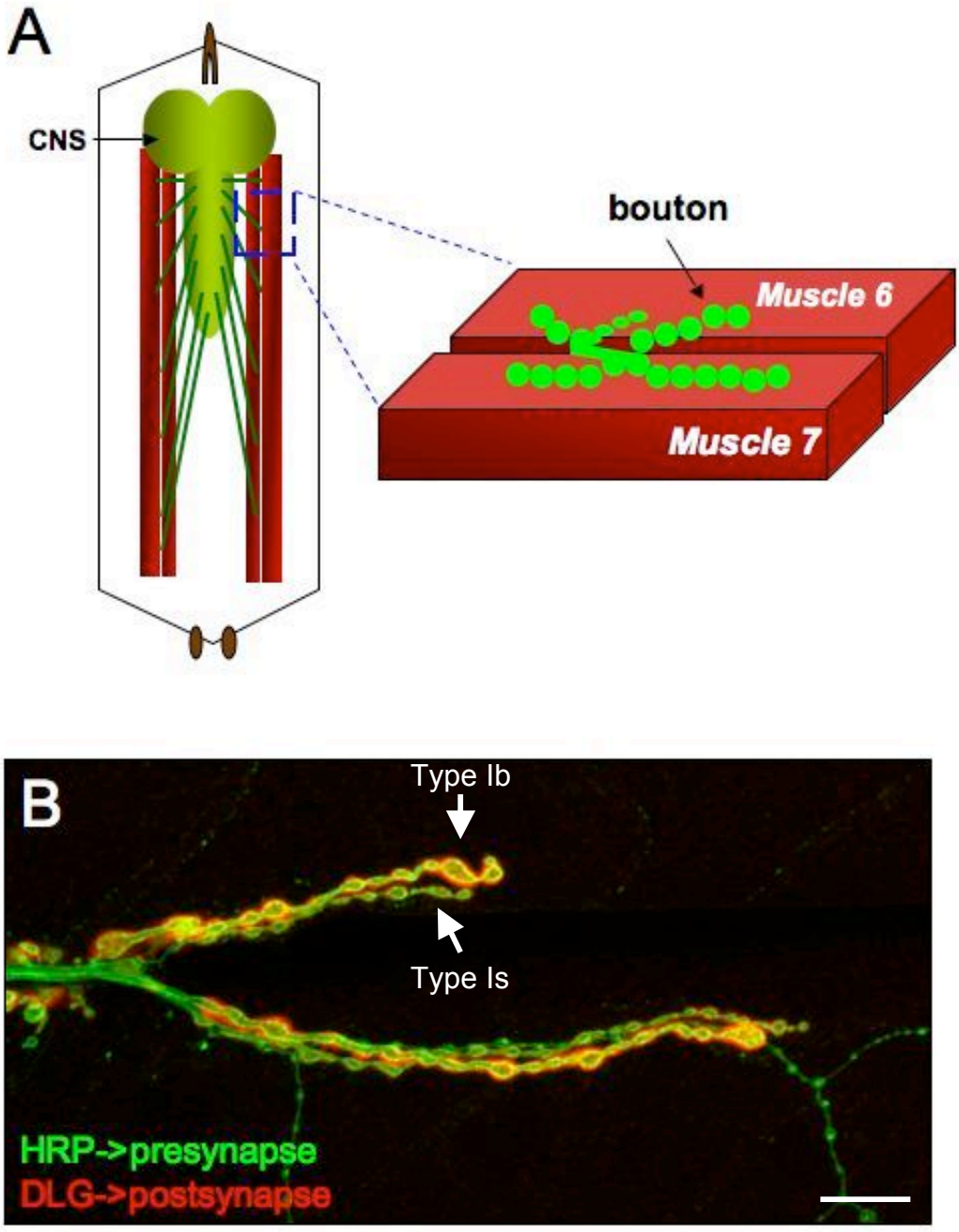
A
CNS
bouton
Muscle 6
Muscle 7
B
Type Ib
Type Is
HRP->presynapse
DLG->postsynapse

Figure 1-2

Figure 1-2. Larval neuromuscular junction. (**A**) (Image courtesy of Yuly Fuentes) The schematic diagram of 3rd instar larva (left) and neuromuscular synapses on Muscle 6&7 (right). (**B**) Typical synaptic boutons from a dissected 3rd instar larval preparation, double-stained with presynaptic membrane marker anti-HRP(green) and postsynaptic protein anti-DLG (red). Arrows indicate type Is and type Ib nerve terminals. Scale bar is 9 μm in B.

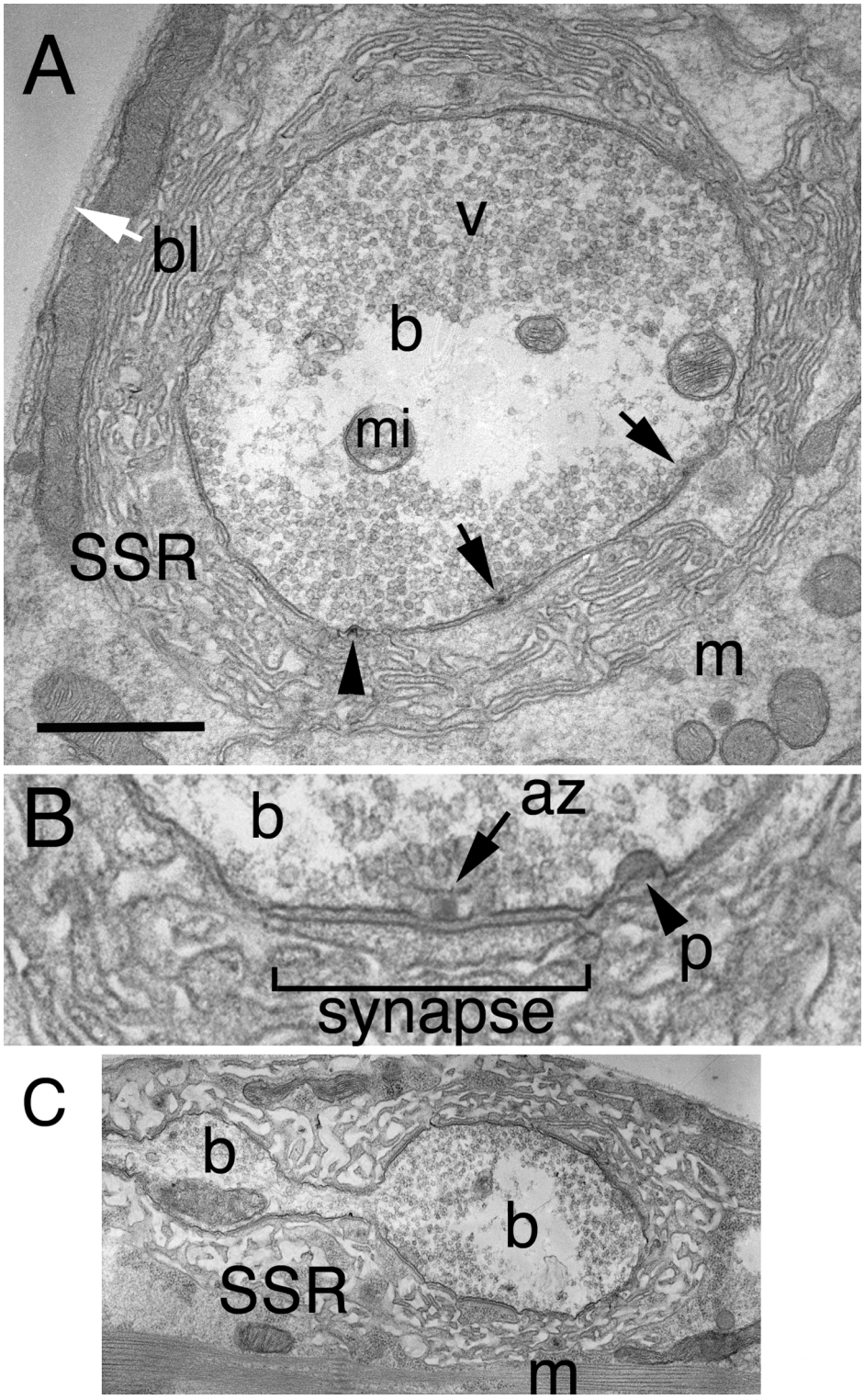

Figure 1 -3

Figure 1-3: (Adapted from (Budnik and Ruiz-Canada, 2006)) Ultrastructure of synaptic boutons. (**A**) Electron micrograph of wild-type type Ib bouton in cross-section (b = bouton, v = synaptic vesicles, mi =mitochondria, bl (white arrow) = basal lamina, SSR = subsynaptic reticulum, m = muscle). Arrows point to active zone T-bars, and arrowheads indicate clathrin coated pits. (**B**) High magnification view of synaptic, area. Arrow points to a T-bar active zone and arrowhead indicates a coated pit (p). (**C**) A longitudinal cross section of two type 1b boutons connected by a neurite process. Calibration bar is 0.8 μm in A, 0.3 μm in B, and 2.5 μm in C.

CHAPTER 2

Wingless Signaling at Synapses is through Cleavage and Nuclear Import of Receptor DFrizzled2

The following work is reprinted from the Science article of the same name published as:

Dennis Mathew, Bulent Ataman, Jinyun Chen, Yali Zhang, Susan Cumberledge and Vivian Budnik. *Science, 25 November 2005: Vol. 310. No. 5752, pp. 1344 – 1347.*

ABSTRACT

Wingless secretion provides pivotal signals during development by activating transcription of target genes. At *Drosophila* synapses, Wingless is secreted from presynaptic terminals and is required for synaptic growth and differentiation. Wingless binds the 7-pass transmembrane DFrizzled2 receptor(Packard et al., 2002), but the events ensuing at synapses are not known. We show that DFrizzled2 is endocytosed from the postsynaptic membrane and transported to the nucleus. The C-terminus of DFrizzled2 is cleaved and translocated into the nucleus, whereas the N-terminal region remains just outside the nucleus. Translocation of DFrizzled2-C into the nucleus, but not its cleavage and transport, is dependent upon Wingless signaling. We conclude that at synapses, Wingless signal transduction occurs through the nuclear localization of DFrizzled2-C for potential transcriptional regulation of synapse development.

TEXT

Members of the WNT signaling family function in synapse formation and maturation (Hall et al., 2000; Krylova et al., 2002; Packard et al., 2002; Packard et al., 2003). In *Drosophila*, the WNT homolog Wingless (Wg) is secreted from presynaptic cells at glutamatergic larval neuromuscular junctions (NMJ) (Packard et al., 2002). The Wg receptor, DFrizzled2 (DFz2), is present in both pre- and postsynaptic cells and is required for synaptic Wg function (Packard et al., 2002). Wg secretion from the presynaptic cell is crucial for both the formation of active zones, regions where synaptic vesicles accumulate adjacent to the presynaptic

membrane, and postsynaptic specializations that assemble during proliferation of synaptic boutons in larval development (Packard et al., 2002). How these Wg-dependent signaling events coordinate synapse differentiation, however, remains unknown. To investigate the effect of Wg signaling on the distribution of its receptor and subsequent signal transduction, we used antibodies to the extracellular amino acids 1-114 (DFz2-N), and to the intracellular amino acids 600-694 (DFz2-C) (Supplemental Figure 2-1). Staining of body wall muscles from third instar larvae showed that DFz2-C antibodies labelled the same NMJs as DFz2-N (Fig. 2-1A and B) (Packard et al., 2002).

Antibodies to DFz2-C also labelled spot-like structures within each of the multiple nuclei in each muscle cell (Fig. 2-1C through F; Supplemental Figure 2-1). Quantification of the number of DFz2-C spots in each nucleus demonstrated that spots were more numerous in nuclei close to the NMJ than in those more distal (Supplemental Figure 2-1). DFz2-N immunoreactive puncta were observed near the nucleus, but unlike DFz2-C immunoreactivity, these puncta were much smaller, were localized outside the nuclear boundary, and were never observed inside the nucleus (Fig. 2-1G through J). Smaller DFz2-C immunoreactive puncta were also observed at the perinuclear area, but their abundance was low (arrowheads in Fig. 2-1C).

Intranuclear localization of DFz2-C was confirmed by double labelling with propidium iodide (PI), and antibodies to the chromatin remodelling protein OSA (Collins et al., 1999; Treisman et al., 1997), which associates with chromosomal DNA (Fig. 2-2A and B). We also labelled preparations with antibody to HP-1,

which labels heterochromatin (James et al., 1989). Regions of the nuclei containing HP-1 had either no DFz2-C spots (Fig. 2-2C), or only marginal coincidence (Fig. 2-2D and E), suggesting that DFz2-C spots are mostly excluded from regions of transcriptionally inactive DNA. Nuclear localization of DFz2-C appeared to be cell-type specific. Although DFz2-C spots were always observed in the nuclei of larval muscles, DFz2-C was not observed in epithelial cells (Supplemental Figure 2-1E) or neurons.

To test whether DFz2 might be cleaved, as are some other membrane receptors such as Notch and Amyloid ß precursor protein (APP)(Fortini, 2002), we transfected *Drosophila* Schneider-2 (S2) cells with full-length DFz2, or with DFz2 fragments containing the N- (amino acids 1-605) or C- (amino acid 606-694) terminal regions. On Western blots of lysate from S2 cells transfected with DFz2, two protein bands were detected, an 83-kD band (full-length DFz2), and an 8-kD band (Fig. 2-2F). The 83-kD band was recognized by both the DFz2-N and the DFz2-C antibodies, but only the DFz2-C antibody recognized the 8-kD band, suggesting that full-length DFz2 may be cleaved to produce a C-terminal fragment. In extracts of wild type body wall muscle, full-length DFz2 was detected at very low levels by Western blots, but the 8-kD band was not detected. However, if full-length DFz2 was overexpressed in muscle cells, an 8-kD fragment was detected (Fig. 2-2G).

We compared the putative amino acid sequence of DFz2 with those of its most related Frizzled counterparts from different species (Corpet, 1988), as regions of functional significance would be highly conserved across phylogenies.

A sequence in the cytoplasmic domain proximal to the transmembrane domain (VWIWSGKTLESW) is virtually identical in all species from flies to humans, and contains a glutamyl-endopeptidase cleavage site (Supplemental Figure 2-2). In eukaryotes, glutamyl-endopeptidase activity is observed in peptidases of the ADAM (A Disintegrin and Metalloprotease) family (Tortorella et al., 1999), and ADAM members have also been implicated in APP (Lammich et al., 1999) and Notch (Pan and Rubin, 1997) receptor cleavage. Although in the case of APP and Notch, ADAM proteases cleave the extracellular domain of the proteins, ADAM proteases are also observed intracellularly (Seals and Courtneidge, 2003).

We used site-directed mutagenesis to construct three mutants: two deleting the coding sequences for KTLES, which contains the glutamyl endopeptidase cleavage site (ΔKTLES and ΔSGKTLESW), and another mutating the adjacent upstream sequence VWIWSG (DFz2-ΔVWIWSG). The amount of cleavage product was reduced in DFz2-ΔKTLES-expressing S2 cells and no cleavage product was detected in DFz2-ΔSGKTLESW cells, but DFz2-ΔVWIWSG cells had normal amounts (Fig. 2-2H). Thus, KTLES is apparently contained in the cleavage site or required for cleavage.

Localization of DFz2-C and DFz2-N fragments into different compartments within and around the nucleus may occur immediately after DFz2 biosynthesis, or DFz2 fragments may translocate to the nucleus through a retrograde pathway after integration into the plasma membrane (Supplemental Figure 2-3). To distinguish between these possibilities we tested whether cell surface DFz2 was

internalized and transported to the nucleus. Larvae were dissected and body wall muscles were incubated in situ in physiological saline containing antibody to DFz2-N. Under these conditions, the antibody was expected to label only surface DFz2 (Mathew et al., 2003). Then unbound antibody was washed away, the preparations were fixed, and secondary antibody conjugated to a blue fluorescent marker (Alexa-647) was added under non-permeabilizing conditions to detect surface DFz2. To determine whether any cell-surface DFz2 had been internalized during the initial incubation, the preparation was permeabilized and then incubated with secondary antibody conjugated to a green fluorescent marker (FITC) (Mathew et al., 2003). A prerequisite for such an experiment is that the antibody should label the extracellular region of DFz2 in situ, and indeed we found that anti-DFz2-N could label NMJs in situ (Fig. 2-3A). A fraction of surface-labelled DFz2 was internalized into the muscle, and appeared as puncta at the NMJ (Fig. 2-3B and C).

To determine whether nuclear DFz2 was derived from receptors that were internalized at the postsynaptic membrane, we conducted an antibody pulse-chase experiment in living preparations. The primary antibody-binding step was done at 4°C to inhibit internalization during antibody incubation. Unbound antibody was washed away and samples were shifted to room temperature for various time intervals before fixation (Fig. 2-3; Supplemental Figure 2-3). In samples that were fixed after a 5-minute shift at room temperature, most of the internalized DFz2 was observed close to the NMJ (Fig. 2-3B and C), but after 60 minutes little internalized DFz2 was observed at the NMJ (Fig. 2-3D through F).

There was a comparatively small decrease in surface DFz2 over time at the NMJ suggesting that only a fraction of labelled DFz2 was internalized (Fig. 2-3A and D). Parallel with the changes in DFz2 internalization at the NMJ, at 5 minutes, minimal internalized DFz2 was observed at the periphery of nuclei (Fig. 2-3G), whereas at 60 minutes, the amount of internalized DFz2 at the nuclear periphery was increased (Fig. 2-3H). Thus, cell-surface DFz2 appears to be transported from the plasma membrane to the nucleus.

If cell-surface DFz2 is endocytosed and transported to the nucleus, then blocking endocytosis or retrograde vesicle transport should block the nuclear localization of DFz2. Therefore, we expressed dominant-negative transgenes that block endocytosis [dominant-negative form of the *Drosophila* Dynamin, Shibire (Shi-DN) (Moline et al., 1999)] or retrograde transport [dominant-negative form of Glued, a component of the dynein-dynactin complex (Allen et al., 1999)] in a subset of muscle cells. In both cases the number of DFz2-C spots per nucleus was reduced (Fig. 2-4A; Supplemental Figure 2-4). These results, together with the *in vivo* internalization assays, indicate that DFz2 is internalized from the plasma membrane and is carried by retrograde transport to the nucleus.

We also tested whether Wg signaling was required for DFz2 transport to the nucleus. To decrease Wg signaling, we used a temperature sensitive wg^{ts} mutant, as well as two conditions that disrupt Wg-dependent DFz2 signaling: overexpression of full-length DFz2 in muscles (Cadigan et al., 1998; Packard et al., 2002) and expressing a DFz2 dominant-negative DFz2 construct (DFz2-DN) (Zhang and Carthew, 1998). We also overexpressed Wg in the presynaptic cells,

which caused those cells to increase Wg secretion (Cadigan et al., 1998; Moline et al., 1999; Packard et al., 2002). Disrupting Wg signaling caused a decrease in the number of DFz2-C spots inside muscle nuclei (Fig. 2-4A). In contrast, when presynaptic secretion of Wg was increased, there was an increase in the number of nuclear spots (Fig. 2-4A; Supplemental Figure 2-4).

We also expressed transgenic DFz2 variants in muscles, full-length DFz2, DFz2ΔSGKTLESW and Myc-NLS-DFz2-C (consisting of a Myc-tagged DFz2-C fragment alone or fused to a nuclear localization sequence). When DFz2 was overexpressed in muscle, bright DFz2-C immunoreactivity accumulated just outside the nucleus (Fig. 2-4B; Supplemental Figure 2-4), suggesting that overexpression of DFz2 does not disrupt retrograde transport of DFz2, but rather the nuclear import of DFz2-C. To further test the model that the DFz2 pool transported to the nucleus is derived by endocytosis from the plasma membrane, and not from an internal pool, we simultaneously expressed DFz2 and the Shi-DN in muscle cells. In the presence of Shi-DN no accumulation of DFz2-C at the perinuclear area was observed (Fig. 2-4C; Supplemental Figure 2-4). Mutations in the DFz2 cleavage site did not alter the endocytosis of DFz2 as expression of transgenic DFz2ΔSGKTLESW in muscles did not suppress the accumulation of perinuclear DFz2-C spots (although it did not enter the nucleus) and the perinuclear spots had a distribution that was indistinguishable from that of cells expressing transgenic wild type DFz2. Muscle cells expressing the DFz2-C transgenes showed diffuse Myc immunoreactivity in the cytoplasm and nuclei.

We also tested whether expressing DFz2, DFz2ΔSGKTLESW, or DFz2-C could rescue the synaptic phenotypes of a mutant of the *dfz2* gene (*dfz2*^{C1}/Df*dfz2*) (Packard et al., 2002). Interfering with DFz2 function prevents the proliferation of synaptic boutons and the formation of pre- and postsynaptic specializations in many boutons (Packard et al., 2002). Like *wg*^{ts} mutants, *dfz2*^{C1}/Df*dfz2* NMJs had irregular and tightly spaced boutons and a reduced number of boutons (Fig. 2-4D; Supplemental Figure 2-5).

Expression of DFz2 in a *dfz2*^{c1}/Df*dfz2* mutant background completely rescued the decrease in bouton number and partially restored the abnormal morphology of the boutons (Fig. 2-4D; Supplemental Figure 2-5). It also restored the presence of nuclear spots in the mutant larvae. In contrast, only a slight rescue was observed when expressing DFz2ΔSGKTLESW, and no rescue was detected when Myc-NLS-DFz2-C was expressed (Fig. 2-4D; Supplemental Figure 2-5). Thus, cleavage of DFz2 appears to be needed for DFz2 signaling at the NMJ and DFz2-C is necessary but not sufficient for DFz2 function. The slight rescuing activity observed in *dfz2*^{c1}/Df*dfz2* mutants expressing DFz2ΔSGKTLESW may indicate that not all of DFz2's function at the NMJ is accomplished through DFz2 cleavage and nuclear import (Lucas et al., 1998).

To test whether Wg is required for nuclear import of DFz2, we treated DFz2-transfected S2 cells with conditioned medium containing soluble Wg (Reichsman et al., 1996) . In the presence of Wg, prominent immunoreactive spots were detected inside the nucleus of DFz2-transfected cells, but not in

DFz2-ΔSGKTLESW-transfected cells nor in transfected cells not exposed to Wg-conditioned medium (Fig. 2-4E through G; Supplemental Figure 2-4).

Our results indicate that at the *Drosophila* NMJ, Wg secretion initiates a signaling mechanism whereby DFz2 receptors at the postsynaptic muscle membrane are endocytosed and undergo retrograde transport to the nucleus. The C-terminal fragment is cleaved during this process and is ultimately transported into the nucleus. We propose that Wg binding to DFz2 may initiate an event that marks the DFz2 C-terminal region. Endocytosed vesicles containing the entire DFz2 receptor travel towards the nucleus. Once at the periphery of muscle nuclei, the C-terminus is cleaved, and only marked C-terminal fragments are imported into the muscle nuclei where they may regulate gene transcription. Our studies help unravel a mechanism by which pre- and postsynaptic cells communicate during the coordinated growth and maturation of synaptic specializations.

Materials and Methods

Fly stocks and expression of transgenes. Flies were reared at 250C except where noted. We used the following mutants: wg^{ts} (wg^{IL114}) (Nusslein-Volhard et al., 1985) , $dfz2^{c1}$ (Chen and Struhl, 1999), and the deficiency of the *dfz2* region Df(3L)ED4782 (referred to as Df*dfz2*). The postsynaptic Gal4 driver was BG487(Budnik et al., 1996), and the presynaptic Gal4 driver was C380 (Budnik et al., 1996). We also used the following reporter UAS strains: UAS- Wg (Binari et al., 1997), UAS-$Shi^{D(K44A)}$ (Moline et al., 1999), UAS-Glued-DN (Allen et al.,

1999), UAS-DFz2-DN (Zhang and Carthew, 1998). We also generated the following UAS-strains: UAS-DFz2, UAS-DFz2-DSGKTLESW, UAS-Myc-NLS-DFz2-C, and UAS-Myc-DFz2-C (see below). Transgenes were expressed at muscles 6 and 7 by using the UAS/Gal4 system (Brand and Perrimon, 1993). wgts was reared at 170C and shifted to 290C for 16 hours prior to dissection. *dfz2*^{C1}/Df*dfz2*, UAS-DFz2/BG487; *dfz2*^{C1}/Df*dfz2*, UAS-DFz2-DSGKTLESW/BG487; *dfz2*^{C1}/Df*dfz2*, UAS-Myc-NLS-DFz2-C/BG487; *dfz2*^{C1}/Df*dfz2*, and wild type controls were reared in enriched medium containing 0.4% agar, 5% sucrose, 5% yeast extract, 2% inactivated yeast, 35µg/ml Doxycycline, 35µg/ml Gentamycin, and 0.5% (9:1) Propionic Acid: Phosphoric acid.

Antibodies and immunocytochemistry. We used the following antibodies for immunolocalization: DFz2-N (Packard et al., 2002), DFz2-C (see below), tubulin (Sigma), Osa (Collins et al., 1999; Treisman et al., 1997), HP-1 (James et al., 1989), Lamin-C (Reichsman et al., 1996), and HRP. The specificity of the DFz2-C immunoreactive spots inside muscle nuclei was determined in mutants expressing a truncated form of DFz2 lacking the C-terminal portion of the receptor (*dfz2*^{C1}). The nuclear staining pattern was eliminated in homozygous *dfz2*^{C1} (Chen and Struhl, 1999) and in *dfz2*^{C1} over a deficiency of the *dfz2* chromosomal region (*dfz2*^{C1}/Df*dfz2*) (Fig. S1B, C). Propidium iodide (PI) was used to stain chromatin, with samples being additionally treated with RNAse A (5µg/µl) for 1 hour prior to PI staining. For immunocytochemistry, *Drosophila* third

instar larvae were dissected and treated as described previously (Packard et al., 2002), and muscles 6 and 7 from abdominal segments 3 and 4 were analyzed. Comparisons between genotypes were performed in samples processed simultaneously and by using the same confocal acquisition parameters using a Zeiss laser scanning confocal microscope.

Statistical Methods. Differences between genotypes were evaluated by analysis of variance (ANOVA) for a mixed model by restricted maximum likelihood (REML) and using an unstructured covariance structure. In the presence of a significant effect of genotype, pairwise comparisons were performed using the Tukey HSD procedure. The distributional characteristics of bouton measurements were evaluated by visual inspection of histograms of residuals from the fitted ANOVA model and by application of the Kolmogorov-Smirnov goodness of fit test for normality.

Internalization assay. The internalization assay was performed and quantified as described before (Mathew et al., 2003). Briefly, samples were dissected in a 0.1mM Ca^{+2} *Drosophila* saline, and antibodies to DFz2-N added prior to incubation for 2 hours at 4^0C. Samples were then shifted to room temperature for defined periods of time, fixed, and labelled with Alexa 647-conjugated secondary antibody under non-permeabilization conditions to label external DFz2. Samples were then permeabilized and labelled with an FITC-conjugated secondary antibody.

Quantifications of images. Nuclear DFz2 immunoreactivity was quantified by counting the average number of distinct DFz2-C immunoreactive spots per nucleus at muscles 6 and 7 (segments A3 and 4), in preparations double stained with antibodies to tubulin and DFz2-C. The boundaries of muscle nuclei were distinguished with antibodies to tubulin (e.g. Fig.1F) or Lamin-C (Fig.S1. Number of samples for each genotype were N= 20 for wild type, 12 for Shi-DN, 12 for Glued-DN, 15 for Wg presynaptic overexpression, 10 for wg^{ts} pulsed to restrictive temperature for 12 hr before the wandering stage, 12 for DFz2 postsynaptic overexpression, and 9 for DFz2-DN.

To measure the differential distribution of nuclear DFz2-C spots in nuclei proximal and distal to NMJs, DFz2-C immunoreactive spots at muscle 6 (segments A3 and A4) were counted. Muscle 6 contains two longitudinal rows of nuclei localized in a stereotypical manner, a row close to muscle 13 (top nuclear row), and a row close to muscle 7 where the NMJ is located (bottom nuclear row). The number of DFz2-C spots in proximal nuclei was determined by averaging the number of spots in the 3 nuclei closest to the NMJ at the bottom nuclear row. The number of spots in distal nuclei was determined by averaging the number of spots in nuclei of the top nuclear row that abutted the segmental boundary. Quantification of the number of DFz2-C-positive spots in each nucleus demonstrated that spots were more numerous in nuclei close to the NMJ compared with those distal, and that this was enhanced by expressing Wg presynaptically (Fig. S1D).

To quantify the accumulation of DFz2 outside the nuclear boundary, the total number of spots juxtaposed to the boundary of every nucleus of muscle 6 (A3, A4) determined by the staining with antibodies to tubulin, was counted in samples double stained with antibodies to tubulin and DFz2-C.

For quantification of signal intensity in the internalization assay we used the Zeiss LSM5 PASCAL (version 3.2) image analysis software. Briefly, the immunolabelled region surrounding individual boutons (at muscles 6 and 7, abdominal segment 3) was manually traced in a single, medial confocal slice, and the mean relative intensities (on a scale of 0-255) of staining in the green channel (internalized DFz2) and the blue channel (external DFz2) across the selected area were measured. For measurements of perinuclear DFz2-N immunoreactivity, the mean intensity of staining in the green channel, in an area between the muscle nucleus and a concentric circle of a radius of 5 μm larger than the nuclear radius, was measured at a nuclear midline confocal slice. A mean intensity value of a similar area away from the nucleus was measured and subtracted from the previous value to normalize background levels in the various samples. Values were normalized by dividing the signal intensities by area of the section and were then plotted.

To determine the number of synaptic boutons in various genotypes, third instar body wall muscles were dissected and stained with antibodies to HRP to visualize NMJs, and boutons were counted under a fluorescence microscope at muscles 6 and 7 (segments A3 and A4). No changes in muscle area were observed in any of the genotypes analyzed, and therefore bouton number was

not normalized to muscle area. Number of samples used for bouton counting are: 43 wild type, 42 *dfz2*^{C1}/Df*dfz2*, 25 UAS-DFz2/BG487; *dfz2*^{C1}/Df*dfz2*; 26 UAS-DFz2ΔSGKTLESW/BG487; *dfz2*^{C1}/Df*dfz2*, 15 UAS-NLS-DFz2-C/BG487; *dfz2*^{C1}/Df*dfz2*.

Schneider-2 (S2)-cell cultures. S2 cell transfection, site directed mutagenesis, and generation of transgenic flies. DFz2 cDNA was cloned into the pAcV5.1/HisB vector (Invitrogen). For all transfections, *Drosophila* Schneider (S2) cells were cultured in SFX (Hyclone) medium containing 10%FBS, penicillin (100U/µl) and streptomycin(100µg/µl). 3x2ml-wells/sample of 60-80% confluent S2 cells were transfected with 1.5µg DNA using Cellfectin and Serum Free Medium (Invitrogen). Thirty-six hours after transfection, cells were harvested, resuspended in homogenization buffer and protein dye. Samples were loaded onto 6% or 15% acrylamide gel for subsequent Western blot procedures. DFz2 mutations were generated using the PCR-based QuikChange site-directed mutagenesis kit (Stratagene). Full length DFz2 in pAcV5/HisB was used as a template. The forward primers TGGATCTGGTCTGGCTGGCGACGCTTCTGG, GGCGTGTGGATCTGGCGACGCTTCTGG and TCGGGCGCGTGGATCTGGGCTGCCAAGACG, and the reverse primers CCAGAAGCGTCGCCAGCCAGACCAGATCC, CCGCCAGAAGCGTCGCCAGATCCACAC and CGTCTTGGCAGCCCAGATCCACGCGCCCG were used for making the DFz2-ΔKTLES, ΔSGKTLESW and DFz2-ΔVWIWSG (VWIWSG to AWIWAA)

constructs respectively. An 8 Myc tag was inserted after aa 616 to create the construct DFz2-8XMyc-C.

To quantify the percentage of S2 cells with nuclear spots, DFz2 transfected S2 cells, with and without Wg-conditioned medium, were double labeled with antibodies to DFz2-C and tubulin. The number of cells with nuclear DFz2 were counted and expressed as a percentage of the total number of transfected cells in a field.

To provide a source of Wg for DFz2-transfected S2 cells we added Wg-conditioned medium as follows. S2HSWG(+)cells were heat shocked to produce WG. GAGs (10µg/ml Heparin and 10µg/ml Chondroitin sulfate) were then added to release WG from the cell surface as described (Reichsman et al., 1996). Next, the conditioned medium was added to transfected S2 cells (Supplemental Figure 2-4F). After 48-60 hours incubation, immunocytochemistry was performed as described before (Chang and Reppert, 2003). When S2 cells are transfected with DFz2 in the absence of Wg, immunoreactive spots are observed in the cytoplasm, but no signal is observed inside the nucleus. The amount of cleaved DFz2-C (8-kD fragment) was not affected by culturing DFz2-transfected S2 cells in the presence of Wg-conditioned medium.

For overexpression and rescue of dfz2 mutant phenotypes, full length DFZ2, ΔSGKTLESW, and DFz2-C region were subcloned using Eag1 and XhoI in frame to a 6 Myc tag at the 5' end of NT-pUAST (kind gift from Dr. Marc Freeman). The Dfz2C fragment (aa 617-aa 694) with a Myc tag

(MEQKLISEEDLNE) and an NLS tag (PKKKRKV) at its N-terminus was cloned into pUAST for germline transformation.

Western Blots: Western blots of S2 cells an body wall muscles were performed as previously described (Ashley et al., 2005). In the Western blots shown in Fig. 2-2 and Supplemental Figure 2-2, proteins in the upper and the lower panels were separated in a 6% or a 15% SDS- PAGE gel respectively. We also examined DFz2 in KC167 cells transfected with DFz2. We observed no DFz2 cleavage product in these cells.

To verify the observations of DFz2 cleavage with a marker independent of the DFz2-C antibody, we also generated a DFz2 construct containing 8 Myc tags inserted after the site of cleavage and expressed it in S2 cells for Western analysis. We found that the cleaved fragment could also be detected with antibodies to Myc antibodies (Supplemental Figure 2-5). We also tested if the amount of DFz2 cleaved was dependent on the presence of Wg. For this experiment, DFz2-S2 cells were cultured in the presence and absence of Wg-conditioned medium, and cell extracts analyzed by Western blot. The amount of Dfz2 cleaved in the two situations was measured using a phosphoimager and expressed as a ratio of full length DFz2. No difference in the amount of DFz2-C was detected in this blot (Supplemental Figure 2-4H).

We also tested whether another member of the DFz family, DFz1 was cleaved in a manner similar to DFz2, although DFz1 lacks the region identified as part of the cleavage site in DFz2. For these experiments, a DFz1 cDNA

containing a V5 tag at its C-terminus was transfected into S2 cells, and cell extracts examined by Western blot. We detected no cleavage of DFz1 (data not shown).

Our immunocytochemical observations suggest that DFZ2-C is not detected in epithelial cells and neurons. We also addressed this issue by performing Western blots of adult heads and imaginal discs overexpressing DFz2. No cleavage product was detected in the blots (data not shown).

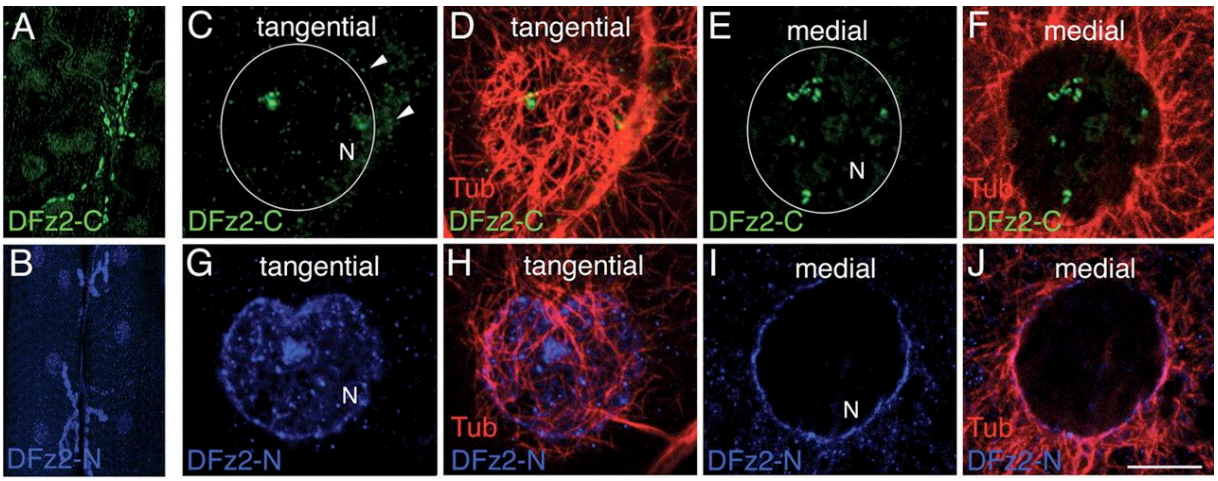
A
DFz2-C
C tangential
N
DFz2-C
D tangential
Tub
DFz2-C
E medial
N
DFz2-C
F medial
Tub
DFz2-C
B
DFz2-N
G tangential
N
DFz2-N
H tangential
Tub
DFz2-N
I medial
N
DFz2-N
J medial
Tub
DFz2-N

Figure 2-1

Figure 2-1. Localization of DFz2-C and DFz2-N to the same NMJs, but to different subcellular compartments — inside the nucleus (DFz2-C) and at the perinuclear region (DFz2-N). (**A**, **B**) Wild type third instar NMJs from muscles 6 and 7 (A3) stained with antibodies to (**A**) DFz2-C, and (**B**) DFz2-N. (**C** through **J**) Representative muscle nuclei at muscle 6 (A3) in preparations double stained with antibodies to (**C** through **F**) DFz2-C (green) and tubulin (red) and (**G** through **J**) DFz-N (blue) and tubulin (red). Note that C-F and G-J were obtained from different preparations. (**C**, **D**, **G**, **H**) show a confocal slice at a focal plane through the nuclear-cytoplasmic boundary (defined by the microtubular array; tangential), and (**E**, **F, I**, **J**) a confocal slice at a focal plane midway through the nucleus (medial). N= nucleus, arrowheads in C point to cytoplasmic DFz2-C. Calibration bar= 9 μm in A-B, and 8 μm in C-J.

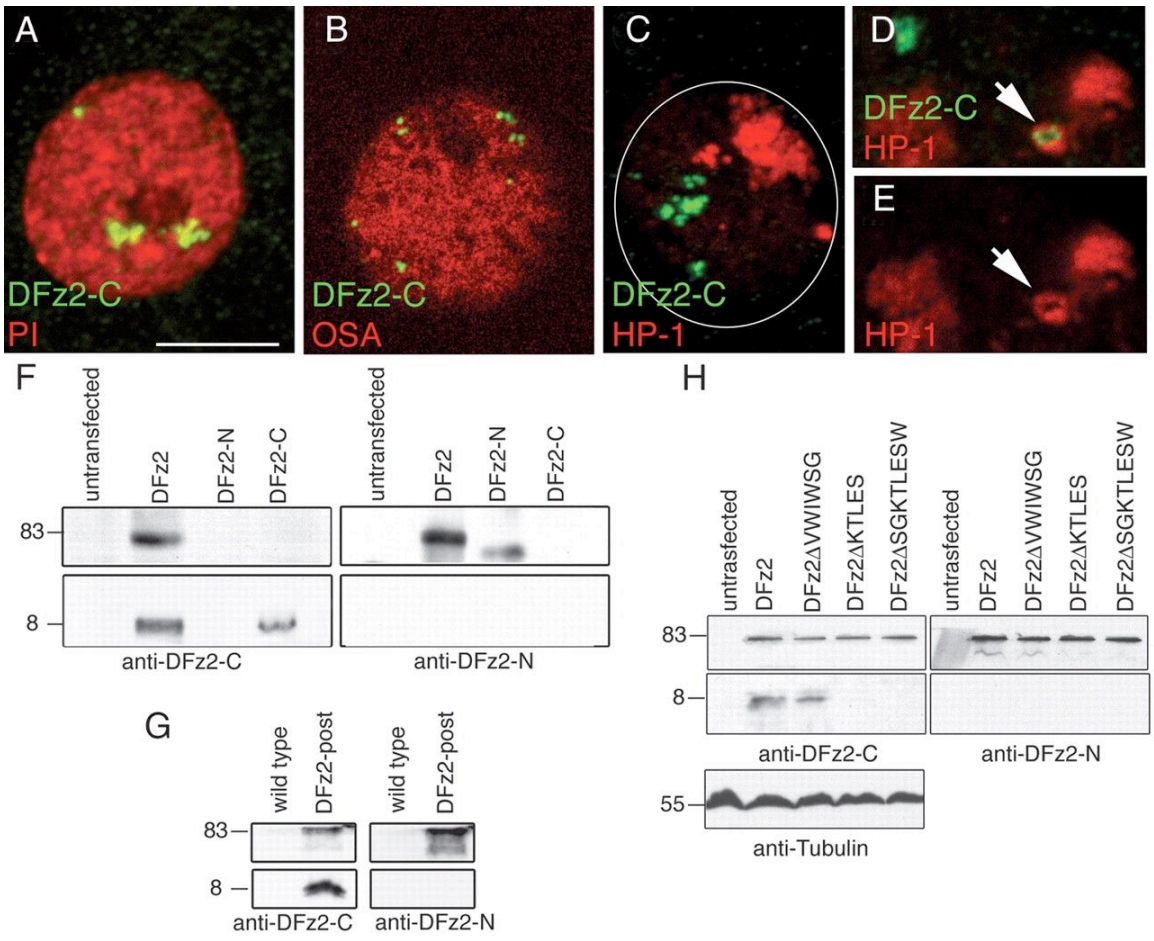
A
DFz2-C
PI
B
DFz2-C
OSA
C
DFz2-C
HP-1
D
DFz2-C
HP-1
E
HP-1
F
untransfected
DFz2
DFz2-N
DFz2-C
83
8
anti-DFz2-C
anti-DFz2-N
G
wild type
DFz2-post
83
8
anti-DFz2-C
anti-DFz2-N
H
untrasfected
DFz2
DFz2ΔVWIWSG
DFz2ΔKTLES
DFz2ΔSGKTLESW
83
8
anti-DFz2-C
anti-DFz2-N
55
anti-Tubulin

Figure 2-2

Figure 2-2. Localization of DFz2-C to euchromatin and evidence for cleavage of DFz2. (**A, B**) Colocalization of (**A**) DFz2-C (green) and PI (red) and (**B**) DFz2-C and OSA. In (**C-E**) muscle nuclei were double labelled with antibodies to the heterochromatin-specific protein HP-1 (red) and DFz2-C (green). Arrows point to regions of adjacent DFz2-C and HP-1 immunoreactivity. Calibration bar= 9 μm in A-C, and 6 μm in D-E. (**F**) Western blot of S2 cells transfected with full-length DFz2, DFz2-N, and DFz2-C. (**G**) Western blots of body wall muscle extracts from wild type larvae, and larvae overexpressing full-length DFz2. (**H**) Western blot of S2 cells and S2 cells transfected with DFz2 constructs. Blots were sequentially probed with antibodies to DFz2-C, DFz2-N, and tubulin.

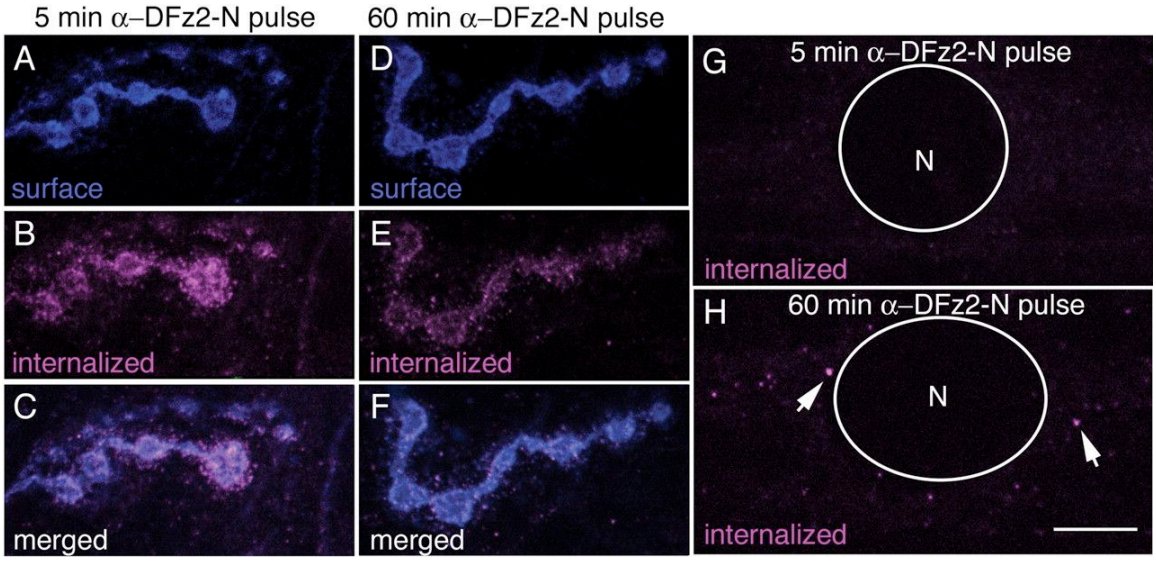
5 min α–DFz2-N pulse
60 min α–DFz2-N pulse
A
surface
B
internalized
C
merged
D
surface
E
internalized
F
merged
G
5 min α–DFz2-N pulse
N
internalized
H
60 min α–DFz2-N pulse
N
internalized

Figure 2-3

Figure 2-3. *In vivo* transport of DFz2 from the cell surface to the nucleus. (**A**-**F**) show anti-DFz2-N immunoreactivity at NMJs during the *in vivo* DFz2 internalization assay. (**A**, **D**) Surface DFz2 (blue), and (**B, E**) internalized DFz2 (magenta) are shown at 5 and 60 minutes after pulse labelling. (**C, F**) correspond to the merged blue and magenta channels. (**G, H**) anti-DFz2-N immunoreactivity around a muscle nucleus at 5 and 60 minutes after pulse labelling. Calibration bar= 9 μm in A-F, and 6 μm in G-H.

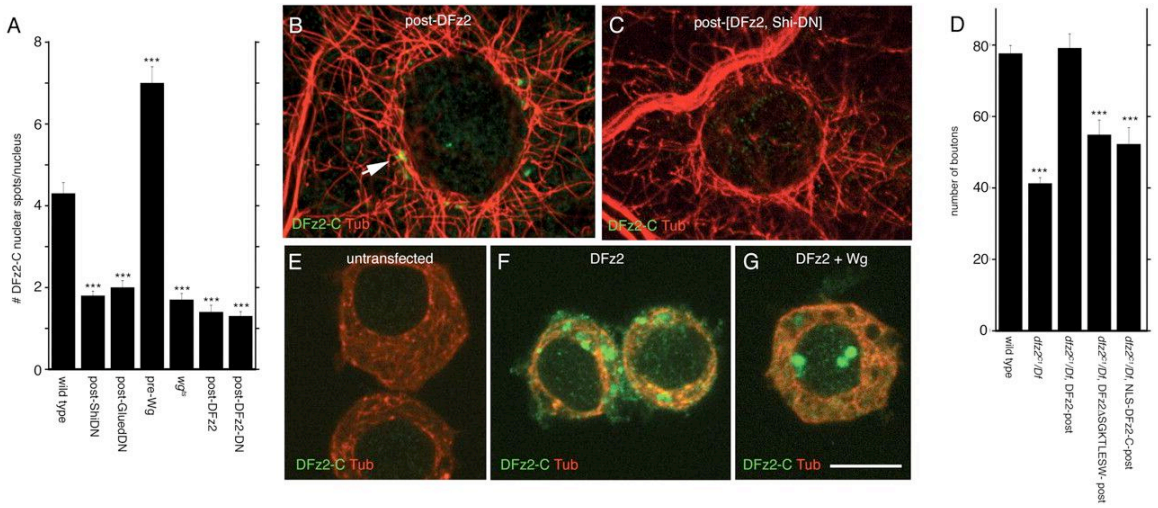
A
DFz2-C nuclear spots/nucleus
wild type
post-ShiDN
post-GluedDN
pre-Wg
wg^ts
post-DFz2
post-DFz2-DN
B
post-DFz2
DFz2-C Tub
C
post-[DFz2, Shi-DN]
DFz2-C Tub
D
number of boutons
wild type
dfz2^1/Df
dfz2^1/Df, DFz2-post
dfz2^1/Df, DFz2ΔSGKTLESW- post
dfz2^1/Df, NLS-DFz2-C-post
E
untransfected
DFz2-C Tub
F
DFz2
DFz2-C Tub
G
DFz2 + Wg
DFz2-C Tub

Figure 2-4

Figure 2-4. Role of endocytosis, retrograde transport, and Wg signaling in DFz2-C nuclear import. (**A)** Mean number of nuclear spots/nucleus in different genotypes. (**B**, **C**) Muscle nuclei in larva expressing (**B**) DFz2 and (**C**) DFz2 and Shi-DN in the muscles. Tissues were double labelled with antibodies to tubulin and DFz2-C. Arrow in B points to DFz2-C spots that accumulate just outside of the nuclear perimeter. (**D**) Number of synaptic boutons in wild type and *dfz2*^{C1}*/Dfdfz2* mutants expressing various DFz2 transgenes in muscle as indicated. *** = $p<0.0001$ compared to wild type [ANOVA (21)]. (**E**-**G**) DFz2-C and tubulin immunoreactivity in (**E**) S2 cells, and (**F-G**) S2 transfected with DFz2, and treated plus and minus Wg-conditioned medium. Calibration bar= 9 μm in B-C, and 7 μm in E-G.

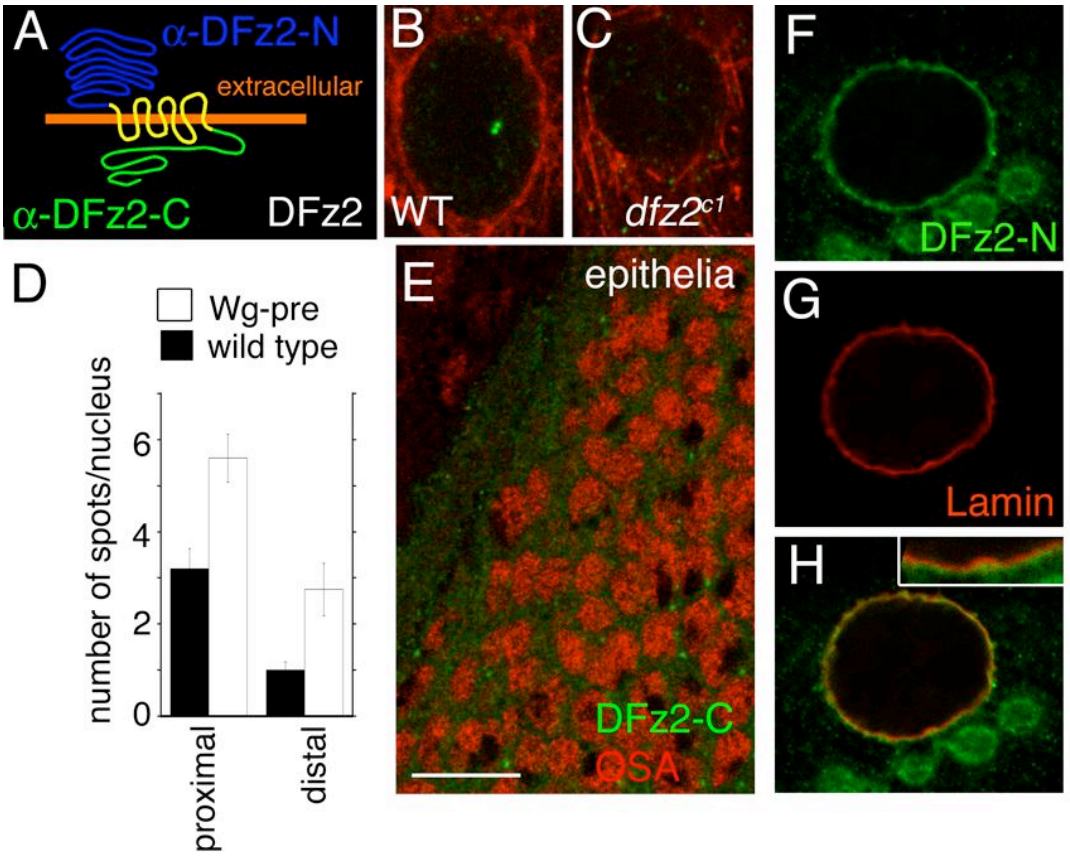

Supplemental Figure 2-1

Supplemental Figure 2-1. DFz2-C is localized to spots in muscle nuclei, but not in the nuclei of epithelial cells. (**A**) Diagram of DFz2 protein showing the regions used for generation of the DFz2-N (blue) and DFz2-C (green) antibodies. (**B**) Second instar wild type and (**C**) *dfz2*^{c1} mutant in preparations double stained with antibodies to DFz2-C (green) and tubulin (red). (**D**) Number of nuclear spots in nuclei adjacent to NMJs (proximal) and in nuclei distant from the NMJ (near the segment boundary; distal) in wild type and in larvae overexpressing Wg in presynaptic neurons. (**E**) Epithelial disc double labelled with the chromatin-remodelling protein OSA (red) and DFz2-C (green). (**F-G**) muscled nucleus double stained with antibodies to DFz2-N and Lamin-C. Inset in H is a high magnification view of the nuclear boundary, showing that DFz2-N is not inside the nucleus. Calibration bar = 8μm in B and C, 10 μm in E-H, and 4 μm in the inset in panel H.

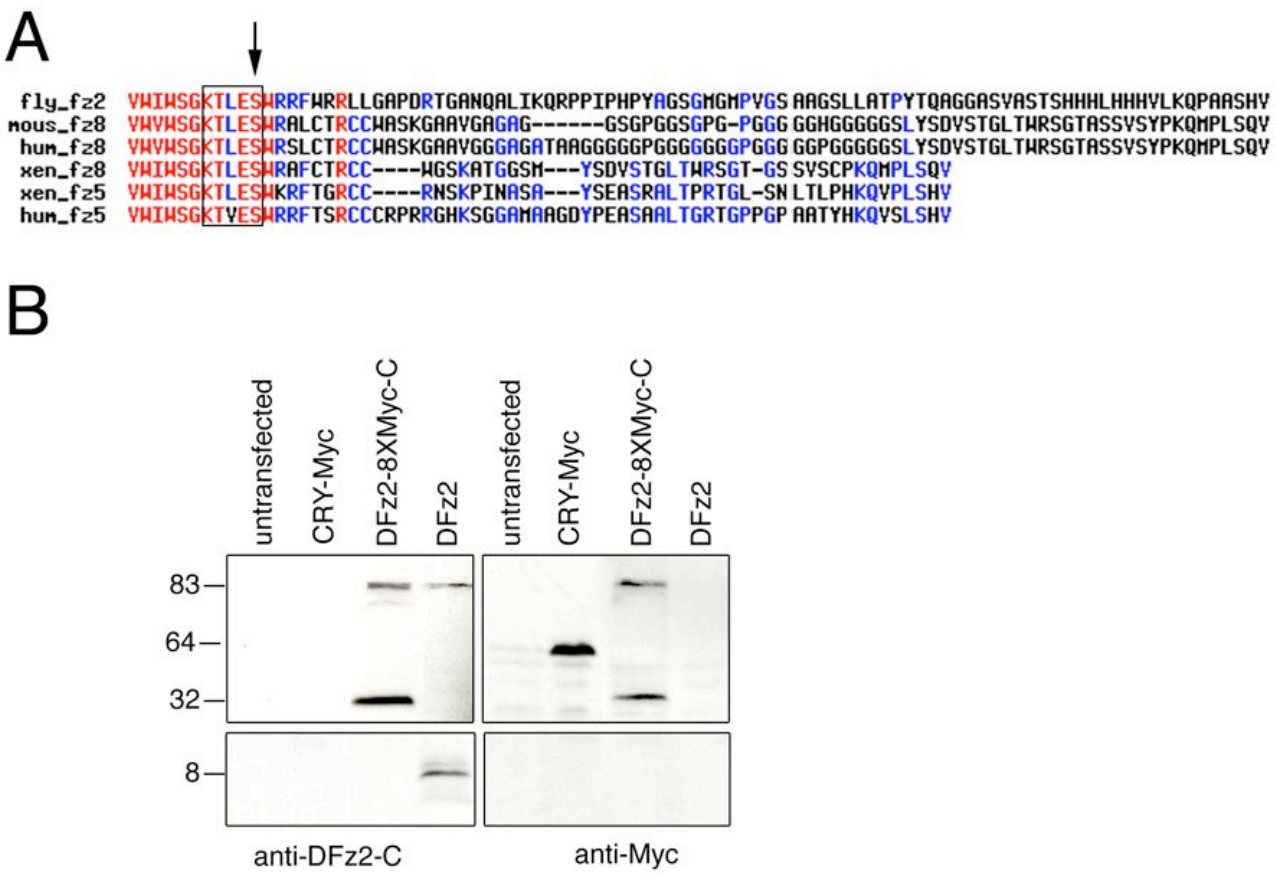

Supplemental Figure 2-2

Supplemental Figure 2-2. DFz2-C is cleaved. (**A**) Alignment of the cytoplasmic domain amino acid sequences of Frizzled proteins most related to DFz2 in several species. Red = high consensus residues, Blue = low consensus residues. Box indicates region deleted in DFz2-DKTLES. Arrow indicates the site of predicted cleavage by a glutamyl-endopeptidase. (**B**) Western blot of S2 cells transfected with CRY-Myc, DFz2-8XMyc-C, and full-length DFz2 sequentially probed with antibodies to Myc and DFz2-C.

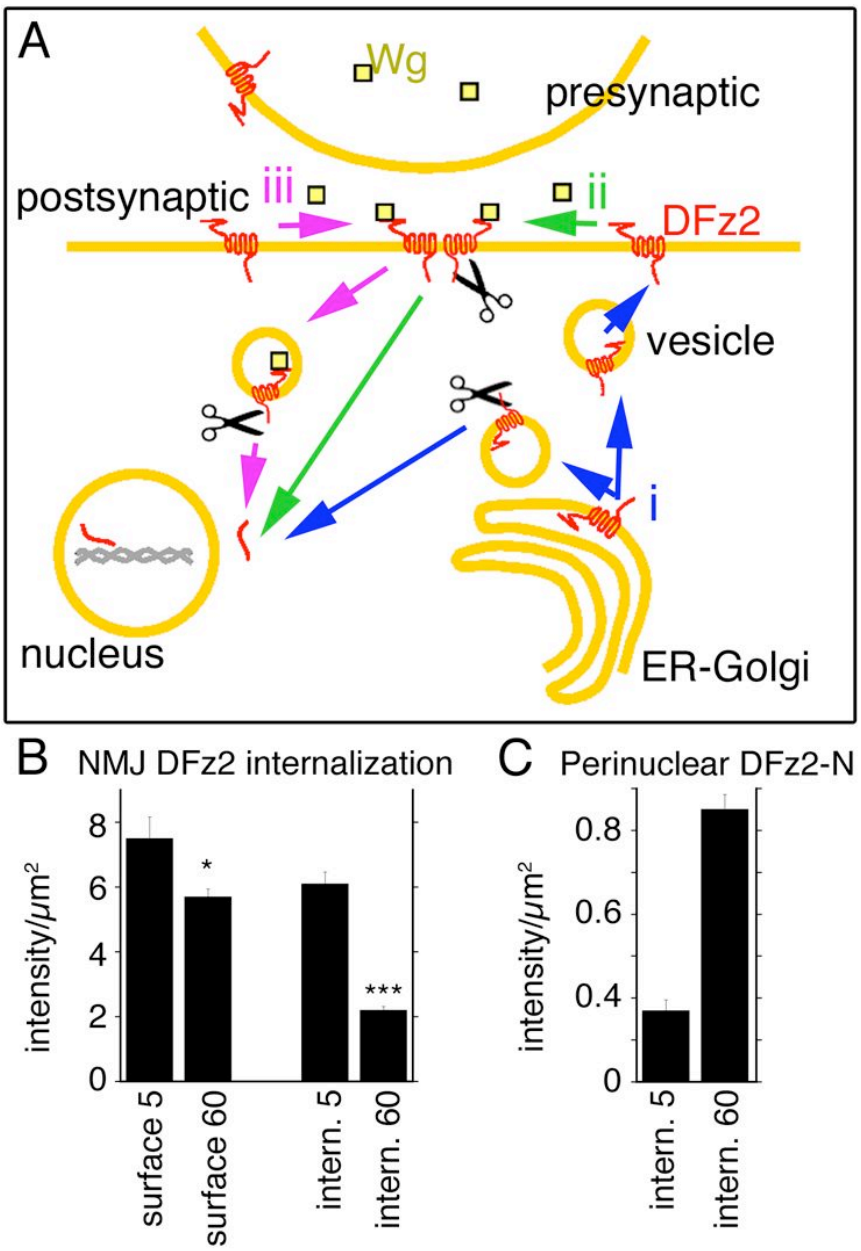

Supplemental Figure 2-3

Supplemental Figure 2-3. *In vivo* trafficking of DFz2 to the nucleus. (**A**) Diagram illustrating potential routes of DFz2-C cleavage and trafficking to the nucleus. (i; blue arrows) DFz2 is cleaved during or after biosynthesis in ER and Golgi; then DFz2-C translocates into the nucleus. (ii; green arrows) DFz2 is cleaved at the plasma membrane, and the DFz2 fragment traffics towards the nucleus where it is imported. (iii; magenta arrows) DFz2 is internalized upon Wg binding, and is transported retrogradely in a transport vesicle towards the nucleus. At the perinuclear area, the C-terminal fragment is cleaved and imported into the nucleus. (**B, C**) Quantification of fluorescence intensity in the internalization assay (B) at the NMJ and (C) at the perinuclear area (N=12 samples). *** = $p<0.0001$, * = $p<0.05$.

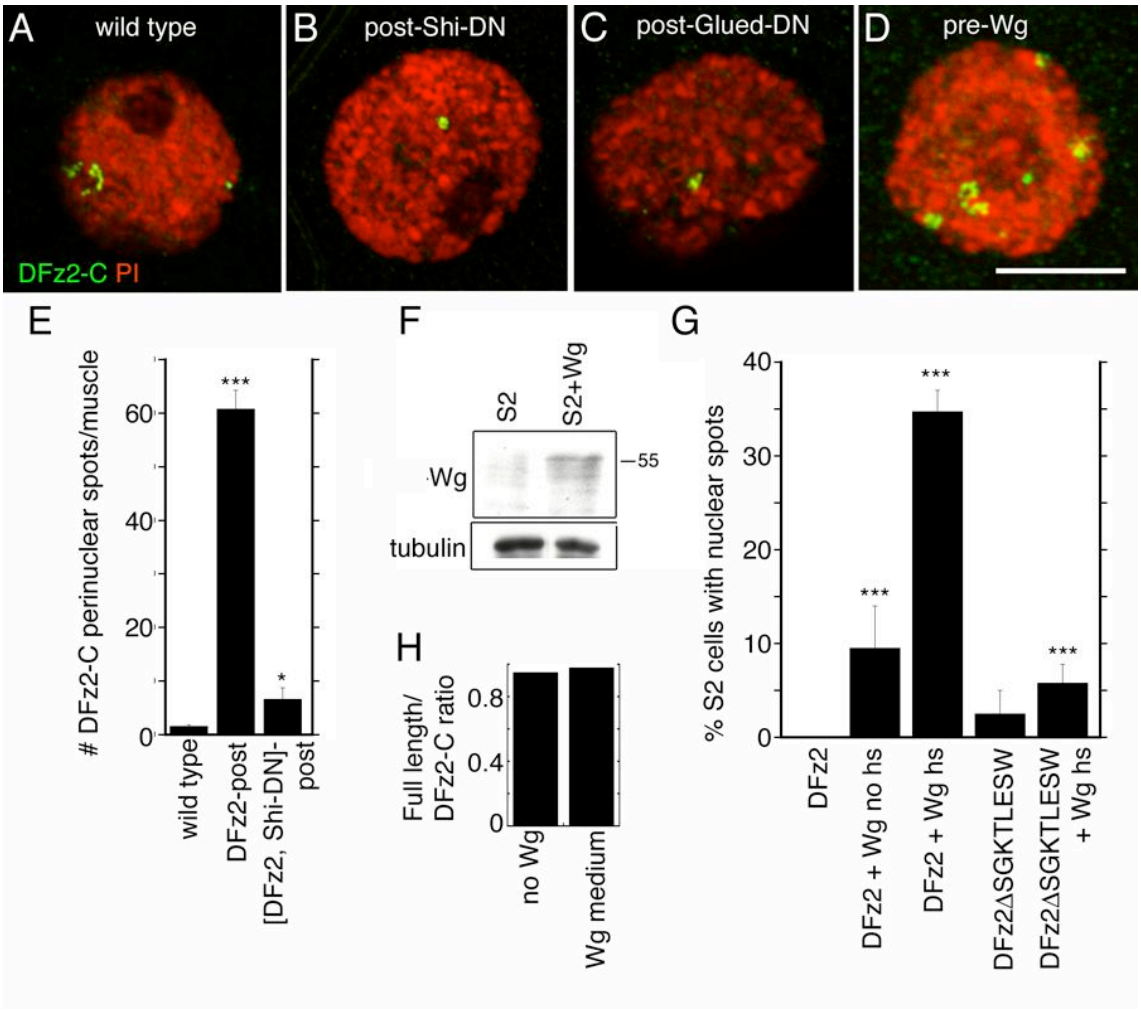

Supplemental Figure 2-4

Supplemental Figure 2-4. DFz2 nuclear import depends on endocytosis, retrograde transport, and Wg signalling. (**A-D**) Muscle nuclei double stained with PI (red) and antibodies to DFz2-C (green) in (**A**) wild type, muscle overexpression of (**B**) Shi-DN, (C) Glued-DN, and (**D**) larvae overexpressing Wg presynaptically. Calibration bar is 9 μm. (**E**) Number of perinuclear spots/muscle in wild type (N=30), postsynaptic DFz2 expression (N=28), and postsynaptic DFz2 and Shi-DN expression (N=20). (**F**) Western blot of S2 cells in the presence and absence of Wg-conditioned medium. (**G**) Percentage of S2 cells containing DFz2-C nuclear spots in S2 cells transfected with DFz2, DFz2 + control Wg conditioned medium (from hs-Wg cell line, but not heat shocked), DFz2 + Wg conditioned medium (from hs-Wg cell line heat shocked, DFz2-DSGKTLESW, and DFz2-DSGKTLESW + Wg conditioned medium. (**H**) Ratio of full length to DFz2-C signal intensity measured from a Western blot of DFz2-S2 cell extracts cultured in the absence or presence of Wg-conditioned medium.

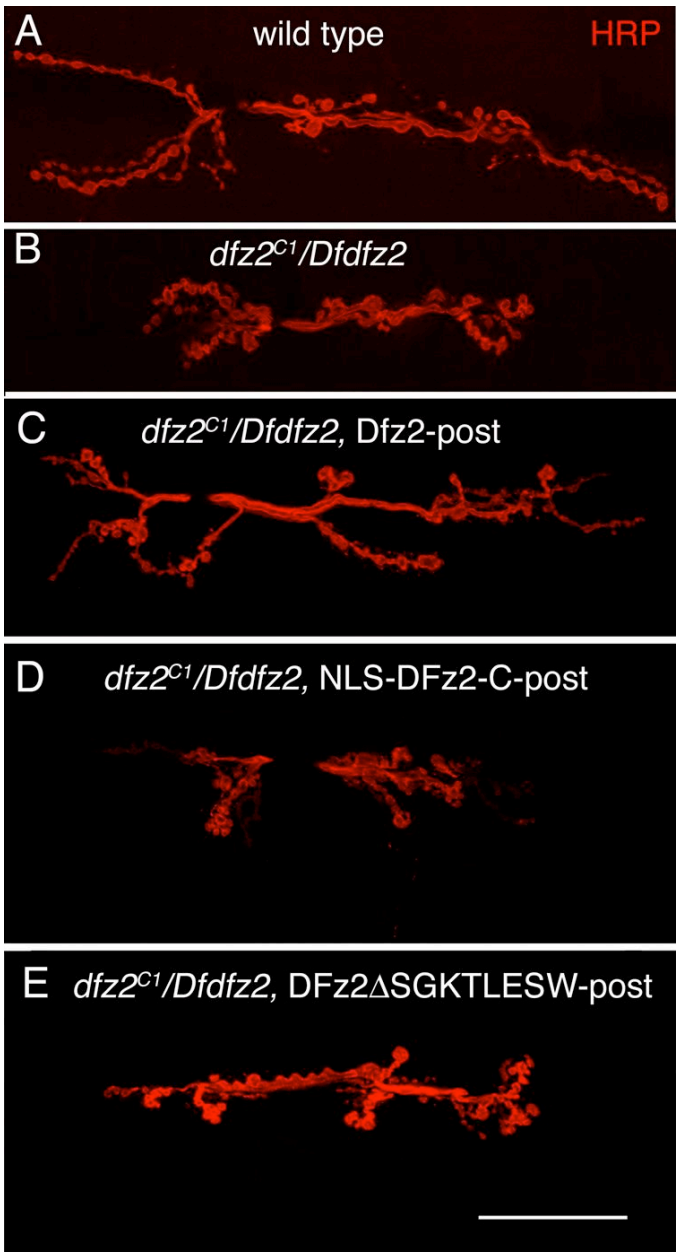

Supplemental Figure 2-5

Supplemental Figure 2-5. *dfz2*^{C1} mutants decrease bouton number, and this defect is rescued by full-length DFz2, but not uncleavable DFz2, or the C-terminal DFz2 fragment alone. The panels show third instar NMJs from abdominal segment 3 in preparations stained with antibodies to HRP in (**A**) wild type, (**B**) *dfz2*^{c1}*/Df*, (**C**) *dfz2*^{c1}*/Df* larvae expressing full-length DFz2, (**D**) *dfz2*^{c1}*/Df* larvae expressing NLS-DFz2-C, and (**F**) *dfz2*^{c1}*/Df* larvae expressing uncleavable DFz2. Calibration bar=6 μm.

CHAPTER 3

Nuclear trafficking of *Drosophila* Frizzled-2 during synapse development requires the PDZ protein dGRIP

The following work is reprinted from the Proceedings of the National Academy of Science (PNAS) article of the same name published as*:*

Bulent Ataman, James Ashley, David Gorczyca, Michael Gorczyca, Dennis Mathew, Carolin Wichmann, Stephan J. Sigrist, and Vivian Budnik. *PNAS, 16 May 2006: Vol.103. No.20, pp. 7841-7846.*

ABSTRACT

The Wingless pathway plays an essential role during synapse development. Recent studies at *Drosophila* glutamatergic synapses suggest that Wingless is secreted by motor neuron terminals and binds to postsynaptic *Drosophila* Frizzled-2 (DFz2) receptors. DFz2 is, in turn, endocytosed and transported to the muscle perinuclear area, where it is cleaved, and the C-terminal fragment is imported into the nucleus, presumably to regulate transcription during synapse growth. Alterations in this pathway interfere with the formation of new synaptic boutons and lead to aberrant synaptic structures. Here, we show that the 7 PDZ protein dGRIP is necessary for the trafficking of DFz2 to the nucleus. dGRIP is localized to Golgi and trafficking vesicles, and *dgrip* mutants mimic the synaptic phenotypes observed in *wg* and *dfz2* mutants. DFz2 and dGRIP colocalize in trafficking vesicles, and a severe decrease in dGRIP levels prevents the transport of endocytosed DFz2 receptors to the nucleus. Moreover, coimmunoprecipitation experiments in transfected cells and yeast two-hybrid assays suggest that the C terminus of DFz2 interacts directly with the PDZ domains 4 and 5. These results provide a mechanism by which DFz2 is transported from the postsynaptic membrane to the postsynaptic nucleus during synapse formation and implicate dGRIP as an essential molecule in the transport of this signal.

INTRODUCTION

Recent studies have implicated the Wingless (Wg)/Wnt pathway as one of the signaling pathways central to synapse differentiation. In vertebrates, Wnt-7a functions as a retrograde messenger that promotes synapse maturation and, additionally, modulates dendritic development (Hall et al., 2000; Koh et al., 1999; Rosso et al., 2005). At the fly neuromuscular junction (NMJ) the Wnt homologue Wg is secreted by presynaptic terminals, and its receptor, *Drosophila* Frizzled-2 (DFz2) is localized both pre- and postsynaptically (Packard et al., 2002). Wg secretion at the synapse is required for the normal proliferation of synaptic boutons during muscle growth and for the differentiation of active zones and postsynaptic specializations (Packard et al., 2002; Packard et al., 2003). Wg/Wnt signaling occurs through a variety of pathways. In some epithelial tissues, Wg operates through a canonical pathway in which Wg binding to DFz initiates a cascade that leads to the formation of a complex between Armadillo/ß-catenin and transcription factors that are imported into the nucleus, where they regulate transcription (Moon et al., 2002). Wnt ligands can also signal through noncanonical pathways that involve G proteins or the release of calcium from intracellular stores (Rosso et al., 2005). A recent study described an alternative pathway in which DFz2 is continuously endocytosed at the plasma membrane of postsynaptic muscles and transported to the perinuclear area. Upon Wg signaling, the C-terminal region of DFz2 is cleaved and imported into the nucleus. In the absence of nuclear import, synaptic proliferation and the formation of synaptic specializations are severely affected (Mathew et al., 2005). The

molecular mechanisms by which DFz2 receptors are trafficked to the nucleus are unknown.

In a search for synaptic proteins involved in synapse development, we identified the *Drosophila* homologue of GRIP, a 7-PDZ protein that, in vertebrates, is thought to be involved in trafficking and scaffolding of several synaptic molecules, including AMPA receptors (Braithwaite et al., 2002; Dong et al., 1997; Hirbec et al., 2003; Liu and Cull-Candy, 2005; Osten et al., 2000), Ephrin ligands and receptors (Contractor et al., 2002; Hoogenraad et al., 2005), and Liprin (Wyszynski et al., 2002). The elucidation of GRIP function in the mammalian nervous system has been complicated by the presence of multiple GRIP PDZ domains and the widespread localization of GRIP isoforms in many tissues. Furthermore, mouse *grip1* knockouts generally die as embryos (Bladt et al., 2002), and the few surviving adults have a wide range of developmental defects, but no neuronal phenotypes have been described (Takamiya et al., 2004). This early lethality, combined with pleiotropic defects, has precluded a study of the specific function of GRIP in the nervous system in an intact organism. A recent study examined the role of GRIP in cultured hippocampal neurons and found that GRIP is required for dendrite morphogenesis (Hoogenraad et al., 2005). However, the validity of these findings for the intact nervous system remains to be tested.

In *Drosophila*, there is a single *dgrip* gene, and a previous study has implicated dGRIP in muscle guidance during embryonic development (Swan et al., 2004); however, its potential function during synapse development was not

addressed. By using a combination of genetic and tissue-specific RNA interference (RNAi) expression tools, we have been able to examine the synaptic phenotypes resulting from synaptic dGRIP loss of function *in vivo*.

We show that dGRIP is present in both presynaptic terminals and postsynaptic muscles in vesicles associated with the microtubule cytoskeleton. Perturbation of dGRIP levels interferes with normal synapse development, and the synaptic defects observed in *dgrip* loss-of-function conditions phenocopy those observed in *wg* and *dfz2* mutants. We also show that dGRIP and the PDZ-binding domain of DFz2 interact and that this interaction is likely to be required for the retrograde transport of DFz2 from the synapse to the nucleus. These results suggest that, at synapses, dGRIP is involved in the transduction of the Wg signaling pathway required to specify the differentiation of pre- and postsynaptic structures.

RESULTS

dGRIP Is Localized to Synapses and to Trafficking Vesicles.

To examine the pattern of dGRIP expression at the NMJ, we generated two antibodies directed against the N and C termini of dGRIP (Fig. 2-1A). The staining with these antibodies was specific because both antibodies gave rise to the same pattern of immunoreactivity at the body-wall muscles, and signal intensity was reduced in *dgrip* mutants or enhanced by dGRIP overexpression (see below). dGRIP was localized both at the pre- and postsynaptic compartments of the NMJ (Fig. 3-1 B, C). At the presynaptic compartment,

dGRIP was observed in a punctate pattern that was enriched along the microtubule bundle that transverses NMJ branches and is labeled by antibodies against the MAP1B-related protein Futsch (Ruiz-Canada et al., 2004) (Fig. 3-1 E–H). dGRIP puncta were also found inside the bouton cytoplasm, especially at distal boutons within an NMJ branch (arrowheads in Fig. 3-1 D and I).

In muscles, dGRIP was localized in puncta and in large well defined spots (~0.5 μm) throughout the muscle cytoplasm (Fig. 3-1 B and C and arrows in E and K). Muscle puncta were found in the muscle cortical region, and their frequency increased at the peribouton area (Fig. 3-1 D and I, long arrows and G and H, arrowheads). In contrast, the large spots had a uniform distribution (Fig. 3-1 B and C). We used several markers to identify the intracellular compartments labeled by dGRIP antibodies. A one-to-one correspondence was found between the large dGRIP spots and Lava lamp (Lva), a Golgi resident protein (Sisson et al., 2000) (Fig. 3-1 J–M, arrows), but the smaller puncta were not associated with Lva (Fig. 3-1M, arrowhead). Although there was a near perfect one-to-one relationship between large dGRIP spots and Lva, Lva and dGRIP immunoreactivity were slightly offset, suggesting that the two proteins may occupy slightly different Golgi subcompartments (Fig. 3-1M Inset). dGRIP spots and Lva were also found to be associated with microtubules in muscles (Fig. 3-1N; see below). Neither large dGRIP-Lva spots nor Lva were found within presynaptic boutons (Fig. 3-1N). Thus, dGRIP is found both pre- and postsynaptically in a punctate pattern, with a fraction of the postsynaptic staining associated with Golgi bodies.

We next examined the relationship between microtubules and dGRIP puncta and spots *in vivo* by expressing dGRIP-red fluorescent protein (RFP) and Tubulin-GFP fusion proteins in muscles by using the UAS/Gal4 system (Brand and Perrimon, 1993). The specificity of the RFP label to dGRIP was confirmed with anti-dGRIP immunoreactivity (data not shown). Dissected larvae were imaged by time-lapse confocal microscopy. Large Lva-dGRIP-RFP spots were juxtaposed to microtubules and appeared to be stationary. In contrast, many of the smaller Lva-negative dGRIP-RFP puncta, which were also juxtaposed to microtubules, were motile (see Movie 1 (PNAS website) and Supplemental Figure 3-1).

Abnormal Synapse Development in Larvae with Decreased dGRIP Levels. The role of dGRIP at the NMJ was investigated by generating mutants and dGRIP-RNAi (Kalidas and Smith, 2002). Two null *dgrip* alleles were available, $dgrip^{ex36}$ (Swan et al., 2004), and $dgrip^{B\text{-}LO1}$ (see Supplemental Figure 3-2G) generated here (Ryder et al., 2004), which deleted the entire *dgrip* genomic region. However, in both alleles, muscle patterning was abnormal ((Swan et al., 2004) and this report), making it difficult to discern which defects were solely of synaptic origin. Therefore, we used a dGRIP-RNAi construct fused to Gal4-binding sites (Fig. 3-1A), allowing us to temporally control dGRIP disruption and circumvent the early roles of dGRIP in muscle patterning when expressed in the postembryonic period. This construct decreased presynaptic dGRIP immunoreactivity by 30–50% when expressed with the presynaptic drivers C380

(Budnik et al., 1996) or elav-Gal4 (Fig. 3-2A–F) and by ~80% when expressed in muscles with the C57 driver (Budnik et al., 1996) (Fig. 3-2 G–I). Real-time PCR analysis further confirmed a specific decrease in *dgrip* mRNA levels in these RNAi lines (Supplemental Figure 3-2G). We also examined a *dgrip* hypomorph, *dgrip*^{f05600}, containing a P-element insertion in the first intron of the gene (Fig. 3-1A). In this mutant, dGRIP was localized in aggregations at extrasynaptic sites at the muscle surface and showed a reduction of dGRIP immunoreactivity at the NMJ, but muscle patterning was mostly normal (Supplemental Figure 3-2).

NMJs expressing the RNAi construct pre- or postsynaptically or from *dgrip*^{f05600} were abnormal in similar ways, having a marked decrease in the number of synaptic boutons (Fig. 3-2J). We also observed boutons with an atypical shape (Fig. 3-3 B, D, and F, arrows), which were clearly marked by the presynaptic marker anti-horseradish peroxidase (HRP), but were completely devoid of postsynaptic DLG immunoreactivity, suggesting that postsynaptic structure was abnormal (Figs. A-3 A–F and 8K). These boutons, which we named "ghost" boutons, had a rounded appearance, as opposed to the more elliptical appearance of Type I boutons. In addition, a thin neuronal process connecting the ghost bouton with a main NMJ branch could occasionally be discerned (Fig. 3-3D, arrowhead).

We examined the localization of several pre- and postsynaptic proteins in ghost boutons. None of the postsynaptic proteins examined, including glutamate receptors (GluRIIA and GluRIII) (Fig. 3-3 G–L, arrows), Scribble, Bazooka, DFz2, and Spectrin were present in ghost boutons, suggesting that the postsynaptic

apparatus was missing or severely defective in ghost boutons. Most ghost boutons were also devoid of active zones, as visualized with monoclonal antibody nc82 (Marrus et al., 2004; Wucherpfennig et al., 2003) (Fig. 3-3 J–L, arrows), although, rarely, a ghost bouton contained a few active zones (e.g., Fig. 3-3J, asterisk). In contrast, synaptic vesicle proteins, such as Synapsin (see Supplemental Figure 3-3) and CSP (data not shown) were present in ghost boutons. We also carried out an ultrastructural analysis of NMJs. We found that, in animals expressing dGRIP- RNAi in postsynaptic muscles, there was a population of synaptic boutons that were filled with synaptic vesicles but were devoid of active zones or postsynaptic specializations, including postsynaptic densities and subsynaptic reticulum (SSR) (Fig. 3-4).

The ultrastructural phenotype observed in dGRIP RNAi-post synapses was distinctly similar to the phenotype observed in *wg* mutations and in genetic manipulations that interfere with DFz2 in postsynaptic muscles (Mathew et al., 2005; Packard et al., 2002). In these mutants, which also have diminished synaptic boutons, a subset of boutons lacking active zones, postsynaptic densities, and SSR, yet containing synaptic vesicles, are observed. Therefore, we examined whether ghost boutons are formed when Wg signaling is disrupted specifically in the postsynaptic muscles by expressing a dominant-negative DFz2 transgene DFz2-C, consisting of just the cytoplasmic region of DFz2, in muscles. We found that, indeed, the number of ghost boutons was increased in DFz2-C-post NMJs, similar to $dgrip^{f05600}$ mutants and dGRIP-RNAi (Fig. 3-2K).

The similarity between these phenotypes pointed to a potential relationship between dGRIP and the Wg pathway at the NMJ. In this alternative transduction mechanism, synaptic DFz2 is endocytosed and transported to the nuclear area, where the C terminus of DFz2 is cleaved and imported into the nucleus (Mathew et al., 2005). To determine whether dGRIP was involved in this process, we examined larvae expressing dGRIP-RNAi in muscle cells, and we used antibodies to the C-terminal region of DFz2 (DFz2-C) to determine the presence of intranuclear DFz2-C spots. We found that the number of DFz2-C-positive nuclear spots was drastically reduced in muscles expressing dGRIP-RNAi (Fig. 3-5A–C).

We next tested whether DFz2 trafficking was altered in dGRIP-RNAi-post flies by using a DFz2 internalization assay that has been used to characterize DFz2 trafficking from synapses to the nucleus (Mathew et al., 2005). In this assay, body-wall muscles dissected in physiological saline are incubated in the cold with an antibody (DFz2-N) that labels the surface pool of DFz2. After the antibody-binding step, excess antibody is washed away, and preparations are shifted to room temperature and fixed at various times. DFz2–antibody complexes remaining at the surface are recognized by using an Alexa Fluor 647-conjugated secondary antibody applied under nonpermeabilizing conditions, and internalized DFz2–antibody complexes are subsequently labeled by a FITC-conjugated secondary antibody after permeabilization. As demonstrated in (Mathew et al., 2005), in wild type at 5 min after the antibody-binding step, internalized DFz2 accumulated around synaptic boutons (Fig. 3-5 D and F–H) but

was not observed at the perinuclear area (Fig. 3-5 E and R). At 60 min, however, internalized DFz2 decreased at the NMJ, and this decrease was accompanied by the presence of DFz2 vesicles at the perinuclear area (Fig. 3-5 D–E, I–K, and S–T, arrowheads). In larvae expressing dGRIP-RNAi postsynaptically, the amount of surface and internalized DFz2 was significantly greater than wild type (Fig. 3-5 D and L–N). In striking contrast to wild type, 60 min after the antibody-binding step, the level of DFz2 at the NMJ was still unchanged, remaining as high as at 5 min (Fig. 3-5 D and O–Q). Also, no DFz2 vesicles were observed at the perinuclear area at either 5 or 60 min (Fig. 3-5 E and U–W). These results provide evidence that severe reductions in dGRIP levels prevent the transport of DFz2 to the perinuclear area and suggest that dGRIP is required for a step in DFz2 trafficking to the nucleus.

DFz2 contains a PDZ-binding motif (ASHV) at the C-terminal tail and is localized around synapses in a pattern similar to that of dGRIP (Fig. 3-6A and B). To determine whether dGRIP was likely to be associated with internalized DFz2 receptors and/or with DFz2-containing endosomes, the above DFz2 internalization assay was performed by using larvae expressing dGRIP-RFP. We found that dGRIP and endocytosed DFz2 strongly colocalized at the bouton and peribouton areas (Fig. 3-6 C–E) and in many DFz2-containing internalized vesicles in the muscle (Fig. 3-6 C'–E'). Thus, internalized DFz2 is present in a subset of dGRIP vesicles, and dGRIP is required to traffic DFz2 to the nucleus.

We also tested the possibility that DFz2 and dGRIP may interact using *Drosophila* Schneider (S2) cells transfected with Myc-DFz2 and V5-dGRIP. We

found that antibodies to Myc (DFz2) immunoprecipitated V5 (dGRIP), suggesting that, indeed, DFz2 and dGRIP can interact (Fig. 3-6F). To determine the likely regions for such an interaction, S2 cells were cotransfected with Myc-DFz2, and either the deletion constructs V5-PDZ1,2,3, V5-PDZ4,5, and V5-PDZ6,7 or full-length V5-dGRIP were cotransfected. As above, anti-Myc antibodies immunoprecipitated full-length V5-dGRIP, but also V5-PDZ4,5 alone (Fig. 3-6G). In contrast, very weak immunoprecipitation of V5-PDZ1,2,3 or V5-PDZ6,7 was observed, suggesting that the interaction is very likely through PDZ4 and -5. The specific interaction between PDZ4 and -5 of dGRIP and the C-terminal region of DFz2 was confirmed by using the yeast two-hybrid assay. This interaction was quite specific for the PDZ4 and -5 domains, because the DFz2 C-terminal did not show any interaction with any of the 3 PDZ domains of DLG or with the 4 PDZ domains of Scribble with the yeast two-hybrid assay (data not shown). Together, the colocalization of internalized DFz2 and dGRIP at the NMJ, the similarity of the phenotypes at synaptic boutons when either protein is decreased or eliminated, and the interactions between these proteins observed by immunoprecipitations and the yeast two-hybrid assay suggest that both proteins may function in the same synaptic development pathway.

DISCUSSION

At the NMJ, the Wg pathway is initiated by the secretion of Wg from the presynaptic cells and its binding to DFz2 receptors present at the postsynaptic muscle cells (Packard et al., 2002). Upon Wg binding to DFz2, the receptor is

internalized and transported to the perinuclear area, where it is cleaved, and the C-terminal DFz2 fragment (DFz2-C) is imported into the nucleus (Mathew et al., 2005). Although the evidence suggested that endocytosis at the postsynaptic membrane and transport via microtubules are required for DFz2 trafficking from synapses to the muscle nucleus, the exact molecular mechanisms of trafficking were unknown. In this study, we provide evidence that the transport of DFz2 to the nucleus depends on interactions between a PDZ-binding motif at the C terminus of DFz2 and PDZ domains of dGRIP. We show that, in postsynaptic muscles, dGRIP is present in Golgi bodies and in a subset of vesicles that is highly concentrated at the postsynaptic area. These vesicles move along microtubules and colocalize with internalized DFz2. We also show that DFz2 and dGRIP can directly interact when expressed in heterologous systems. Manipulations that lead to severe reduction of dGRIP mimic all of the synaptic phenotypes resulting from mutations in *wg* or *dfz2*. Furthermore, in these *dgrip* mutants, internalized DFz2 accumulates at the postsynaptic region and is not transported to the nucleus. We suggest that dGRIP is required at synapses to mediate the trafficking of DFz2 to the nucleus to properly regulate the expansion of the NMJ during muscle growth.

Synaptic Functions of GRIP in Mammals and Flies.

Studies suggest that GRIP is involved in the clustering and trafficking of AMPA receptors at mammalian synapses (Dong et al., 1997; Liu and Cull-Candy, 2005; Setou et al., 2002; Wyszynski et al., 2002). GRIP has also been found to interact

with Ephrin ligands and Eph receptors (Contractor et al., 2002; Hoogenraad et al., 2005), neuronal RAS guanine nucleotide exchange factor (GRASP1) (Ye et al., 2000), members of the Liprin-α/syd2 family of proteins (Wyszynski et al., 2002), the KIF5 microtubule motor kinesin (Setou et al., 2002), and extracellular matrix protein FRAS1 (Takamiya et al., 2004). This large number of partners identified is perhaps not surprising, given that GRIP contains at least seven modular protein-interaction domains.

Studies have shown that, similar to dGRIP, rat GRIP is also localized to both presynaptic axons and postsynaptic dendritic structures and is enriched in vesicular profiles that closely associate with microtubules (Dong et al., 1999; Wyszynski et al., 1999). Furthermore, a recent study shows that knockdown of GRIP-1 using siRNA in primary hippocampal neurons interfered with the formation and growth of dendrites in developing neurons and the maintenance of dendrites in mature neurons (Hoogenraad et al., 2005). In this study, we similarly found that interfering with GRIP function hampered synaptic bouton formation and growth in larval glutamatergic synapses. Additionally, elimination of postsynaptic dGRIP led to loss of the postsynaptic apparatus and presynaptic active zones and, presumably, to either the retraction or deficient stabilization of new synaptic boutons (see below). These results imply that GRIP family proteins have a conserved role in both the formation and the stabilization of synapses in the nervous system.

In *Drosophila*, dGRIP is involved in the guidance of embryonic muscle precursors to establish the proper body-wall muscle pattern (Swan et al., 2004),

whereas here, we show that dGRIP is required for synapse differentiation. These results are not surprising, given the recurrent theme that many molecules necessary for early pattern formation in the embryo, such as members of the TGF-β pathway, the Wg pathway, and the tumor suppressor proteins DLG and Scribble (Scrib) are used again during synapse development (Packard et al., 2003).

Involvement of dGRIP in DFz2 Trafficking During Synapse Development. Evidence that dGRIP and DFz2 might interact arises from the observation that manipulations that lead to alterations in both proteins give rise to remarkably similar phenotypes, including decreased NMJ expansion and the presence of ghost boutons, which lack all postsynaptic proteins studied and the subsynaptic reticulum, and are devoid of active zones but filled with synaptic vesicles. These ghost boutons may represent boutons that initiated their differentiation presynaptically but never fully matured by forming corresponding pre- and postsynaptic specializations. Alternatively, the ghost boutons may represent boutons that are initially formed (including differentiation of both pre- and postsynaptic specializations) but subsequently retracted. However, studies have suggested that retraction of mature boutons at the *Drosophila* NMJ is accompanied by the presence of "synaptic footprints," in which postsynaptic proteins are still present, despite the absence of a presynaptic bouton (Eaton et al., 2002). In our mutants, we observe the opposite phenotype, where synapses have some presynaptic proteins but are devoid of a postsynaptic apparatus.

Interestingly, synaptic footprints are observed when the retrograde signaling mediated by TGF-β is disrupted (Eaton and Davis, 2005). In contrast, ghost boutons are observed when the Wg pathway is abnormal. The Wg pathway at the NMJ has been shown to function in an anterograde manner, but the possibility that it also functions in a retrograde manner has not been studied. These findings suggest that, at the *Drosophila* NMJ, synapse retraction can be induced both pre- and postsynaptically, as in the vertebrate NMJ (Balice-Gordon et al., 1993; Colman et al., 1997; Walsh and Lichtman, 2003). It would be interesting to determine whether anterograde Wg and retrograde TGF-β signaling pathways crosstalk and coordinate synapse stability during development. Taken together, our studies suggest that one function of dGRIP at the NMJ is in trafficking DFz2 to the nucleus, which, in turn, regulates synaptic growth.

MATERIALS AND METHODS

Flies. Flies were reared in standard *Drosophila* medium. The following fly stocks were used: the wild-type strain Canton-S (CS), $dgrip^{B\text{-}L01}$, $dgrip^{f05600}$ (Exelixis, Harvard Medical School, Boston), UAS-Tubulin-GFP (Grieder et al., 2000), UAS-6xMyc-DFz2-C (Mathew et al., 2005), and the Gal4 strains BG487, C57, C380, and C164 (Budnik et al., 1996; Torroja et al., 1999). We also generated the following UAS strains: UAS-dGRIP (ORF of RE14068), UAS-dGRIP-RFP, and UAS-dGRIP-RNAi. The $dgrip^{B\text{-}LO1}$ was generated (Ryder et al., 2004) by using the CB-5266-3 and 5-SZ-3429 FRT insertions (Szeged Stock Centre, Szeged, Hungary) located 401 bp upstream of the *dgrip* 5' UTR and 2,083 bp downstream

of the *dgrip* 3' UTR, respectively. To maximize the expression of transgenes by using the UAS/Gal4 system, mutant and control larvae were reared at 29C°.

Antibodies and immunocytochemistry. Drosophila third-instar larvae were dissected and processed as in (Budnik et al., 1996). Antibody conditions, morphometric analysis, internalization assay, yeast two-hybrid assay, real-time PCR, and constructs used are described in *Supporting Materials and Methods*. Electron microscopy was performed as in (Packard et al., 2002). S2 cell transfection and immunoprecipitations from S2 cells were carried out as in (Ashley et al., 2005).

Antibodies and Immunocytochemistry. FITC- or Texas red-conjugated anti-horseradish peroxidase (HRP) (1:200; Sigma), anti-DLG (1:10,000) (Koh et al., 1999), anti-Futsch (22C10) and anti-Spectrin (1:100 and 1:50, respectively; Developmental Studies Hybridoma Bank, Iowa City, IA), anti-Lva (1:2,000; gift of J. Sisson, University of Texas, Austin) (Sisson et al., 2000), anti-GFP (1:200; Molecular Probes), anti-Tubulin (1:1,000; Sigma), anti-V5 (1:3,000; Invitrogen), anti-Myc (1:1,000; Roche), anti-nc82 (1:100; gift of A. Hofbauer, University of Regensburg, Regensburg, Germany), anti-GluRIII (1:2,000; gift of A. Diantonio, Washington University School of Medicine, St. Louis) (Marrus et al., 2004), anti-DFz2-N and anti-DFz2-C (1:100) (Marrus et al., 2004), anti-dCSP ab49 (1:100; gift of K. E. Zinsmaier, University of Arizona, Tucson), and anti-OSA (1:100; gift of M. Buszcak, Carnegie Institution of Washington, Baltimore) (Collins et al.,

1999). Secondary antibodies (Jackson ImmunoResearch) were used at 1:200. Two anti-dGRIP antibodies (used at 1:300) were made by immunizing rats and rabbits with bacterially produced affinity-purified proteins (either dGRIP N-terminal amino acids 1–82 or C-terminal amino acids 906–1058) generated by using the pET system (Novagen).

Morphological Analysis. Muscles 6 and 7 from abdominal segment 3 were analyzed for synaptic bouton numbers. No changes in muscle size were observed in any of the genotypes analyzed. Comparisons between genotypes were performed in samples processed simultaneously and by using the same confocal acquisition parameters with a Zeiss LSM confocal microscope and PASCAL 3.0 software. Student *t* tests were performed to assess significance levels. Numbers in histograms represent mean ± SEM.

In Vivo Time-Lapse Imaging. Live images were acquired on a Zeiss Pascal Confocal microscope using a water immersion ×25 (0.8 N.A.) objective. The sequential images were collected at 3-second intervals over a 5-minute period. The preparation was a standard larval dissection of a third instar that was bathed in a solution of HL-6 saline (Macleod et al., 2002) containing 0.1 mM Ca^{+2}.

Internalization Assay. The internalization assay was performed as described in (Mathew et al., 2005). Briefly, samples were dissected in 0.1 mM Ca^{+2} saline and anti-DFz2-N added before incubation for 2 h at 4C°. Samples were then washed

to remove unbound antibody and shifted to room temperature for 5 or 60 min, fixed and labeled with Alexa Fluor 647-conjugated secondary antibody under nonpermeabilization conditions to label external DFz2. Samples were then permeabilized and labeled with FITC-conjugated secondary antibody to label internalized DFz2.

Quantification of Images. Changes in dGRIP fluorescence-intensity levels were calculated as follows: for presynaptic boutons, signal intensity was measured by using the PASCAL software in a 2-m m^2 area at the center of the bouton, in a slice going through the middle of the bouton. Measurements of postsynaptic intensity were performed in a 20-mm^2 area of the muscle surface. Nuclear DFz2 immunoreactivity was evaluated by counting the average number of distinct DFz2-immunoreactive spots per nucleus at muscles 6 and 7 (segments 3 and 4), in preparations double-stained with anti-Tubulin and anti-DFz2-C (4). Quantification of DFz2-N signal intensity at synapses and the perinuclear area in the internalization assay was performed as described in (Mathew et al., 2005).

S2 Cell Cultures, Biochemistry, and Yeast Two-Hybrid Assay. Drosophila Schneider (S2) cells were cultured and transfected as (Ashley et al., 2005). Full-length dGRIP cDNA, PDZ1-2-3 (amino acids 1–430), PDZ4-5 (amino acids 431–747) and PDZ6-7 (amino acids 748–1058) were cloned into the pAcV5.1/HisA or -B vector (Invitrogen) with V5 tags for S2 cell transfections. Immunoprecipitations from S2 cell extracts were carried out as (Ashley et al., 2005). Yeast two-hybrid

interaction assay was carried out as described (Tejedor et al., 1997). A C-terminal Dfz2 construct (amino acids 610–698) was cloned into pB42AD, and dGRIP constructs described above were cloned into pLexA. The individual PDZ domains of DLG and Scrib were also cloned into pLexA and tested against Dfz2C-pB42AD.

Quantitative Real-Time PCR. The expression levels of *dgrip* mRNA in pre-dGRIP-RNAi (with OK6-Gal4 driver), post-dGRIP-RNAi (with MHC-Gal4driver), and *dgrip*-null alleles were determined. Total RNA was extracted (RNeasy mini kit; Qiagen, Valencia, CA) from 20 male larvae of each genotype as well as their corresponding controls (OK6/w^1, MHC/w^1, and w^1). Random hexamer-primed cDNA was synthesized (Omniscript), and relative amounts of *dgrip* message in *dgrip* alleles and the control cDNAs were quantified by QuantiTect SYBR green PCR kit (Qiagen) using the dGRIP PDZ 7-specific primers forward: 5'-TCATCAACAGGATTCGCAGC-3' and reverse: 5'TCAGTAGGCCGCACATATCG-3'. Quantitative real-time PCR was performed in GeneAmp 5700 Sequence Detection System (PerkinElmer Applied Biosystems). Obtained values were calibrated against the total cDNA levels measured by RT-PCR primers 5'-AAGCCCGTGCCCGTATTATG-3' and 5'-AAGTCATCCGTGGATCGGGAC-3' for tbp-1 (TaT-binding protein-1), a housekeeping gene. Transcript levels are normalized to the level of control transcript detected.

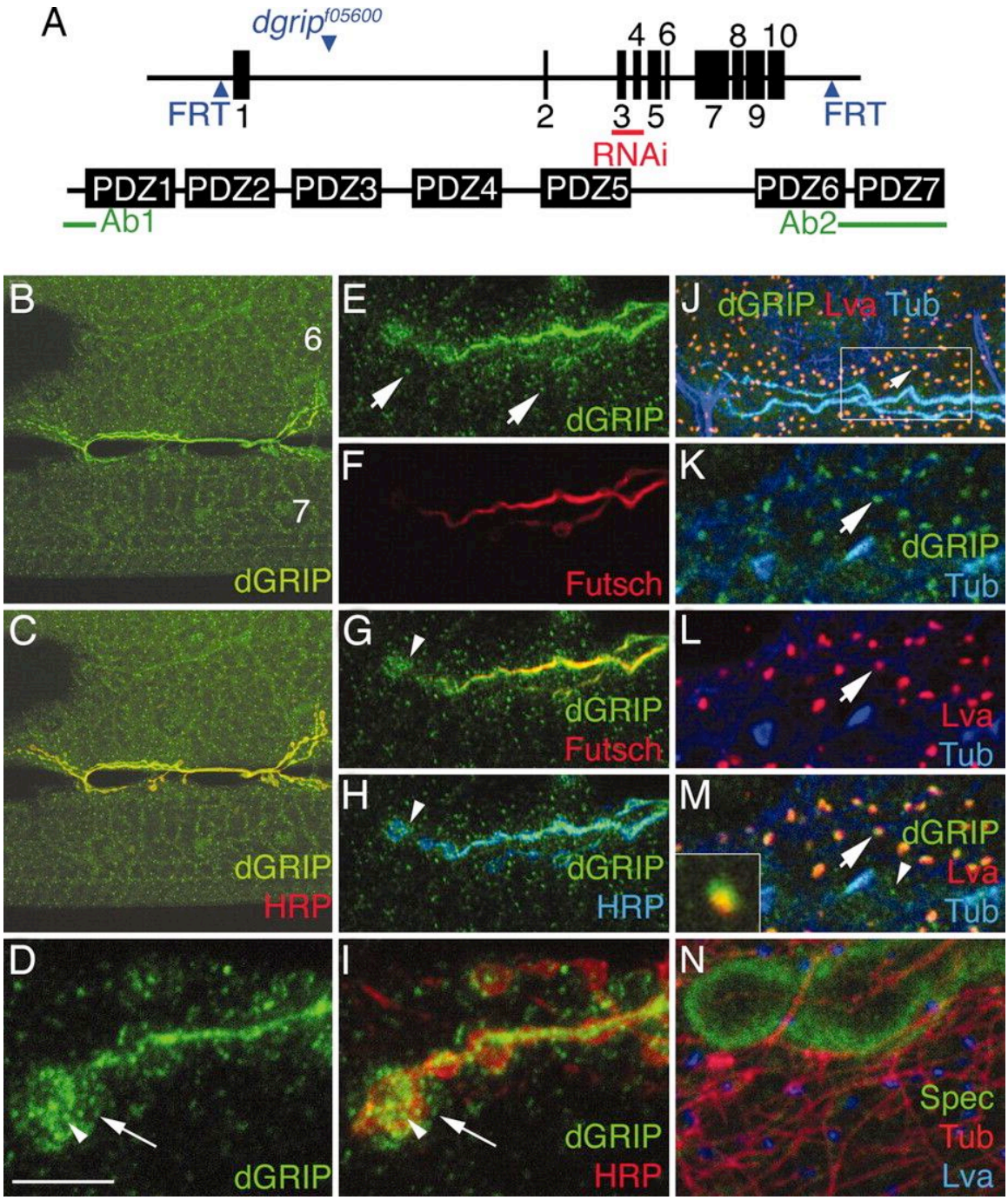
A
dgrip f05600
4 6
8 10
FRT 1
2
3 5
7 9
FRT
RNAi
PDZ1 PDZ2 PDZ3 PDZ4 PDZ5 PDZ6 PDZ7
Ab1
Ab2
B
6
7
dGRIP
E
dGRIP
J
dGRIP Lva Tub
F
Futsch
K
dGRIP
Tub
C
dGRIP
HRP
G
dGRIP
Futsch
L
Lva
Tub
H
dGRIP
HRP
M
dGRIP
Lva
Tub
D
dGRIP
I
dGRIP
HRP
N
Spec
Tub
Lva

Figure 3-1

Figure 3-1. Localization of dGRIP at the NMJ. (A) Genomic structure of dgrip showing exons 1–10. Blue, localization of dgripf05600 and the 2 FRT insertions used to generate the null allele; red, region targeted by dGRIP-RNAi (Upper). Protein structure of dGRIP and organization of PDZ domains (Lower).Green, regions used to generate dGRIP antibodies. (B–D and I) dGRIP immunoreactivity at the NMJ and muscles in a preparation stained with antibodies against dGRIP (green) and HRP (red) shown at low (B and C) and high (D and I) magnification in muscles 6 and 7. Arrowheads, punctate dGRIP immunoreactivity at presynaptic boutons; arrows, punctate dGRIP at the postsynaptic muscle area. (E–H) Localization of dGRIP at the presynaptic microtubule bundle, shown in a preparation labeled with antibodies against dGRIP (green), Futsch (red), and HRP (blue). Arrows, large dGRIP muscle spots; arrowhead, punctate dGRIP immunoreactivity at the peribouton area. (J–M) Localization of large dGRIP spots to Golgi bodies shown at low (J) and high (K–M) magnification in a preparation stained with antibodies against dGRIP (green), Tubulin (blue), and Lva (red). Arrow, Lva-positive dGRIP spot; arrowheads, Lva-negative dGRIP puncta. (M Inset) High-magnification view of a GRIP-Lva spot. (N) Association of Lva-positive spots with microtubules shown in a preparation labeled with Lva (blue), Tubulin (red), and Spectrin (green). All are single confocal slices, except for B, C, and J, which are a Z-series projection. [Scale bar, 70 μm (B and C), 17 μm (E–H), 13 μm (J), 8 μm (D, I, and K–N), and 2.5 μm (M Inset).]

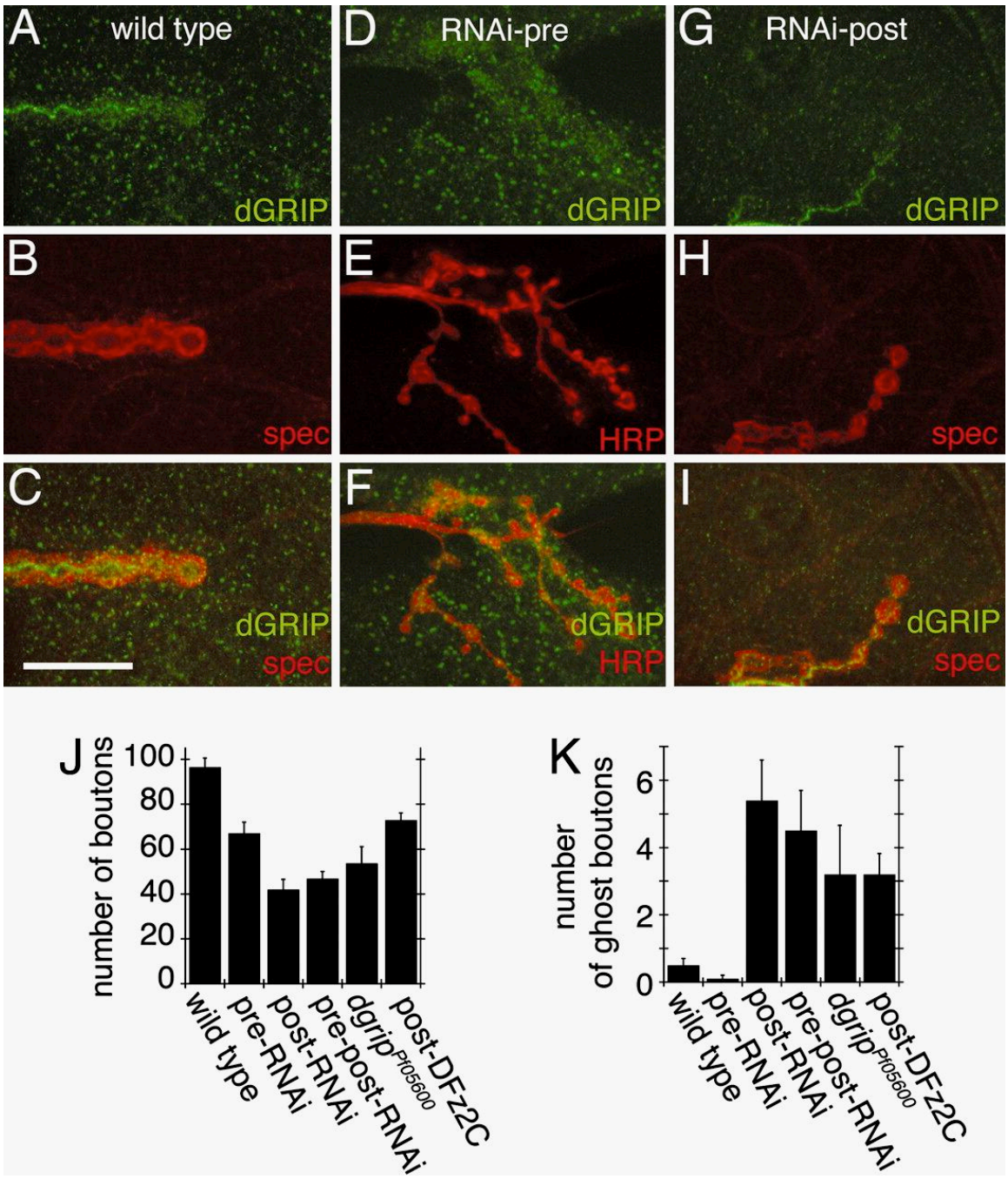
A
wild type
dGRIP
D
RNAi-pre
dGRIP
G
RNAi-post
dGRIP
B
spec
E
HRP
H
spec
C
dGRIP
spec
F
dGRIP
HRP
I
dGRIP
spec
J
number of boutons
100
80
60
40
20
0
wild type
pre-RNAi
post-RNAi
pre-post-RNAi
dgrip^PI05600
post-DFz2C
K
number of ghost boutons
6
4
2
0
wild type
pre-RNAi
post-RNAi
pre-post-RNAi
dgrip^PI05600
post-DFz2C

Figure 3-2

Figure 3-2. dGRIP immunoreactivity and quantification of NMJ morphology in larvae expressing dGRIP-RNAi. (A–I) dGRIP immunoreactivity at the NMJ in preparations labeled with antibodies against dGRIP (green) and Spectrin (red) (A–C and G–I) or dGRIP (green) and HRP (red) (D–F), in wild-type larvae (A–C) and larvae expressing dGRIP-RNAi in motor neurons (D–F) or muscles (G–I). (J and K) Number of synaptic (J) and ghost (K) boutons at muscles 6 and 7 (A3) in third-instar larvae of various genotypes. (Scale bar, 13 μm.)

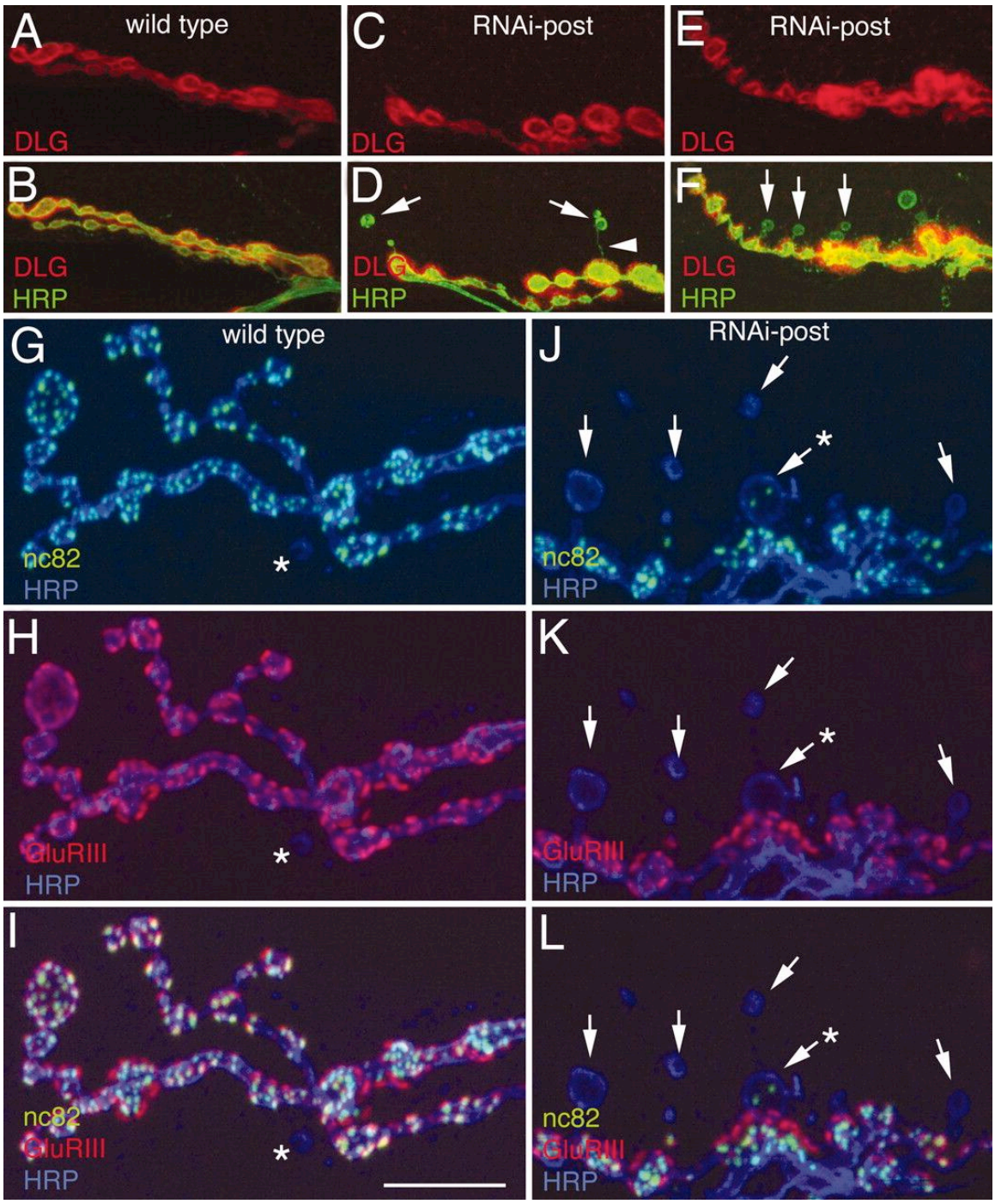
A
wild type
DLG
C
RNAi-post
DLG
E
RNAi-post
DLG
B
DLG
HRP
D
DLG
HRP
F
DLG
HRP
G
wild type
nc82
HRP
J
RNAi-post
nc82
HRP
H
GluRIII
HRP
K
GluRIII
HRP
I
nc82
GluRIII
HRP
L
nc82
GluRIII
HRP

Figure 3-3

Figure 3-3. Ghost boutons lack postsynaptic proteins and most active zones. (A–L) Third instar NMJs in wild-type larvae (A, B, and G–I) and in larvae expressing dGRIP-RNAi postsynaptically (C–F and J–L) in preparations labeled with anti-HRP (green) and anti-DLG (red) (A–F), and anti-HRP (blue), anti-GluRIII (red), and nc82 (green) (G–L). Arrows, ghost boutons; asterisks in G–I, uncommon ghost bouton observed in wild type; arrowhead, HRP-labeled process connecting a ghost bouton with the main arbor; asterisks in J–L, ghost bouton containing nc82 immunoreactivity. [Scale bar, 15 μm (A–F) and 12 μm (G–L).]

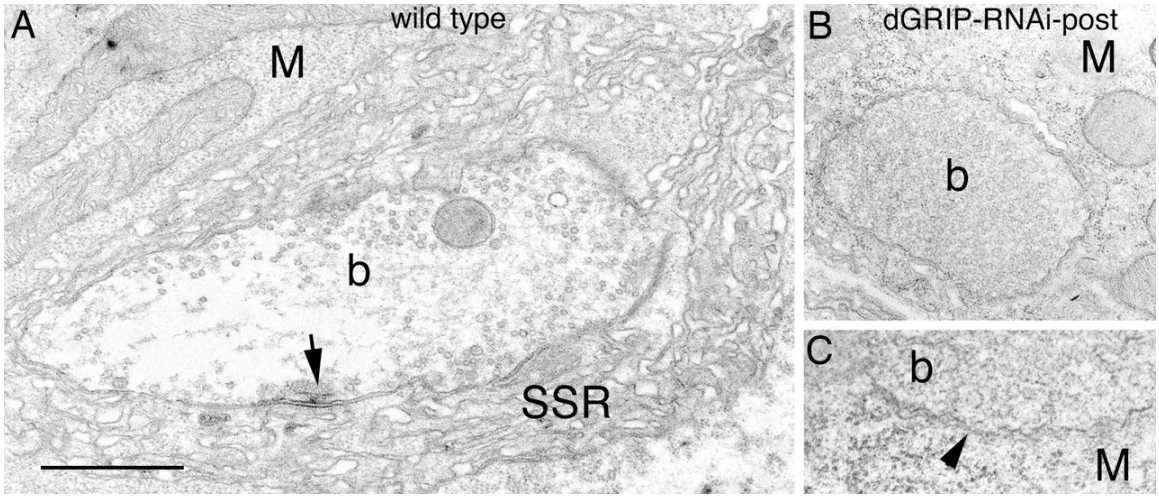

Figure 3-4

Figure 3-4. Disrupted synaptic structure in larvae expressing dGRIP-RNAi-post. Crosssection through a type I bouton in wild type (A), and a ghost bouton lacking active zones and SSR (B and C) dGRIP-RNAi-post; arrow, active zone. (C) High-magnification view of a ghost bouton membrane (arrowhead), showing its abnormal ruffled appearance. M, muscle; b, bouton. [Scale bar, 1.2 μm (A and B) and 0.3 μm (C).]

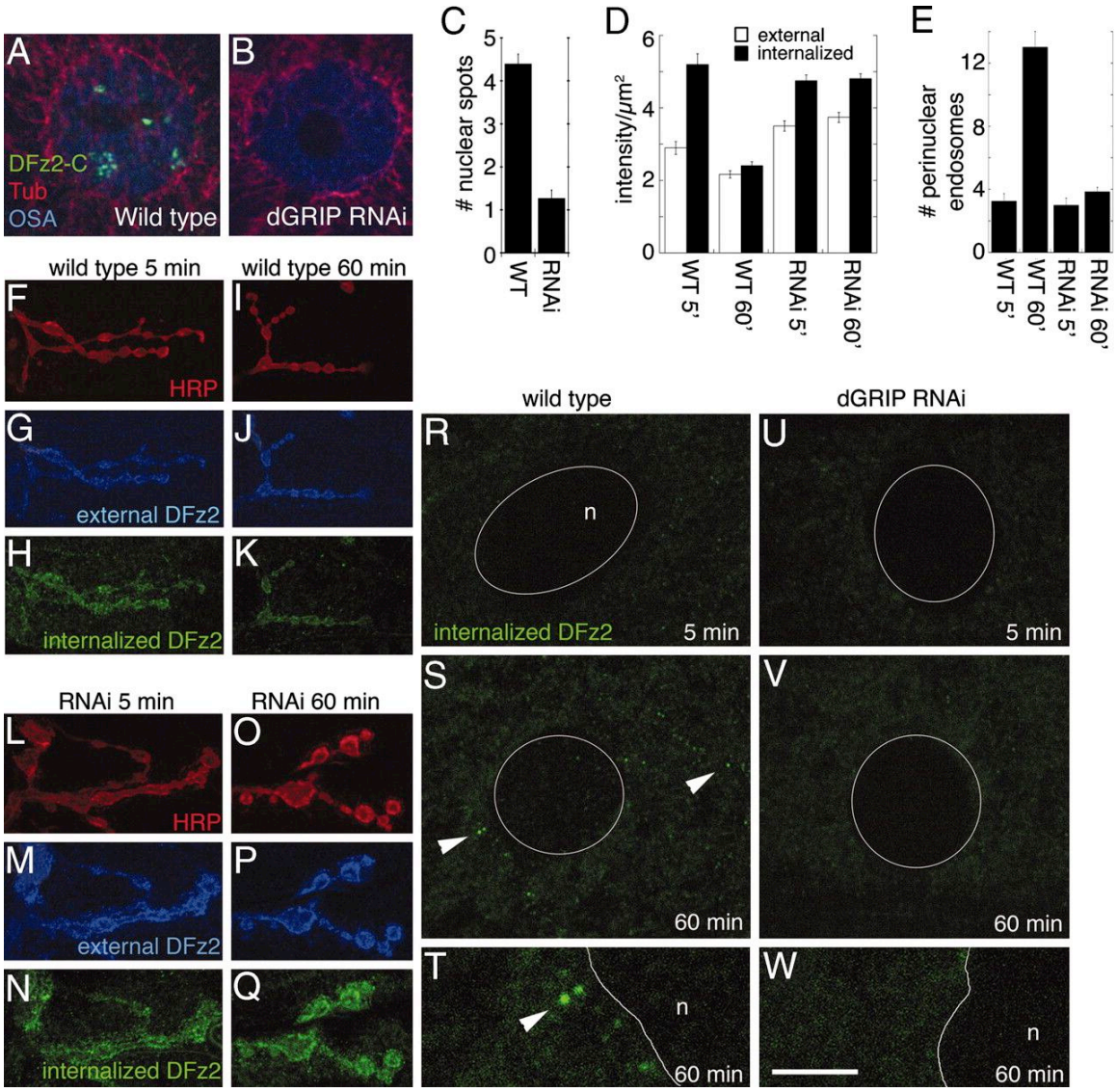
A
DFz2-C
Tub
OSA
Wild type
B
dGRIP RNAi
C
nuclear spots
WT
RNAi
D
external
internalized
intensity/μm²
WT 5'
WT 60'
RNAi 5'
RNAi 60'
E
perinuclear endosomes
WT 5'
WT 60'
RNAi 5'
RNAi 60'
wild type 5 min
wild type 60 min
F
HRP
I
G
external DFz2
J
H
internalized DFz2
K
RNAi 5 min
RNAi 60 min
L
HRP
O
M
external DFz2
P
N
internalized DFz2
Q
wild type
dGRIP RNAi
R
n
internalized DFz2
5 min
U
5 min
S
60 min
V
60 min
T
n
60 min
W
n
60 min

Figure 3-5

Figure 3-5. Abnormal trafficking of DFz2-C from the synapse to the nucleus in larvae expressing dGRIP-RNAi-post. (A and B) Muscle nucleus in wild type (A) and in a dGRIP-RNAi-post larva (B) in preparations stained with antibodies against DFz2-C (green), Tubulin (red), and OSA (blue). (C) Number of DFz2-C immunoreactive nuclear spots. (D) External and internalized DFz2 signal intensity at the NMJ. (E) Number of DFz2-N-positive perinuclear vesicles in the internalization assay. (F–Q) External (blue) and internalized (green) DFz2 at the NMJ of wild type (F–K) and dGRIP-RNAi post (L–Q), at 5 (F–H and L–N) and 60 (I–K and O–Q) min after the antibody-binding step in the internalization assay. NMJs are visualized by the anti-HRP staining (red). (R–W) Internalized DFz2 (green) at the perinuclear area in wild-type (R–T), and dGRIP-RNAi-post (U–W) larvae, at 5 (R and U) and 60 (S, T, V, and W) min after the antibody-binding step. (T and W) Highmagnification views of a region in S and V. Arrowheads, internalized DFz2 vesicles at the perinuclear area. n, nucleus. [Scale bar, 10 μm (A and B), 20 μm (F–Q), 12 μm (R–V), and 3 μm (T and W).]

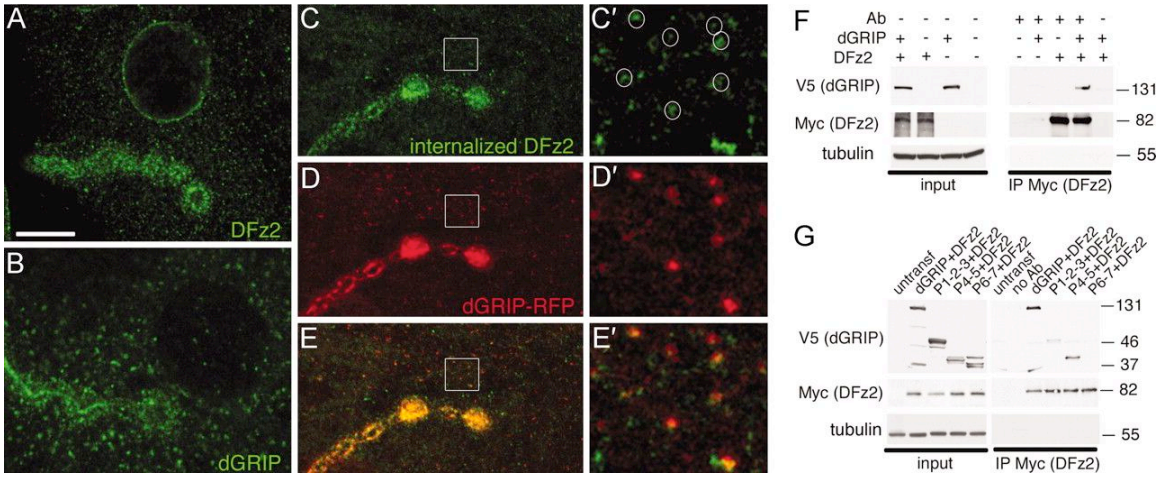
A
DFz2
B
dGRIP
C
internalized DFz2
C′
D
dGRIP-RFP
D′
E
E′
F
Ab
dGRIP
DFz2
V5 (dGRIP)
Myc (DFz2)
tubulin
131
82
55
input
IP Myc (DFz2)
G
untransf
dGRIP+DFz2
P1-2-3+DFz2
P4-5+DFz2
P6-7+DFz2
no Ab
V5 (dGRIP)
Myc (DFz2)
tubulin
131
46
37
82
55
input
IP Myc (DFz2)

Figure 3-6

Figure 3-6. Colocalization of internalized DFz2 with dGRIP and interactions between dGRIP and DFz2. (A and B) Localization of DFz2 (A) and dGRIP (B) at the NMJ. (C–E) Colocalization between dGRIP-RFP (red) and internalized DFz2 (green) at the NMJ. (C'–E') High-magnification views of the regions enclosed by squares in C–E. (F) Coimmunoprecipitation of V5 (dGRIP) by anti-Myc (DFz2) in S2 cells. (G) Coimmunoprecipitation of dGRIP deletion constructs. Input lanes in F and G correspond to 10% of the initial extract. Molecular masses are shown in kDa. [Scale bar, 10 μm (A–E) and 2 μm (C'–E').]

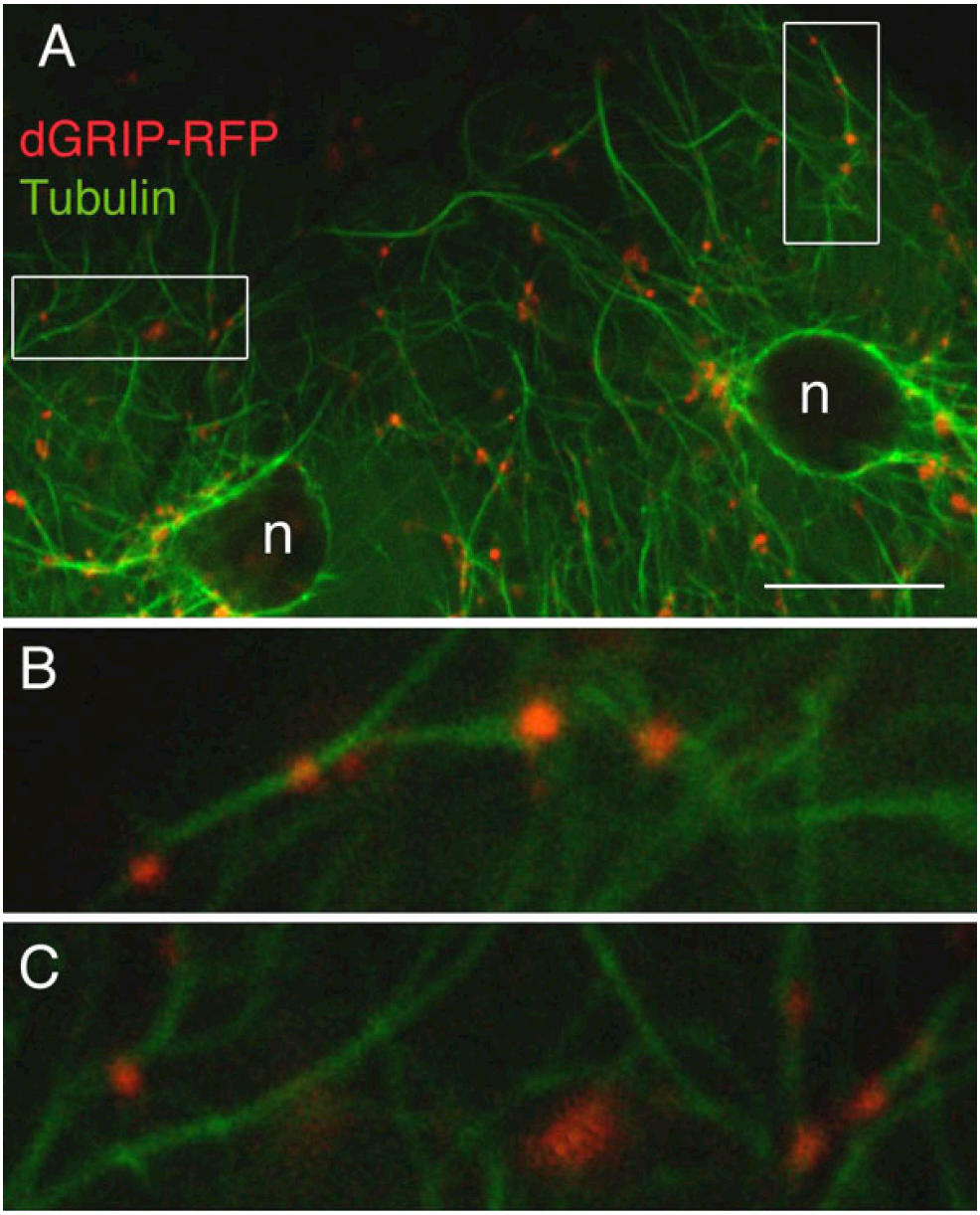

Supplemental Figure 3-1

Supplemental Figure 3-1. dGRIP-RFP in postsynaptic muscle cells associates with microtubules. Live image of a larval body-wall muscle preparation expressing dGRIP-RFP (red), and Tubulin-GFP (green). (A) Low-magnification image from muscle 6 of segment A3. (B and C) High-magnification of Insets in A. n, muscle nucleus. [Scale bar, 16 μm (A) and 5 μm (B and C.)]

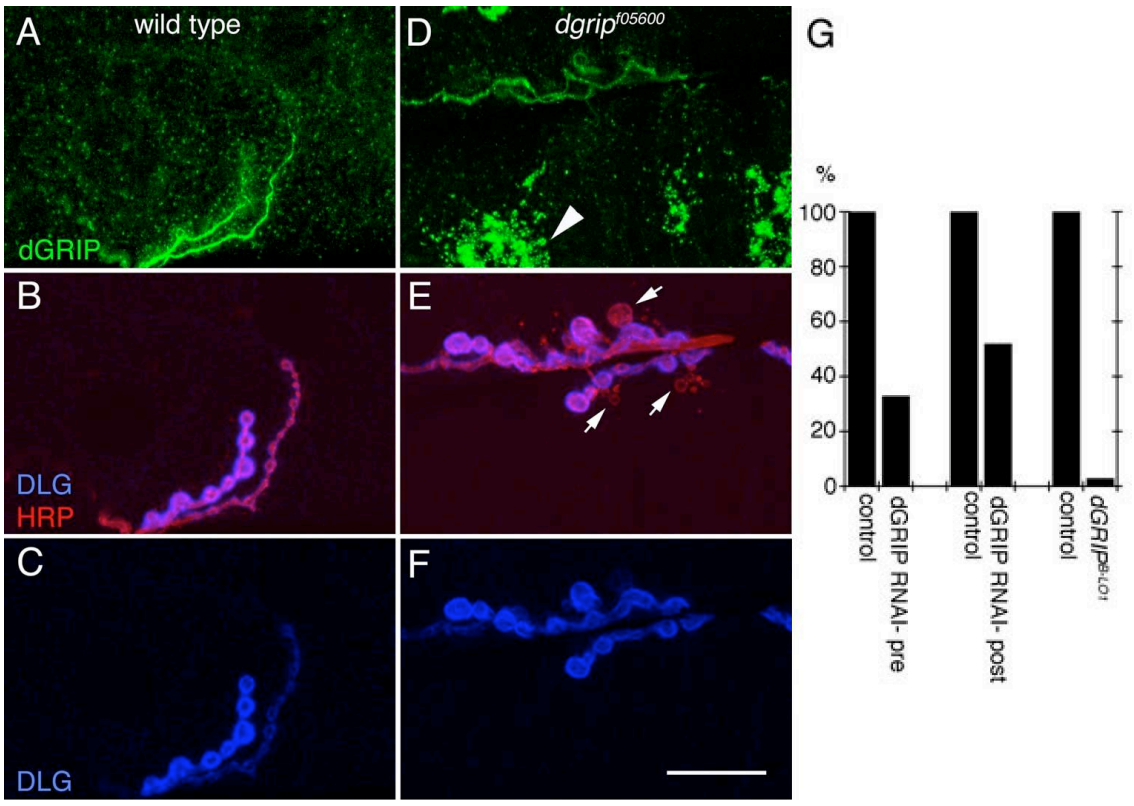

Supplemental Figure 3-2

Supplemental Figure 3-2. Reduction of synaptic dGRIP immunoreactivity and presence of ghost boutons in *dgrip*^{f05600} mutants. Neuromuscular junctions (NMJs) at muscles 6 and 7 in wild-type (A–C) and dgripf05600 (D–F) preparations labeled with antibodies against dGRIP (green), DLG (blue), and HRP (red). Arrowhead in D points to extrasynaptic dGRIP aggregations in dgripf05600. Arrows in E point to ghost boutons. (G) Real-time PCR analysis in dGRIP-RNA interference (RNAi)-pre (with OK6-Gal4) and -post (with MHC-Gal4) as well as dgripB-LO1 alleles demonstrates significant reduction of dgrip mRNA levels. (Scale bar, 16 μm.)

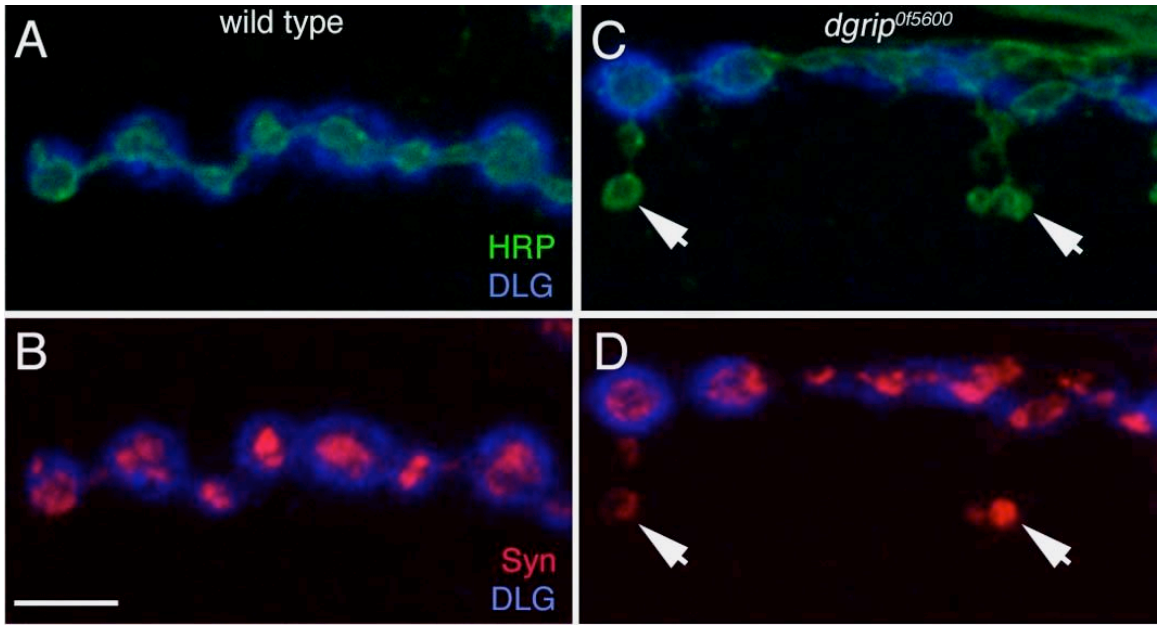

Supplemental Figure 3-3

Supplemental Figure 3-3. Synaptic vesicle-associated protein Synapsin is present in ghost boutons. NMJs at muscles 6 and 7 in a wild-type (A and B) and a dgripf05600 (C and D) preparation triple-labeled with antibodies against HRP (green), DLG (blue), and Synapsin (red). Arrows in C and D point to ghost boutons. (Scale bar, 5 μm.)

CHAPTER 4

Rapid Activity-Dependent Modifications in Synaptic Structure and Function Require Bidirectional Wnt Signaling

The following work is the original manuscript accepted to Neuron on January 25, 2008 and is currently in press. Author list is:

Bulent Ataman, James Ashley, Michael Gorczyca, Preethi Ramachandran, Wernher Fouquet , Stephan J. Sigrist, and Vivian Budnik.

SUMMARY

Activity-dependent modifications in synapse structure play a key role in synaptic development and plasticity, but the signaling mechanisms involved are poorly understood. We demonstrate that glutamatergic *Drosophila* neuromuscular junctions undergo rapid changes in synaptic structure and function in response to patterned stimulation. These changes, which depend on transcription and translation, include formation of motile presynaptic filopodia, elaboration of undifferentiated varicosities, and potentiation of spontaneous release frequency. Experiments indicate that a bidirectional Wnt/Wg signaling pathway underlies these changes. Evoked activity induces Wnt1/Wg release from synaptic boutons, which stimulates both a postsynaptic DFz2 nuclear import pathway, as well as a presynaptic pathway involving GSK-3ß/Shaggy. Our findings suggest that bidirectional Wg signaling operates downstream of synaptic activity to induce modifications in synaptic structure and function. We propose that activation of the postsynaptic Wg pathway is required for the assembly of the postsynaptic apparatus, while activation of the presynaptic Wg pathway regulates cytoskeletal dynamics.

INTRODUCTION

Synaptic plasticity has been placed at the foundation of complex brain functions, such as learning and memory and the refinement of synaptic connections. In these processes, correlated changes in electrical activity lead to

long-term modifications in synaptic efficacy, which are often accompanied by structural changes in synapse shape and/or number (Chklovskii et al., 2004; Kandel, 2001). Although understanding the mechanisms for the induction of these changes has been the focus of intense efforts, many of the mechanisms downstream of activity remain unclear.

An important breakthrough has been the realization that many of the secreted molecules that play fundamental roles in pattern formation during early development function later in the nervous system to signal synapse development and plasticity. These include brain-derived neurotrophic factor (BDNF), Bone Morphogenetic Protein (BMP) and Wnts (Lu, 2003; Marques, 2005; Speese and Budnik, 2007). However, the extent of their participation and the cellular processes they initiate are for the most part unclear. Recent studies demonstrate that members of the Wingless (also known as Wg/Int (Wnt)) family of secreted signaling proteins are pivotal players during differentiation of synapses (Ciani and Salinas, 2005; Speese and Budnik, 2007), and misregulation of Wnt signaling is associated with a number of cognitive disorders such as schizophrenia and Alzheimer's (De Ferrari and Moon, 2006). However, a potential involvement of Wnts in activity-dependent changes at synapses is just beginning to be recognized (Chen et al., 2006; Wayman et al., 2006). A microarray analysis of dentate gyrus genes regulated by induction of long-term potentiation (LTP) led to the identification of several members of Wnt transduction pathways. Further, interfering with Wnt function reduced the magnitude of late LTP (Chen et al., 2006).

Both activity and the Wg pathway influence the development of synapses at the *Drosophila* larval neuromuscular junction (NMJ) (Budnik et al., 1990; Mosca et al., 2005; Packard et al., 2002; Schuster et al., 1996b). The larval NMJ is continuously forming and stabilizing new synapses in order to maintain synaptic efficacy as the postsynaptic muscle cells grow in size (Griffith and Budnik, 2006). NMJ expansion is stimulated by chronic intensification of both motorneuron activity and Wnt-1 (Wg) signaling (Budnik et al., 1990; Mosca et al., 2005; Packard et al., 2002). Mutations that decrease *wg* or the gene encoding its receptor, D-Frizzled-2 (DFz2), result in underdeveloped NMJs containing fewer synaptic boutons. A subset of these boutons remain undifferentiated, lacking active zones and postsynaptic specializations (Packard et al., 2002).

Current observations suggest that Wg might operate in a bidirectional manner, as DFz2 receptors are present in both pre- and postsynaptic compartments (Packard et al., 2002). In postsynaptic muscles, Wg secretion by presynaptic boutons activates an unconventional pathway, the Frizzled Nuclear Import (FNI) Wg pathway, in which the DFz2 receptor is endocytosed, cleaved, and the C-terminal fragment (DFz2C) is translocated into the nucleus (Ataman et al., 2006a; Mathew et al., 2005). The signal transduction pathway activated by Wg in the presynaptic compartment is less clear. Studies show that the Wnt/Wg family of proteins utilizes a divergent canonical pathway involving the regulation of the microtubule cytoskeleton through the action of glycogen synthase kinase 3ß (GSK-3ß/Shaggy (Sgg)) on microtubule-associated proteins (Ciani et al., 2004; Speese and Budnik, 2007). GSK-3ß is enriched at presynaptic boutons,

and mutations in *sgg* have a positive effect on bouton proliferation, consistent with Wg inhibition of GSK-3ß activity. Moreover, mutations in *wg* and *sgg* result in opposing defects in presynaptic microtubule cytoskeleton organization (Franco et al., 2004; Packard et al., 2002).

Here we establish that activity-dependent modifications in synapse structure at the larval NMJ are not simply the result of chronic changes in activity levels throughout development. Rather, rapid changes leading to the formation of new synaptic structures can be elicited by acute stimulation. These rapid structural changes depend on bidirectional Wg signaling and new protein synthesis. Our results support the notion that Wg is released from synaptic boutons in an activity-dependent manner, and that Wg functions downstream of activity to regulate synapse development and function. Thus, these studies establish a mechanistic link between acute activity changes and modifications in synaptic structure, and identify an important transduction cascade underlying these changes.

RESULTS

Activity induces rapid changes in synaptic structure

As in mammalian synapses, developmental changes in presynaptic activity have a substantial influence on the expansion of the *Drosophila* NMJ. Alterations that increase excitability throughout development result in enhanced proliferation of synaptic boutons, and this phenotype can be rescued by

mutations that lower excitability (Budnik et al., 1990; Mosca et al., 2005). The mechanisms by which enhanced presynaptic activity induce these morphological changes are still poorly understood. Moreover, it is unclear whether these changes arise as a result of long-term exposure to augmented activity during development, or whether acute activity is sufficient to regulate synaptic structure.

To address the latter question directly preparations expressing a membrane tethered GFP (mCD8-GFP) in motorneurons were imaged live before and after acute intervals of stimulation induced by high K^+ depolarization paradigms. Spaced depolarization, in a pattern similar to that required to induce morphological changes in dendritic spines in mammalian hippocampal cultures (Wu et al., 2001), was found to be most effective in inducing rapid changes. Two striking changes were observed after repetitive, spaced depolarizations, consisting of 4-5 high (90 mM) K^+-pulses spaced by 15 min of rest (Fig. 4-1B). First, after approximately 2 hr from the beginning of the stimulation paradigm numerous, short, filopodia-like structures began to extend and retract from the NMJ with a time course of minutes (Fig. 4-1A, D and Supplemental Movie 1). These filopodia were 0.5 to 5.5 μm long (average 2.44±0.15 μm; n=47), and remained at their maximal length from 4 sec to over 100 sec (average = 33.8±3.9 sec; n=33).

Many of these filopodia-like processes, which we termed synaptopods, appeared from the stretch of neurite between two boutons, but some also appeared to emerge from boutons themselves. Synaptopods could also be observed in unstimulated controls, or immediately after dissection, although their

frequency was significantly lower (Fig. 4-1C), and they were much shorter (1.12±0.13 μm; n=23) compared to those observed after stimulation (2.44±0.15 μm; n=47). Synaptopods were usually not preserved by fixation, limiting their study to live preparations.

We also observed the appearance of synaptic varicosities that were often large and quite rounded (Fig. 4-2A top row; arrows). Unlike synaptopods, we were able to preserve these varicosities by our fixation protocol (Fig. 4-2A bottom row). However, similar to synaptopods the thin process connecting them to the main arbor was most often destroyed by fixation. Our ability to fix the newly formed varicosities allowed us to determine their nature by using a number of synaptic markers. Notably, they were devoid of postsynaptic proteins, such as Discs-Large (DLG; Fig. 4-2A bottom right panel, B, C arrows) or glutamate receptors (GluRs; Fig. 4-2F left panel arrows), and they rarely contained active zone markers such as nc82/Brp (Kittel et al., 2006b) (Fig. 4-2F right panel). In contrast, they were labeled with synaptic vesicle markers such as Cysteine String Protein (CSP) (Zinsmaier et al., 1994) (Fig. 4-2D arrows) and Synapsin (not shown). These varicosities resembled a certain type of synaptic bouton previously referred to as a “ghost bouton” (Ataman et al., 2006a), which contains synaptic vesicles, but lacks active zones and postsynaptic structures. Ghost boutons have been shown to increase substantially in number upon genetically interfering with the Wg pathway at the NMJ, and in that case their appearance is accompanied by a dramatic decrease in normal bouton number (Ataman et al., 2006a; Packard et al., 2002). Here, upon spaced stimulation ghost boutons

formed *de novo*, and did not arise from retraction of existing boutons (Fig. 4-2A, E; Supplemental Figure 4-1A). Therefore, these ghost boutons likely represent an undifferentiated bouton state, as they lack both pre- and postsynaptic specializations. Indeed, ghost boutons are also observed in unstimulated wild type preparations, albeit at very low frequency (Ataman et al., 2006a). Thus, acute depolarization induces rapid changes in synaptic structure.

To determine if the formation of synaptopods represented a normal physiological process during NMJ growth, and whether ghost boutons developed into mature boutons, we imaged wild type unstimulated NMJs through the cuticle of intact early third instar larvae. NMJs were labeled by expressing mCD8-GFP or myristylated-mRFP (myr-mRFP) in motorneurons. In some experiments larvae also expressed either a postsynaptic GFP-tagged GluRIIA transgene driven by the endogenous promoter (Rasse et al., 2005), or a presynaptic GFP-tagged Brp transgene (Wagh et al., 2006). We observed several instances of motile synaptopods at these NMJs (Supplemental Movie 2), suggesting that they are a normal occurrence during NMJ development. In addition we observed the appearance of ghost boutons, which as expected, were labeled by presynaptic myr-mRFP but were virtually devoid of postsynaptic GluR clusters (Fig. 4-3A,C arrows) and Brp-positive active zones (Fig. 4-3 D, E arrows). To establish if ghost boutons eventually acquired GluR or Brp clusters, larvae were returned to the food, and the same NMJ imaged at 12-18 hr intervals until the beginning of pupariation. We found several instances in which ghost boutons acquired GluR (Fig. 4-3A, C arrows) or Brp (Fig. 4-3D, E) clusters *de novo*, and that the number

of GluR clusters increased over time (Fig. 4-3B). Therefore, ghost boutons are likely to represent an immature synaptic bouton state, which can differentiate into a mature bouton over prolonged periods.

We also determined some of the cellular and physiological requirements for enhanced ghost bouton formation. Dissected samples were stimulated with different depolarization paradigms and/or in the presence of specific pharmacological agents. A frequent appearance of synaptopods and ghost boutons required at least 4-5 cycles of spaced depolarization (Fig. 4-2E red arrows; Fig. 4-4A). Fewer cycles of spaced stimulation or pseudo-massed stimulation (same total stimulation period consisting of longer high K^+ depolarization times and fewer stimulation/rest cycles, (Fig. 4-1B; Fig. 4-4A) or eliminating Ca^{++} from the external solution (Fig. 4-4B) did not lead to an increase in ghost bouton formation.

The spaced stimulation dependency was reminiscent of the patterned training required for long-term plasticity in a variety of systems (Kogan et al., 1997; Mauelshagen et al., 1998; Wu et al., 2001; Yu et al., 2006), a process that depends on transcription and new protein synthesis. As both of these phenomena require spaced stimulation, we examined whether activity-dependent ghost bouton formation also required transcription and translation. Bath application of either the transcriptional inhibitor actinomycin (5mM) or the translational inhibitor cycloheximide (100mM) during stimulation prevented the formation of ghost boutons (Fig. 4-4B). Thus, activity dependent synapse remodeling depends on transcription and translation.

Just blocking action potentials in neurons by shifting the temperature sensitive neuronal Na^+ channel mutant *paralytic* (*para*^{ts}) (Wu and Ganetzky, 1980) to restrictive temperature during high K^+ stimulation prevented the formation of ghost boutons (Fig. 4-4C), even though high K^+ depolarization should allow neurotransmitter release in the absence of action potentials. This observation indicates that neurotransmitter release is not the only factor mediating rapid activity-dependent synapse modification, but that normal action potentials are also required.

Spaced stimulation potentiates spontaneous release frequency

We next determined the physiological consequences of spaced 5X K^+ depolarization by recording from the postsynaptic muscles after the spaced depolarization paradigm. In these animals the frequency of spontaneous excitatory potentials (mEJPs) was increased on average by about 3-fold compared to controls (Fig. 4-5A, B), suggesting a presynaptic modification. Presynaptic potentiation was evaluated through a frequency potentiation index, which is arrived at by dividing the mEJP frequency after stimulation by the control mEJP frequency (Fig. 4-5C).

A small but significant increase in mEJP amplitude was also observed upon spaced depolarization (Fig. 4-5D). This might result from multiquantal release, changes in postsynaptic receptor function, or activity-dependent changes in the size of synaptic vesicles (Steinert et al., 2006). No change in the amplitude of nerve-evoked responses was observed (Supplemental Figure 4-

1B). This was not due to a change in quantal content, as determination of quantal content by failure analysis (Del Castillo and Katz, 1954; Petersen et al., 1997) revealed no differences between 5X K^+ stimulated and non-stimulated samples (quantal content in unstimulated samples was 1.3±0.12 vs. 1.3±0.07 in 5X K^+ stimulated samples; n=4 and 5 respectively).

To assess if the changes in NMJ morphology and physiology could be elicited by patterned stimulation of motor nerves at frequencies comparable to those observed upon endogenous activity (Budnik et al., 1990), we also stimulated motor nerves with patterned 10 Hz frequency and examined the consequences for mEJPs and NMJ structural changes. A precise spaced pattern of high frequency stimulation (5 stimulation cycles, each consisting of 5 min of stimulation (2 sec at 10 Hz interspersed by 3 sec rest) and 15 min of rest; Fig. 4-5F blue and black) was required to elicit mEJP frequency potentiation (Fig. 4-5B, C), and structural synapse dynamics, as illustrated by the rapid motility of synaptopods (Fig. 4-5E arrows). The average magnitude of these changes was only slightly smaller than the 5X K^+-induced depolarization results in wild type (Fig. 4-5C). However, examining individual experiments in a probability plot indicated that the high frequency nerve stimulation paradigm was not as effective as the spaced K^+-induced depolarization paradigm (Fig. 4-5B).

As an additional independent way to establish that the observations with K^+ depolarization were physiologically relevant in the intact organism, experiments were also carried out by stimulating undissected larvae. For these experiments larvae expressing the light activated channel Channelrhodopsin-2

(ChR2;(Nagel et al., 2002; Schroll et al., 2006)) were fed all-trans-retinal containing food and subjected to light stimulation paradigms using 470nm illumination from an LED controlled by a stimulator. Patterned light stimulation similar to the electrical stimulation paradigm (5 stimulation cycles, each consisting of 5 min of light stimulation [2 sec illumination interspersed by 3 sec rest] and 15 min of rest; Fig. 4-5F purple and black) indeed potentiated mEJP frequency on average to the same level as nerve stimulation (Fig. 4-5B, C), and induced structural synaptic changes including the formation of ghost boutons (Fig. 4-4A, 5G). Recording from the postsynaptic muscles of ChR2 expressing larvae, while subjecting them to the light paradigm, demonstrated that the light stimulation elicited bursts of synaptic activity which did not exceed 50 Hz, as previously reported (Fig. 4-5F; (Schroll et al., 2006)). It is also noteworthy that light-induced mEJP potentiation lasted for at least 2-3 hrs. Thus, an acute increase in activity by direct nerve stimulation in dissected preparations or by light in ChR2-expressing intact larvae also leads to rapid modifications in synaptic structure and function. These observations also provide compelling evidence that the changes induced by high K^+ depolarization are physiologically relevant.

Rapid activity-dependent changes in synaptic structure and function depend on Wg signaling

The similarity between ghost boutons observed upon spaced stimulation and those found in mutations that interfere with the Wg pathway led us to investigate a potential relationship between the activity-dependent changes

described above and Wg signaling. Reducing Wg dosage by using heterozygous wg^{ts}/+ mutants shifted to restrictive temperature for 16 hr prior to dissection, or homozygous wg^{1} hypomorphic mutants, completely prevented the observed increase in ghost bouton formation (Fig. 4-6A blue; compare to red) upon spaced 5X K^+ depolarization. This phenotype could be rescued by expressing Wg in motorneurons in the wg^{ts}/+ mutant background (Fig. 4-6A green). These changes were not simply due to a decreased excitability in wg^{ts}/+ mutants, since 0X K^+ wg^{ts}/+ larvae had mEJP frequency and amplitude as well as EJP amplitudes which were undistinguishable from wild type controls (Fig. 4-6D and Supplemental Figure 4-1C).

Enhancing Wg secretion by overexpressing a *wg* transgene in motorneurons (c380/+;;UAS-Wg/+) resulted in an increase in ghost boutons upon 5X K^+ spaced depolarization similar to wild type (Fig. 4-6A orange; compare to red). However, in NMJs overexpressing Wg in motorneurons, only 3 cycles of spaced stimulation (compared to the usual 5 in wild type) were sufficient to enhance ghost bouton formation, quite unlike wild type NMJs with 3 cycles (Fig. 4-6A orange; compare to red). This enhancement was again suppressed by reducing *wg* dosage in c380/+; wg^{ts}/+; UAS-Wg/+ larvae (Fig. 4-6A green). The effect of overexpressing Wg in motorneurons was unlikely to result from increased excitability at these NMJs, as mEJP amplitude was not significantly different in 0X K+ wild type and UAS-Wg-pre controls (Fig. 4-6D). Further, these larvae actually had a small but statistically significant decrease in EJP amplitude (Supplemental Figure 4-1C). Thus, spaced depolarization induces ghost bouton

formation in a Wg-dependent fashion, and enhancing Wg secretion can bypass some of the stimulation requirements for inducing ghost bouton formation.

We next examined whether the potentiation in mEJP frequency observed upon spaced 5X K^+ stimulation was also dependent on Wg signaling. Notably, this potentiation was prevented by reducing *wg* gene dosage (Fig. 4-6 B, C blue). When stimulated NMJs overexpressing Wg in motorneurons were compared to stimulated wild type NMJs, on average there was no statistically significant difference in the mEJP frequency (Fig. 4-6C orange). However, many stimulated NMJs overexpressing Wg in motorneurons displayed a significant shift towards higher mEJP frequencies when comparing individual experiments in a probability plot (Fig. 4-6B), further indicating that Wg release is involved in this potentiation. Interestingly, mEJP amplitude was also increased in all genotypes, suggesting that unlike mEJP frequency, the increase in mEJP amplitude did not depend on Wg (Fig. 4-6D). Just as wild type stimulation, there was also no significant change in evoked EJP amplitude (Suppl. Fig 1C). Thus the induction of ghost boutons and mEJP frequency potentiation after spaced 5X K^+ depolarization depends on the Wg pathway.

Acute depolarization enhances Wg secretion

The suppression of activity-dependent structural and functional modifications by reducing *wg* dosage and the partial bypass of the stimulation requirements by increasing presynaptic Wg levels suggested that presynaptic activity might regulate Wg secretion. A measure of Wg release can be obtained

by calculating the mean intensity of Wg staining within the immediate postsynaptic volume (as defined by the extent of DLG immunoreactivity and exclusion of the labeling by the presynaptic membrane marker anti-HRP (Jan and Jan, 1982) (Fig. 4-7A) by using 3D volumetric quantification of confocal stacks. Consistent with our hypothesis, the mean intensity of Wg immunoreactivity in the postsynaptic junctional volume displayed a small but statistically significant increase upon spaced 5X K^+ depolarization (Fig. 4-7A, B; Supplemental Figure 4-2). This effect was suppressed by eliminating Ca^{++} from the external solution (Fig. 4-7B). The levels of secreted postsynaptic Wg upon 5X K^+ depolarization was also substantially reduced when neurotransmitter release was temporally blocked (Fig. 4-7C, blue). This was achieved by expressing a temperature sensitive dominant-negative Dynamin transgene (Shibire-DN^{ts}; $ShiDN^{ts}$) (Kitamoto, 2001) in motorneurons and shifting the samples from permissive temperature to restrictive temperature, which blocks neurotransmission in a reversible manner by interfering with vesicle recycling (Koenig and Ikeda, 1989) (Fig. 4-7C, blue; controls in Supplemental Figure 4-3C). Similarly, the secretion of Wg was also substantially reduced by blocking action potentials in *para*^{ts1} mutants shifted to restrictive temperature (Fig. 4-7C, blue). Notably, the levels of presynaptic Wg did not change significantly after 5X K^+ depolarization (Fig. 4-7B, red) suggesting that, as demonstrated by studies of peptidergic vesicles (Shakiryanova et al., 2006) activity might induce the mobilization of vesicles into active terminals. This notion is also consistent with the observation that in $ShiDN^{ts}$ and *para*^{ts1} synapses, there was a decrease in

presynaptic Wg (Fig. 4-7C, red). Thus, activity regulates rapid synapse remodeling, most likely by stimulating Wg release from presynaptic boutons in a Ca^{++}-dependent manner.

Acute and chronic alterations in electrical activity modulate the postsynaptic Wnt Frizzled Nuclear Import pathway at the NMJ

The above observations demonstrated that NMJs can undergo rapid structural changes in response to activity in a Wg-dependent fashion. A short-term consequence of these changes is the formation of ghost boutons, which lack postsynaptic proteins and structures. Earlier studies have demonstrated that in postsynaptic muscles Wg secretion activates the postsynaptic FNI pathway (Mathew et al., 2005). Mutations that interfere with this pathway reduce DFz2C import into postsynaptic muscle nuclei. In contrast, enhancing Wg secretion from motorneurons leads to substantial increase in nuclear DFz2C entry. Therefore, if increased activity enhances Wg secretion we would expect to observe that acute spaced stimulation should result in augmentation of nuclear DFz2C entry. We found that the number of intranuclear DFz2C spots was significantly higher upon 5X K^+ spaced depolarization (Fig. 4-8A).

We also tested the effects of blocking activity on DFz2C nuclear import by expressing $ShiDN^{ts}$ in motorneurons and shifting the larvae to restrictive temperature for various time periods. Blocking neurotransmitter release significantly reduced the number of DFz2C nuclear spots (Fig. 4-8B). This decrease in nuclear DFz2C import was a function of the duration of the

neurotransmitter block. While blocking synaptic transmission for 90 min before dissection led to a small but significant reduction in nuclear DFz2C import, increasing cumulative durations of the temperature shift led to increasingly larger reductions in nuclear DFz2C import when compared to their wild type controls (Fig. 4-8B; temperature controls in Supplemental Figure 4-3A). A similar reduction in DFz2C nuclear import was observed when action potentials in neurons where blocked by shifting *para*^{ts} mutants to restrictive temperature (Fig. 4-8C). In these mutants K^+ depolarization would still elicit neurotransmitter release, suggesting that neurotransmitter release is not the only relevant process in the regulation of muscle DFz2C nuclear import. Thus levels of activity are directly correlated to the magnitude of DFz2C nuclear import.

A prediction of the above experiments is that chronic changes in activity should also lead to an increase in DFz2C nuclear import. This was tested by examining the hyperexcitable mutant *eag Sh* which was previously reported to stimulate the development of new synaptic boutons and active zones (Budnik et al., 1990; Jia et al., 1993b). We found a dramatic increase in the number of nuclear DFz2C spots in *eag Sh* mutants (Fig. 4-8D, E). This enhancement was completely suppressed by reducing *wg* gene dosage in a heterozygous *wg* mutant, corroborating a dependency on FNI (Fig. 4-8D). An enhancement in DFz2C nuclear import was also found when larvae expressing ChR2 in motorneurons were stimulated by the light paradigm every 12 hr for the last 3 days of larval development (Fig. 4-8D). Thus, the acute changes in DFz2C nuclear import are further enhanced by augmenting activity in a chronic fashion.

Rapid changes in presynaptic structure and function depend on GSK-3ß/Sgg function in motorneurons

While the above results implicate a role for the postsynaptic Wg signaling pathway, most of the immediate changes we observed in synaptic structure were presynaptic. Presynaptic activation of a Wg pathway has been previously suggested through studies of the Shaggy/GSK-3ß kinase (Franco et al., 2004; Packard et al., 2002). A major outcome of activation of the canonical and divergent canonical Wnt/Wg pathways is the inhibition of GSK-3ß. The latter pathway has been implicated in cytoskeletal rearrangements during axonal remodeling and in the differentiation of presynaptic terminals (Ciani and Salinas, 2005; Speese and Budnik, 2007). This regulation is thought to occur through GSK-3ß-dependent phosphorylation of microtubule associated proteins (MAPs), which in turn influence microtubule dynamics (Goold and Gordon-Weeks, 2004). Studies have also provided evidence that GSK-3ß is localized to actin-rich regions of the growth cone where it controls axonal growth (Eickholt et al., 2002). Studies at the larval NMJ demonstrate that GSK-3ß is enriched within presynaptic terminals, and that mutations in the GSK-3ß gene *sgg* result in alterations in bouton number and the organization of the microtubule cytoskeleton (Franco et al., 2004; Packard et al., 2002). These changes are, as expected from the inhibition of GSK-3ß by Wg signaling, the opposite of those elicited by mutations in Wg.

The Wg-dependent modifications in the structure of presynaptic arbors upon spaced stimulations raised the question of whether Sgg, a key component of Wg signaling, was involved in this process. This question was investigated by enhancing or decreasing Sgg function specifically in motorneurons, either by presynaptic expression of a full-length Sgg transgene, which was previously shown to antagonize Wg signaling (Bourouis 2002), or by presynaptic expression of a dominant-negative kinase-null Sgg transgene (SggDN) which was reported to phenocopy *sgg* loss-of-function at the NMJ (Franco et al., 2004). Presynaptic expression of Sgg completely suppressed the activity-dependent induction of ghost boutons (Fig. 4-8F blue; compare to red). In contrast, inhibiting presynaptic Sgg by expressing the SggDN transgene did not interfere with ghost bouton formation upon 5X K^+ spaced depolarization, although this increase was slightly less robust than wild type (Fig. 4-8F orange). Notably, in agreement with the notion that inhibiting Sgg mimics the activation of the Wg pathway, the number of ghost boutons was significantly increased even upon just 3 cycles of stimulation upon expressing SggDN in motorneurons as compared to the requirement of 4-5 cycles of stimulation in wild type (Fig. 4-8F orange). Thus, while activity activates the FNI pathway in postsynaptic muscles, our results are consistent with a concomitant activation of a divergent canonical Wg pathway mediated by Sgg in the presynaptic motorneuron.

We also determined if potentiation of mEJP frequency was influenced by enhancing or decreasing Sgg activity. Overexpressing Sgg resulted in an increase in mEJP frequency after 5X K^+ spaced stimulation, although this

increase was less than 2-fold compared with a 3-fold enhancement in stimulated wild type larvae (Fig. 4-8G, I blue; compare to red). Interestingly, potentiation of mEJP frequency was augmented by almost 4-fold upon presynaptic expression of SggDN (Fig. 4-8G, I orange). These results are in agreement with the previously suggested hypothesis that Wg activates a canonical or divergent canonical presynaptic pathway that leads to Sgg inhibition. Increasing Sgg function partially or completely bypassed Wg-dependent inhibition, preventing the activity-dependent increase in ghost boutons, and decreasing mEJP potentiation. Reducing Sgg function in presynaptic motorneurons did not interfere with activity-dependent potentiation of mEJP frequency and enhanced ghost bouton formation close to wild type levels (Fig. 4-8F, G, I). Similar to all other genotypes (Fig. 4-6D), Sgg transgenic flies also exhibited a small but significant increase in mEJP amplitude upon spaced 5X K^+ depolarization (Fig. 4-8J). These observations provide evidence for simultaneous activation of pre- and postsynaptic Wg signaling in response to patterned activity and place a bidirectional Wg pathway as a critical downstream component of activity-dependent synapse remodeling.

DISCUSSION

Understanding how neuronal circuits can be modified in the mature brain requires knowledge of the mechanisms by which synapses can be shifted from a relatively stable state to a dynamic condition that allows new synaptic growth or

elimination. Here we have shown that rapid activity-dependent changes in synapse development and function can be induced at the *Drosophila* glutamatergic NMJs in a process that depends on spaced stimulation, akin to changes observed in dendritic spines of hippocampal neurons in culture (Yao et al., 2006). During the postembryonic period after initial formation of synaptic contacts, synaptic boutons continuously proliferate in conjunction with changes in postsynaptic target size (Griffith and Budnik, 2006). Chronic increases in activity, induced by mutations in ion channels, significantly enhance the formation of new synaptic boutons (Budnik et al., 1990; Schuster et al., 1996a). Here we demonstrate that activity-dependent changes are not simply the result of a developmental elevation in overall neuronal excitability, but rather that the ability of synapses to respond to changes in activity through structural and functional dynamics is an acute process, which is rapidly established upon patterned stimulation. Further, we have identified an important downstream mechanism, the Wnt pathway, which links activity-dependent changes to structural and functional synaptic modifications.

Together, the findings that (1) activity can induce Wg release from presynaptic boutons, (2) patterned activity elicits acute changes in synapse function and structural dynamics in a Wg-dependent fashion, (3) increasing Wg secretion can bypass some of the activity requirements, (4) intensifying or blocking activity has a corresponding influence on DFz2C entry into the nucleus in the postsynaptic muscle cell, and (5) activity modifications can be completely or partially suppressed by modulating GSK-3ß in the presynaptic cell,

demonstrate that bidirectional Wg signaling is a key downstream mediator of activity-dependent synaptic plasticity.

We propose the following model on bidirectional regulation of synapse structure and function by the Wg pathway (Fig. 4-8H). Spaced stimulation results in the release of Wg by presynaptic boutons, which binds to DFz2 receptors present both pre- and postsynaptically (Packard et al., 2002). In the presynaptic compartment, Wg release likely regulates cytoskeletal dynamics through inhibition of Sgg activity, leading to synaptopod dynamics and formation of ghost boutons in a process that depends on transcriptional and/or translational activation. In the postsynaptic compartment Wg release activates the FNI pathway, resulting in DFz2C cleavage and import into the nucleus where it may induce the transcription of synaptic genes (Fig. 4-8H). Disrupting the Wg pathway during synapse development dampens the maturation of new synaptic boutons resulting in NMJs containing fewer mature boutons as well as a larger number of undifferentiated ghost boutons (Ataman et al., 2006a; Packard et al., 2002). While our results are consistent with this model, alternative possibilities must be also considered. For example, changes in Wg signaling might alter excitability (beyond the parameters examined in this study) and these changes might trigger parallel transduction pathways that modulate synaptic structure and function. In addition, it is unlikely that Wg alone is responsible for all activity-dependent mechanisms. For example, the participation of a retrograde BMP signaling pathway in the regulation of synaptic bouton proliferation is well-established (Marques, 2005). It is highly likely that multiple signaling pathways, including Wg,

BMPs and others collaborate in the orchestration of activity-dependent synapse modifications.

Acute changes in synapse structure and function

The most striking structural changes we observed were the *de novo* formation of synaptopods and ghost boutons. Although the nature of synaptopods is unclear, they might represent an initial stage during synaptic bouton formation like the filopodia observed at dendritic spines in normal animals and in response to activity (Niell et al., 2004; Yuste and Bonhoeffer, 2004). However, in our studies we never observed a transition from synaptopod to bouton. Another possibility is that they might correspond to exploratory structures that convey a signal to pre- and/or postsynaptic sites. This function has also been suggested for dendritic filopodia (Dunaevsky and Mason, 2003; Yuste and Bonhoeffer, 2004) as well as for growth cone filopodia prior to target innervation (Kalil and Dent, 2005).

Ghost boutons, on the other hand, represent rapid *de novo* formation of undifferentiated boutons. Their formation is not the result of retraction of mature boutons. They are found to contain synaptic vesicles, but virtually lack pre- and postsynaptic specializations. Our live imaging studies showed that these boutons could acquire postsynaptic GluR and presynaptic Brp clusters over a relatively long period after their initial formation.

The above morphological changes required transcription and/or translation, akin to late LTP and long-term memory (Kandel, 2001), but the

step(s) at which they are required remains unclear. Potential scenarios include an activity-dependent increase in *wg* mRNA or Wg protein synthesis as observed in the mammalian brain (Wayman et al., 2006). They could also involve the activation of alternative pathways such as PKA and CREB-dependent mechanisms (Davis et al., 1998; Davis et al., 1996; Wayman et al., 2006).

Previous live imaging studies of wild type intact larval NMJs did not report the occurence of synaptopods and ghost boutons (Zito et al., 1999). However, in that study a postsynaptic marker (mCD8-GFP-Sh) was used to label the NMJ, and thus synaptopods and ghost boutons would not have been observed.

We also observed a Wg-dependent potentiation of mEJP frequency after spaced stimulation. An increased mEJP frequency has also been observed at the embryonic NMJ upon high frequency stimulation, although the accompanying structural changes were not examined in that preparation (Yoshihara et al., 2005). The potentiation of mEJP frequency that we observed did not result from the addition of ghost boutons, as ghost boutons only rarely contain active zones(Ataman et al., 2006a). In addition, it occurred without any change in the number of nc82/Brp puncta in existing boutons (data not shown), suggesting that this potentiation is unlikely to emerge from the recruitment of new active zones. However, nc82/Brp is thought to label just the T-bar component of the active zone (Kittel et al., 2006a), and many active zones lack T-bars (Atwood et al., 1993). Thus, this possibility cannot be completely ruled out. Alternatively, the increase in mini frequency might arise from unsilencing of existing synapses as

shown in mammals (Yao et al., 2006) or from changes in their intrinsic properties.

Potentiation of spontaneous release frequency has been widely implicated in synapse maturation (Zucker, 2005). At the *Xenopus* NMJ repetitive neuron stimulation also results in the potentiation of spontaneous synaptic activity which is associated with synapse maturation (Lo et al., 1991). Expressing SynCaM, a homophilic cell adhesion molecule that drives synaptic maturation, also increases the frequency of spontaneous release (Biederer et al., 2002). At the *Drosophila* embryonic NMJ mutations that block the potentiation of spontaneous release frequency, such as mutants lacking both DGluRIIA and DGluRIIB, as well as mutations in *syntaxin*, and *synaptotagmin IV,* exhibit abnormal NMJ development. These mutants all show a lack of presynaptic maturation, as demonstrated by a maintained growth cone structure (Yoshihara et al., 2005). In the mammalian nervous system spontaneous release has been shown to regulate postsynaptic local protein synthesis which is thought to stabilize synaptic function (Chung and Kavalali, 2006). Thus, the mEJP frequency potentiation observed here may play an initial role in postsynaptic maturation.

Importantly, spaced stimulation also induced a small but significant increase in mEJP amplitude that did not depend on Wg. Thus, activity is likely to regulate additional Wg-independent pathways. For example, elevated Ca^{++} induces the mobilization of vesicles to release sites, thereby increasing the number of active zones containing more than one docked vesicle, and thus

eliciting multi-quantal release (Koenig et al., 1993). Recent studies have also suggested an activity-dependent increase in the size of synaptic vesicles (Steinert et al., 2006). However, the change in mEJP amplitude was not accompanied by modifications in the amplitude of evoked responses, as expected if quantal size was larger, and further, we did not see a change in quantal content as determined by failure analysis.

Activity-dependent Wg release and role of Wg in functional and structural synaptic changes

Wg secretion was also found to be regulated by activity. Spaced depolarization increased the levels of Wg at the postsynaptic area, and conversely, temporally blocking activity in *para*^{ts1} and by expressing ShiDN^{ts} in motorneurons decreased secreted Wg. Given that diminishing *wg* gene dosage prevented the rapid activity-dependent changes, these results suggest that Wg operates downstream of activity to promote these changes. This conclusion is further supported by the observation that increasing Wg secretion by overexpressing Wg in motorneurons, or activating the presynaptic Wg pathway by expressing a SggDN in motorneurons, partially bypassed the requirement for activity.

Notably, we found that activity-dependent Wg release did not decrease presynaptic Wg levels. In contrast, reducing Wg release through *para*^{ts1} and ShiDN^{ts} diminished Wg levels in presynaptic boutons. This is in agreement with recent studies documenting activity-dependent trafficking of peptidergic vesicles

at the *Drosophila* NMJ (Shakiryanova et al., 2005; Shakiryanova et al., 2006). In resting terminals peptidergic vesicles are relatively immobile, but activity induces a rapid mobilization of these vesicles to active terminals. Alternatively (or in addition), activity (or lack thereof) might influence the transcription and/or translation of Wg, consistent with the requirement of transcription and/or translation in ghost bouton formation.

Wnts and activity at mammalian synapses

Tetanic stimulation in hippocampal slices induces NMDA receptor-dependent release of Wnt3a by postsynaptic cells, the translocation of ß-Catenin into the nucleus, and the upregulation of Wnt target genes (Chen et al., 2006). Further, altering Wnt signaling levels caused corresponding changes in the magnitude of LTP (Ahmad-Annuar et al., 2006; Chen et al., 2006). Members of the Wnt pathway are also involved in activity-dependent dendritic arborization (Wayman et al., 2006; Yu and Malenka, 2003). Activation of an NMDA receptor- and Ca^{++}-dependent pathway resulted in CREB responsive transcription of Wnt-2, through activation of CaM kinase kinase (CaMKK), that coupled neuronal activity with dendritic development (Wayman et al., 2006). Similarly, other studies suggest that the enhancement of dendritic growth induced by depolarization requires ß-Catenin and an increased Wnt release (Yu and Malenka, 2003).

To date, mammalian Wnts have been shown to be secreted by postsynaptic cells (Ciani and Salinas, 2005). However, multiple members of the Wnt family exist both in *Drosophila* and in mammalian systems, and different

members might be released by different synaptic compartments. Alternatively, the anterograde, retrograde, or autocrine nature of Wnt signaling at synapses might have changed through evolution.

Notably, spaced, but not massed stimulation of cultured hippocampal neurons and dentate gyrus explants resulted in the persistent extension of postsynaptic filopodia and spine-like structures in dendrites (Wu et al., 2001). As in our experiments, the induction of these structures depended on calcium and did not begin to appear until the 3rd-4th spaced stimulation cycle (Wu et al., 2001). Spaced depolarization also led to an increase in mEPSC frequency thought to emerge from the activation of silent synapses (Yao et al., 2006). Our findings in this study indicate that the cellular processes underlying rapid activity-dependent changes in synaptic structure and function appear to be conserved in presynaptic arbors of the NMJ.

Our results also implicate presynaptic GSK-3ß in the presynaptic compartment during rapid activity-dependent changes at the larval NMJ. GSK-3ß is known to regulate microtubule and actin cytoskeletons. In the case of microtubules, it phosphorylates MAP1B and tau, thereby influencing microtubule stability (Goold and Gordon-Weeks, 2004). In agreement with those observations, GSK-3ß/Sgg phosphorylates the *Drosophila* MAP1B-related protein Futsch (Gogel et al., 2006), and Futsch is required for Sgg function in synaptic growth (Franco et al., 2004). Further, in *sgg* mutants the number of bundled/stable microtubule loops within synaptic boutons were dramatically

increased, exactly the opposite phenotype of *wg* mutants (Franco et al., 2004; Packard et al., 2002).

In summary, our studies demonstrate that rapid modifications in synapse structure and function can be elicited in glutamatergic synapses at the larval NMJ, and identify Wg signaling as a critical effector of activity-dependent synaptic plasticity. These studies also provide a prominent *in vivo* model system to examine structural and physiological consequences of acute activity in a genetically tractable organism.

MATERIALS AND METHODS

Fly strains. Flies were reared in standard *Drosophila* medium at 25C° except where indicated. The following stocks were used Canton-S, wg^{ts} (wg^{lL114}) (Nusslein-Volhard et al., 1985), wg^{1} (Couso et al., 1994), UAS-Wg (Binari et al., 1997), GluRIIA-GFP (Rasse et al., 2005), UAS-Brp-GFP (Wagh et al., 2006), $para^{ts1}$ (Wu and Ganetzky, 1980), UAS-ShiDN^{ts1} (Kitamoto, 2001), eag^{1} Sh^{133} (Budnik et al., 1990), UAS-mCD8:GFP (Lee and Luo, 1999), UAS-Sgg and UAS-SggDN (A81T) (Bourouis, 2002), UAS-ChR2 (Schroll et al., 2006) and motorneuron Gal4 driver C380 (Budnik et al., 1996).

Immunocytochemistry. Larvae were dissected in Ca^{++} free saline and fixed for 10-15 minutes in 4% paraformaldehyde as in (Budnik et al., 1996), unless otherwise stated. Anti-Wg 1:200 (Packard et al., 2002), anti-DLG 1:20,000 (Koh et al., 1999), anti-GluRIII 1:1000 (Marrus et al., 2004), nc82 monoclonal antibody 1:100 (Kittel et al., 2006b), anti-cystein string protein monoclonal antibody ab49 1:100 (Zinsmaier et al., 1994) (gift from K.Zinsmaier), anti-DFz2-C 1:100 (Mathew et al., 2005), and FITC- or Texas Red-conjugated anti-HRP 1:200 (Sigma). Secondary antibodies conjugated to FITC, Texas Red, or Cy5 (Jackson Immunoresearch) were used at a concentration of 1:200. Imaging of fixed preparations was performed using a Zeiss Pascal confocal microscope.

Spaced High K^+depolarization Paradigm. Body wall muscles from third instar larvae were dissected in normal-HL3 saline (Stewart et al., 1994) containing 0.1mM Ca^{++}, leaving the CNS and peripheral nerves innervating the body wall muscles intact. High K^+ (90 mM) HL3 (Roche et al., 2002) adjusted for osmolarity changes (in mM; 40 NaCl, 90 KCl, 20 $MgCl_2$-$6H_2O$, 1.5 $CaCl_2$, 10 $NaCO_3$, 5 Sucrose, 5 Trehalose, 5 HEPES, pH=7.2) was applied to unstretched semi-intact preparations with 2, 2 ,2 ,4 and 6 minute pulses respectively with each pulse separated by a 15 minute incubation in normal-HL3. Experimental preparations were kept in normal-HL3 for 15 min after the last high K^+-pulse, and then were either live-imaged or fixed with 4% paraformaldehyde for 15 min followed by immunostaining with selected antibodies. Control larvae for all experiments were dissected and incubated using the same protocol as above but with only normal-HL3. For the pseudo-massed stimulation paradigm in Fig. 4-1B, larvae were subjected to 5, 5, and 6 min depolarization in high K^+ (same total depolarization period as the spaced protocol; 16 min), each separated by 15 min rest in normal HL3. For the experiments with transcriptional and translational inhibitors either 100 mM cycloheximide (Sigma) or 5 mM actinomycin (Sigma) were included in the normal and high K^+ HL3.

Heat shock paradigms. *wg^{ts}*/+ larvae reared at 17°C were shifted to 29°C for 16 hr prior to dissection. For UAS-*ShiDN^{ts}* or *$para^{ts1}$* the restrictive temperature (RET) was 32˚C and the permissive temperature room temperature. For experiments where UAS-*ShiDN^{ts}* was driven in motorneurons using C380, the

following heat shocks at the restrictive temperature (RET) of 32˚C where carried out: *90 min*: 3X 30 min at RET during late 3rd instar larval stage separated by 30 min at room temperature [RT]; *150min*: the above 90 min temperature shift paradigm plus 30 min at RT followed by 60 min at RET; *developmental block*: 75 min at RET twice a day for 3 days, beginning from second instar larval stage (total of 450 min at RET). For *para*^{ts1} heat pulses, the 150 min paradigm described above was applied. For the stimulation of activity in *para*^{ts1} larvae, dissected larvae were shifted to RET either from the beginning (Fig. 4-7C) or after the 2nd K^+ pulse (Fig. 4-4C) of the spaced 5X K^+-paradigm (see below). For the ShiDN^{ts} experiment in Fig. 4-7C, larvae were shifted to RET for 90 min prior to the 5X K^+ paradigm.

Channelrhodopsin-2 Light Paradigm. Larvae were raised on 100 μM all-trans-retinal food, as described in (Schroll et al., 2006). Multiple blue light (470nm) LEDs were driven using an ITC-16 computer interface (InstruTech, PortWashington, NY), commanded by Heka pulse software (HEKA Electronik, Lambrecht/Pfalz, Germany), to stimulate intact larvae expressing ChR2 in motorneurons. The acute light paradigm used timing and spacing identical to the paradigm used in nerve stimulation experiments (see above), except that during the 2 sec stimulation light was constant. For developmental stimulation (Fig. 4-8D), late 2nd instar larvae were stimulated with this paradigm every 12 hours for 3 days.

Live-imaging of intact larvae. Live imaging of undissected larvae was conducted in muscle 14, 30 and 27 as in (Rasse et al., 2005). Briefly, early 2nd or 3rd instar larvae expressing dGluRIIA-GFP in muscles and UAS-myr-mRFP , UAS-mCD8-GFP or UAS-Brp-GFP in motorneurons, were anaesthetized with isofluorane (Webster Veterinary), desflurane (Baxter) or Sevoflurane (Baxter), and imaged through the cuticle using either a Leica AOBS confocal microscope using a 63X (1.36 N.A.) objective, or an Improvision Spinning Disk confocal microscope using 40X (1.2 N.A.) objective.

Quantification of nuclear DFz2C spots, ghost boutons and synaptopods. Measurements were done at muscles 6 and 7 abdominal segment 3. Intranuclear DFz2C spots and ghost boutons were quantified as in (Ataman et al., 2006a; Mathew et al., 2005). Synaptopods were quantified from confocal images of live preparations. Statistical significance in two-way or multiple group comparisons was determined using a Student t-test and a one way ANOVA with a Tukey *post hoc* test respectively. Numbers in histograms represent mean± SEM.

Quantification of Wg. Secreted Wg was calculated as in (Gorczyca et al., 2007). Briefly, confocal stacks were collected from samples that were processed simultaneously, using the same confocal acquisition parameters and were then analyzed using Volocity 4.0 software (Improvision). Postsynaptic volume was determined via 3D quantitation of confocal stacks measuring the volume occupied by DLG and excluding the DLG signal within the volume occupied by

HRP immunoreactivity. Mean Wg fluorescence intensity was measured in the above postsynaptic volume for each genotype and normalized to wild-type controls.

Electrophysiology. Third instar larvae were dissected and continuously superfused with 1.5mM $CaCl_2$ HL3.1 saline (Feng et al., 2004). Electrophysiological recordings were carried out as in (Ashley et al., 2005). For nerve stimulation, the uncut A3 segmental nerve was carefully pulled into the tip of a suction electrode with a 10μm lumen, and samples were stimulated with cycles of 10 Hz for 2 sec followed by 3 sec rest, for 5 min. After 15 min rest, the above procedure was repeated 4 additional times. Voltage recordings of high K^+- or nerve stimulated samples were carried out as in (Ashley et al., 2005). The frequency of mEJPs was determined by measuring the average frequency over 5 sec intervals for a total of 2 min per sample. The frequency potentiation index was calculated by dividing the mean mEJP frequency of each stimulated sample by the mean frequency of unstimulated controls.

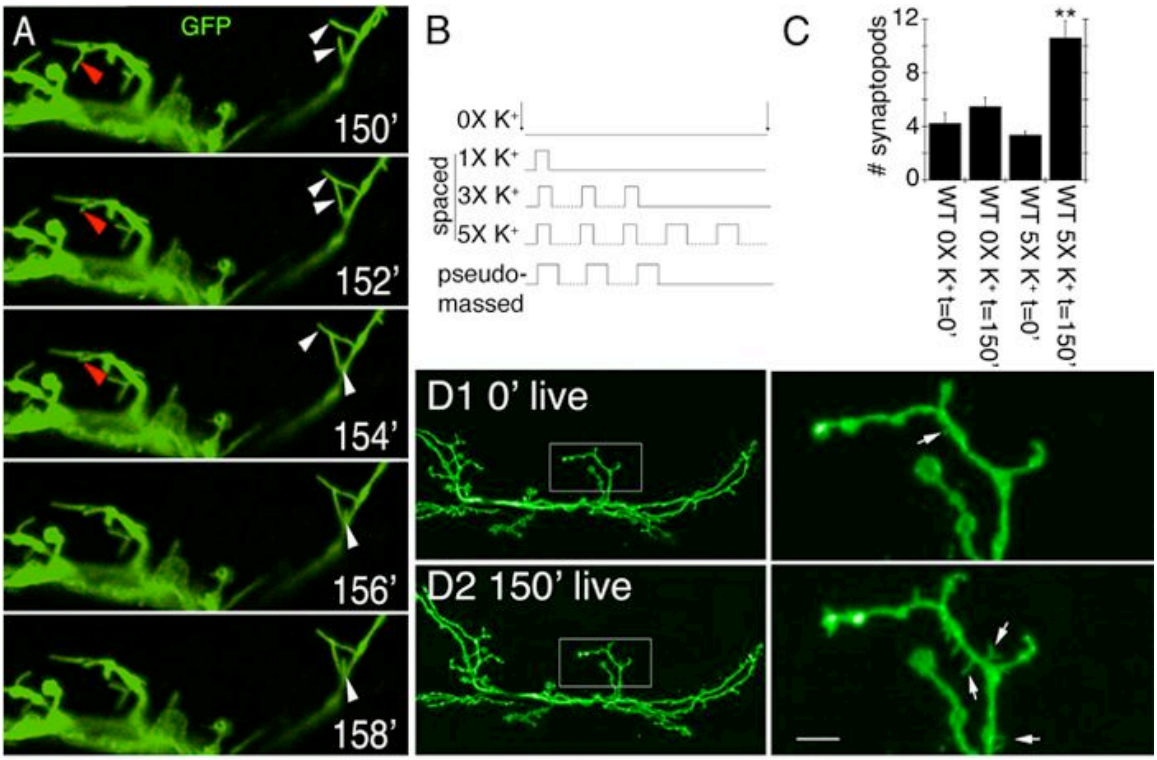

Figure 1
Ataman et al.

Figure 4-1

Figure 4-1. Acute spaced stimulation induces the formation of synaptopods at the NMJ. (**A**) Time lapse images of live NMJs expressing membrane tethered GFP in motorneurons about 2.5 hr from the beginning of spaced depolarization (exact time is stated in minutes in each panel). Red arrowheads point to a retracting synaptopod. White arrowheads point to elongating synaptopods. (**B**) High K^+-induced depolarization paradigms. (**C**) Number of synaptopods per NMJ arbor in wild type controls and preparations stimulated with spaced high K^+ depolarization. (**D**) Comparison of a representative NMJ arbor imaged live (**D1**) before and (**D2**) after 2.5 hrs from the beginning of spaced high K^+ depolarization, showing the increase in synaptopod frequency and length. Left column shows an entire NMJ at muscle 6 and 7, and right column is a high magnification view of the NMJ area circumscribed by the box in the left column panels. Arrows point to synaptopods. N [#arbors; #animals] in (C) is (from left to right): [4;3], [4;3], [21,9] and [21; ** = $p < 0.001$. Calibration scale is 4.5 μm in A, 23 μm in D left column, and 5 μm in D right column.

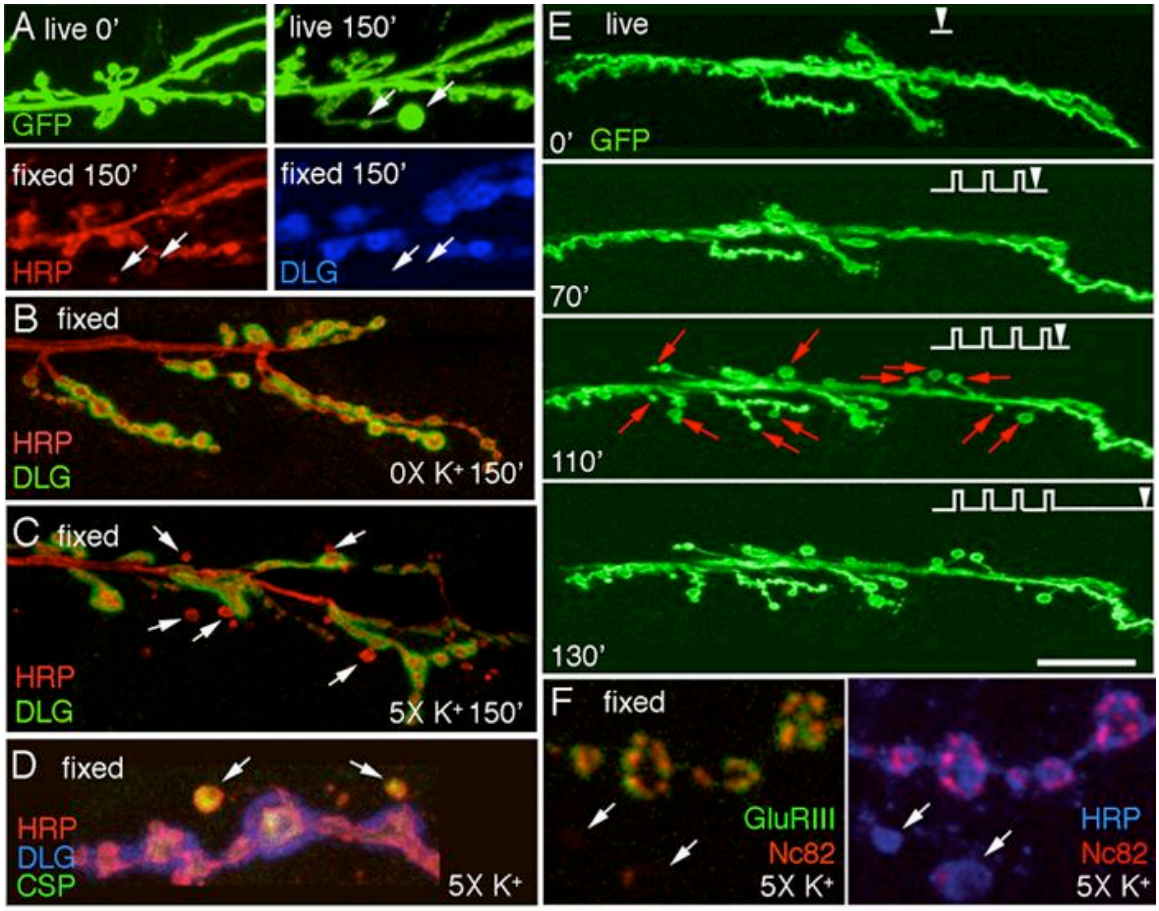
A live 0'
GFP
live 150'
fixed 150'
HRP
fixed 150'
DLG
B fixed
HRP
DLG
0X K+ 150'
C fixed
HRP
DLG
5X K+ 150'
D fixed
HRP
DLG
CSP
5X K+
E live
0' GFP
70'
110'
130'
F fixed
GluRIII
Nc82
5X K+
HRP
Nc82
5X K+
Figure 2
Ataman et al

Figure 4-2

Figure 4-2. Acute spaced stimulation induces the formation of undifferentiated "ghost boutons". (**A**) *De novo* ghost bouton formation observed live, after 150 min from the beginning of spaced depolarization. In **A** (bottom row) the same sample shown in (**A** top right panel) is exhibited after fixation and immunocytochemical staining with anti-HRP (left panel) and anti-DLG (right panel) antibodies, Arrows point to two ghost boutons in the live and fixed preparations. (**B, C**) NMJs double stained with anti-HRP and anti-DLG antibodies in (**B**) a control unstimulated preparation, and (**C**) a sample subjected to spaced 5X K^+ depolarization, fixed and imaged at 2.5 hrs after dissection. Arrows in (**C**) point to ghost boutons, which are recognized by labeling with anti-HRP antibodies, while lacking DLG immunoreactivity. (**D, F**) View of ghost boutons (arrows) in preparations fixed after stimulation and triple stained with (**D**) HRP, DLG, and CSP antibodies showing that ghost boutons contain a synaptic vesicle marker, and (**F**) HRP, NC82, and GluRIII antibodies showing that ghost boutons are devoid of GluR clusters and most active zones. (**E**) Time-lapse image series in which the preparation was imaged before stimulation and at the indicated times during the spaced stimulation protocol (arrowheads). Note the sudden appearance of ghost boutons (red arrows) after the 4^{th} depolarization pulse. Calibration scale is 12 μm in (A); 17 μm in (B, C); 6.5 μm in (D, F); and 24 μm in (E). 9].

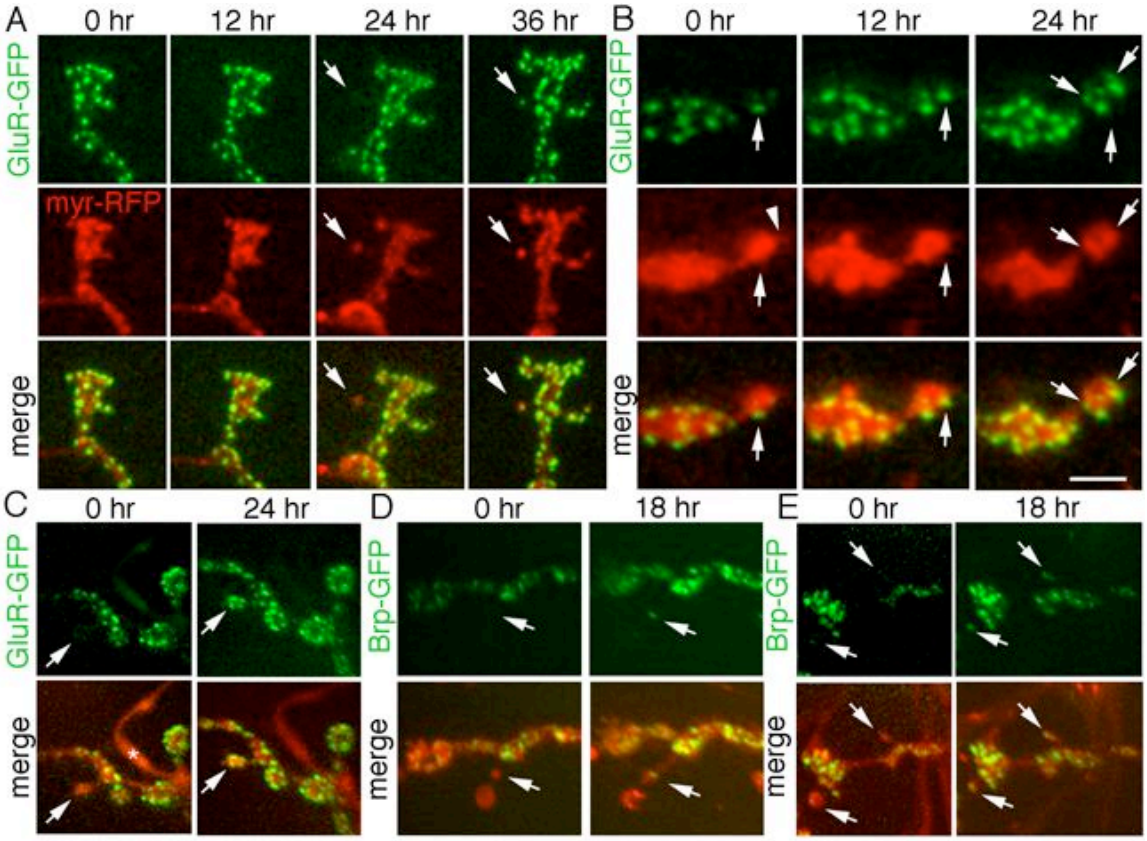

Figure 3
Ataman et al.

Figure 4-3

Figure 4-3. Ghost boutons form *de novo* in intact undissected larvae and develop into mature boutons by acquiring postsynaptic GluR and presynaptic Brp clusters. Time-lapse imaging through the intact cuticle of NMJs expressing presynaptic myr-RFP (red) and either postsynaptic GluR-GFP (green) or presynaptic Brp-GFP (green) showing **(A)** *de novo* formation of a ghost bouton (arrows) in muscle 27 at 24hr and clustering of GluR receptors on the ghost bouton (arrows) at 36hr. **(B)** Progressive increase in the number of GluR clusters (arrows) in a differentiating bouton, on muscle 27, over a 24hr period. Arrowhead in myr-RFP at 0 hr points to a synaptopod **(C)** Another example of a ghost bouton (arrows) in muscles 14 and 30 imaged at 0hr, which acquired GluR clusters (arrows) at 24 hours. * = peptidergic ending, which normally lacks GluR clusters. **(D, E)** Ghost boutons (arrows) in muscles 14 and 30 at 0hr, which acquired Brp clusters at 18 hr (arrows). Thin neurites may appear invisible, next to bright mRFP signal of boutons. Calibration scale is 5 μm in A, 3 μm in B, and 8 μm in C-E.

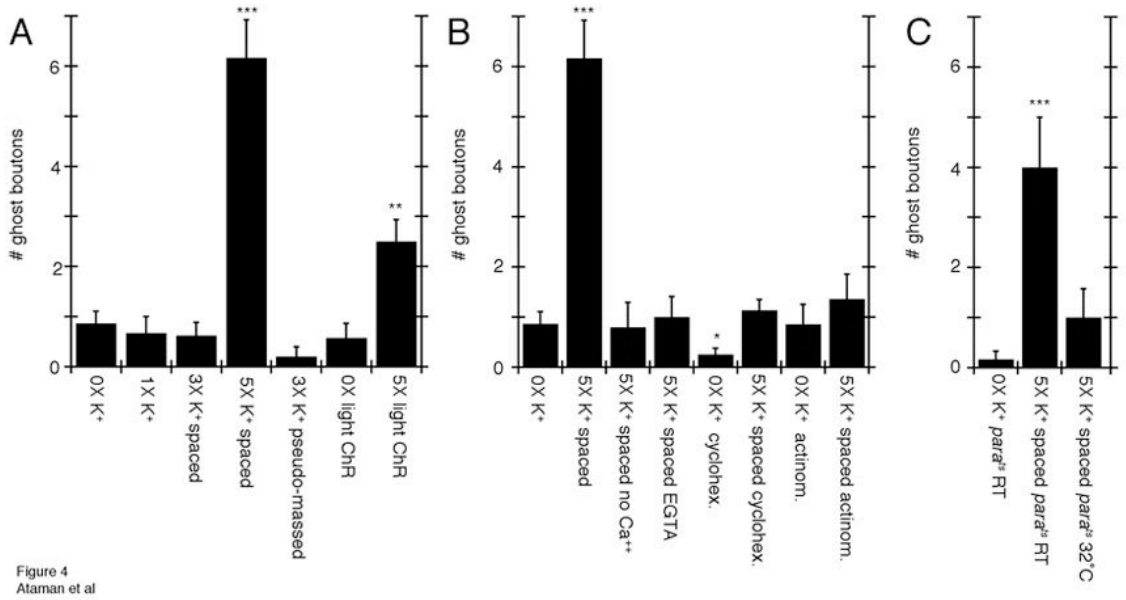
A
B
C
ghost boutons
0X K+
1X K+
3X K+ spaced
5X K+ spaced
3X K+ pseudo-massed
0X light ChR
5X light ChR
5X K+ spaced no Ca++
5X K+ spaced EGTA
0X K+ cyclohex.
5X K+ spaced cyclohex.
0X K+ actinom.
5X K+ spaced actinom.
0X K+ para^ts RT
5X K+ spaced para^ts RT
5X K+ spaced para^ts 32°C
Figure 4
Ataman et al

Figure 4-4

Figure 4-4. Activity-dependent ghost bouton formation depends on spaced stimulation, Ca^{++}, as well as transcription and translation. (**A-C**) Number of ghost boutons upon K^{+} depolarization induced (**A**) by using alternative stimulation protocols, (**B**) in the presence of different drugs and Ca^{++} conditions (no Ca^{++} and 0.5 mM EGTA) and (**C**) in *para*^{ts} mutants. N [# arbors; # animals] is (from left to right): (A): [22;11], [7;4], [8;4], [18;9], [6;4], [7;4], [12;6]; (B): [22;11], [18;9], [6;4], [13;7], [12;6], [16;8], [12;6], [11;6]; (C): [6;4], [15;8], [14;7].

*= p<0.05, **= p<0.001, ***=p<0.0001.

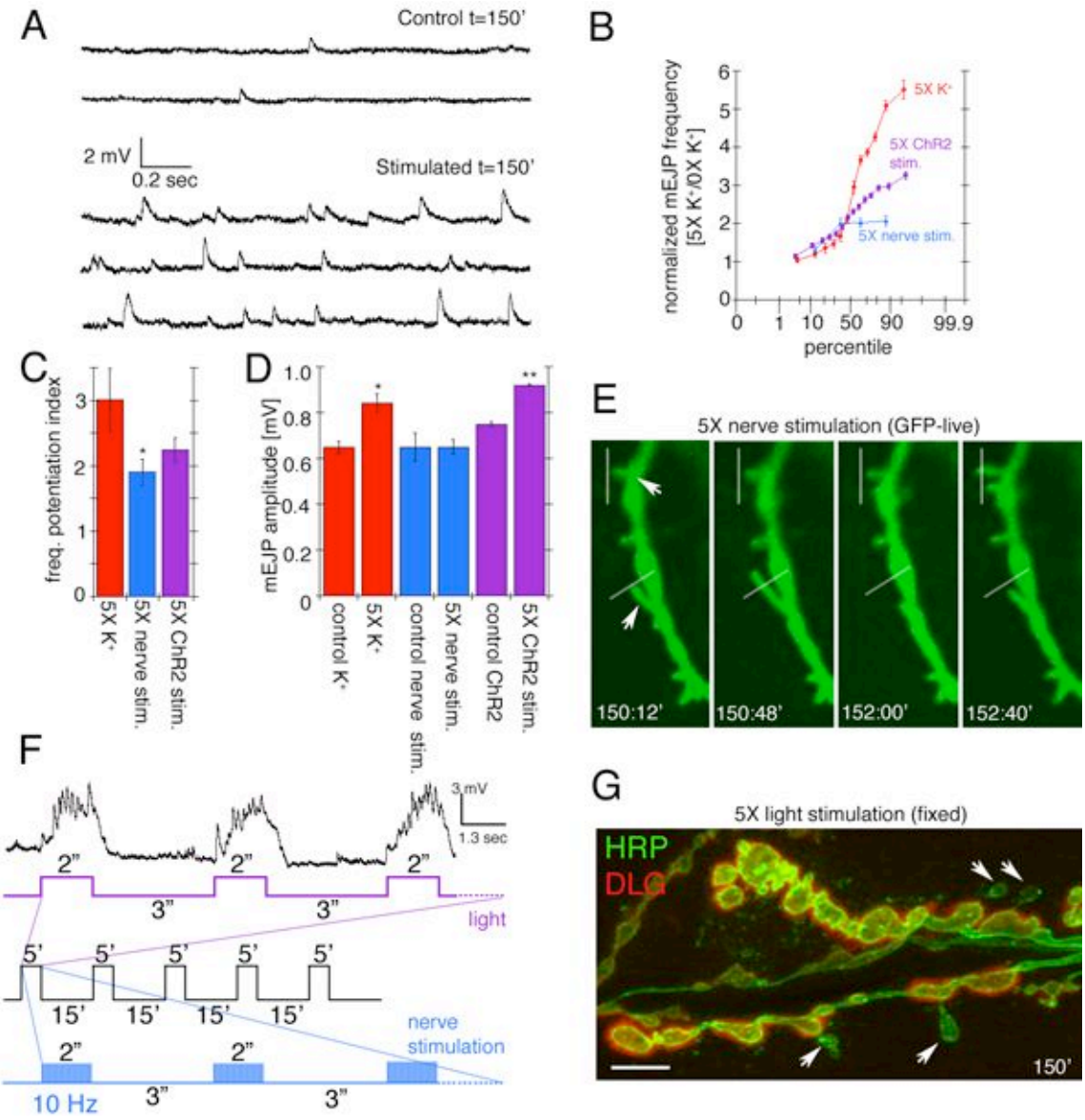

Figure 5
Ataman et al.

Figure 4-5

Figure 4-5. Potentiation of spontaneous release frequency after spaced K^+ depolarization, nerve stimulation, and light induced stimulation of motorneurons by using ChR2. (**A**) mEJP traces in (top) controls and (bottom) samples subjected to spaced 5X K^+ depolarization. (**B**) Normalized probability distribution of mEJP frequencies, obtained by dividing the mEJP frequency of experimental samples by the mean control frequencies, after spaced 5X K^+ depolarization (red), 5X nerve stimulation (blue), or 5X light stimulation of presynaptic ChR2 (purple). (**C**) mEJP frequency potentiation index (mEJP frequency in experimental samples divided by the mean control frequency). (**D**) Mean mEJP amplitude after the above stimulation paradigms. (**F**) Paradigms for nerve and light stimulation and postsynaptic recording of responses to the 5X light ChR2 paradigm. Traces below the recording correspond to (purple) LED lights on and off cycles and (blue) nerve stimulation, with the entire 5X paradigm shown in black. (**E, G)** Morphological plasticity of NMJs upon (**E**) 5X nerve and (**G**) 5X ChR2 stimulation. (**E**) shows an instance of extending and retracting synaptopods (arrows mark moving synaptopods, white lines are fiduciary markers) in a presynaptic mCD8-GFP-labeled preparation imaged live. (**G**) shows an example of enhanced ghost bouton formation (arrows) in a fixed preparation double labeled with anti-HRP (green) and anti-DLG (red) antibodies. N [#experimental; #control animals] is (from left to right): C, D: [12;6], [5;5], [13;9]. *= $p<0.05$, **=$p<0.001$. Calibration scale is 3 μm in E and 6 μm in G.

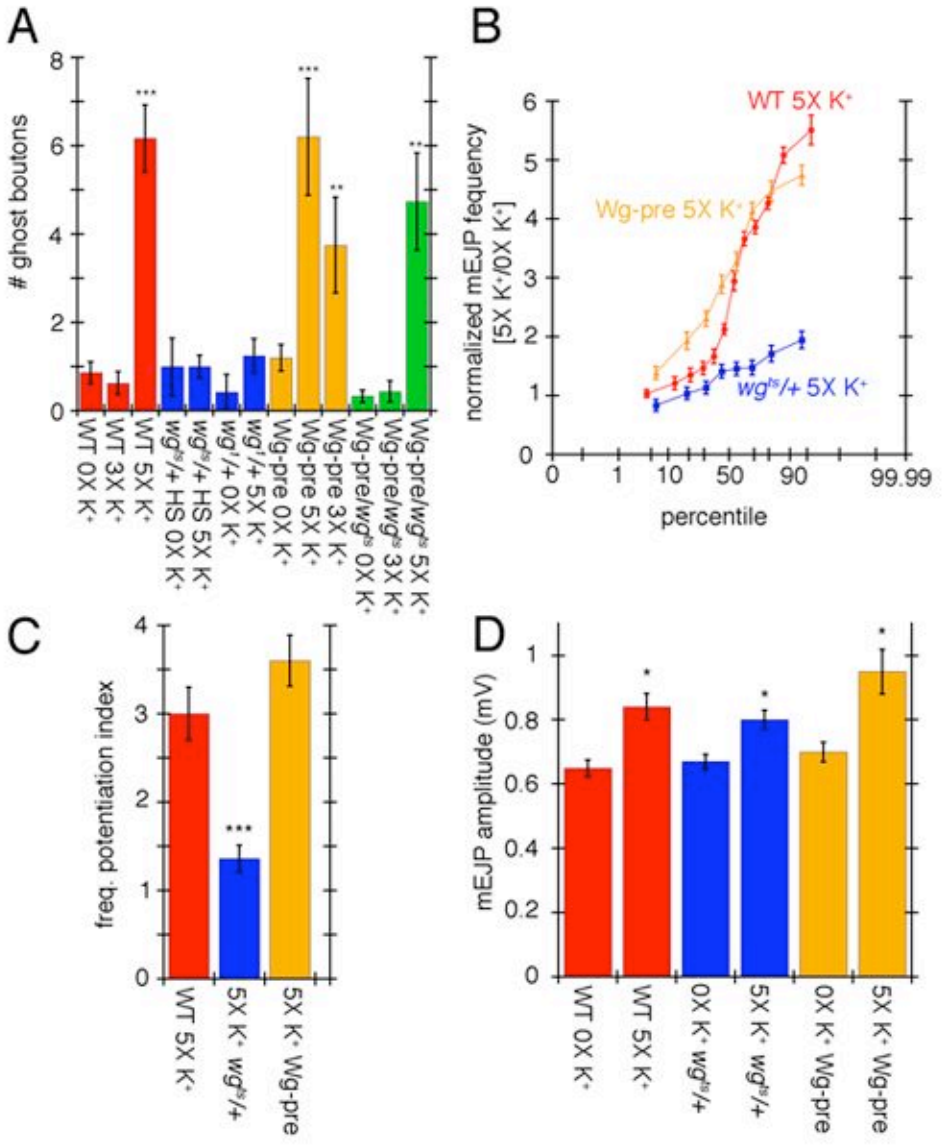

Figure 6
Ataman et al

Figure 4-6

Figure 4-6. Wg signaling regulates ghost bouton formation and mEJP potentiation. **(A)** Number of ghost boutons after 0X, 3X, or 5X spaced K^+ stimulation in controls (red), wg^{ts}/+ heterozygous and wg^{1} homozygous mutants (blue), upon expressing UAS-Wg in motorneurons (orange), and upon rescuing wg^{ts} with UAS-Wg in motorneurons (green). (**B**) Normalized probability distribution of mEJP frequencies in the indicated genotypes after spaced 5X K^+ stimulation. Normalization was obtained by dividing the frequency of experimental samples by the mean control frequencies. (**C)** Frequency potentiation index. (**D**) Mean mEJP amplitude in the indicated genotypes in controls and samples subjected to spaced 5X K^+ stimulation. N [# arbors; # animals] is (from left to right): (A): [22;11], [8;4], [18;9], [12;6], [15;8], [12;6], [16;8], [12;6], [13;7], [14;7], [12;6], [9;5], [15;8]. In (B-D) N [# experimental; # control animals] is [12;6], [7;7], and [6;8]. *= p<0.05, **= p<0.001, ***=p<0.0001.

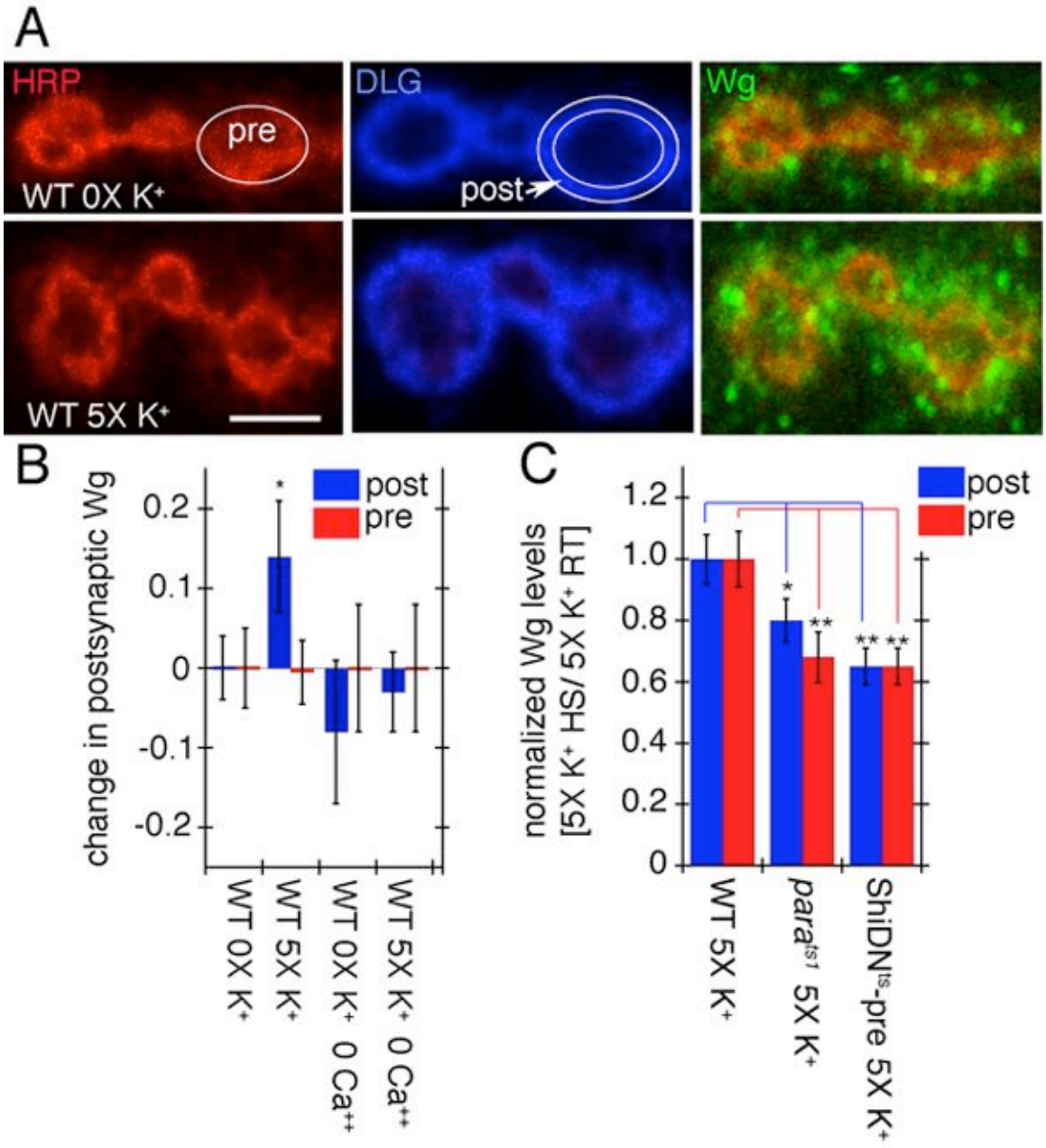

Figure 7
Ataman et al.

Figure 4-7

Figure 4-7. Activity-dependent Wg secretion by synaptic boutons. (**A**) Wg immunoreactivity (green) at synaptic boutons of wild type (top row) controls and (bottom row) specimens subjected to spaced 5X K^+ depolarization in samples triple stained with anti-HRP (red), anti-DLG (blue) and anti-Wg (green). Images correspond to single confocal slices. The postsynaptic (DLG minus HRP) and the presynaptic (HRP) areas are outlined in white in the middle-upper and the left-upper rows respectively. (**B**) Pre- (red) and postsynaptic (blue) Wg levels in wild type controls and samples subjected to spaced 5X K^+ depolarization, in the presence or absence of Ca^{++}. Numbers in the Y-axis correspond to the difference in mean Wg intensity levels between control and experimental samples. (**C**) Pre- (red) and postsynaptic (blue) Wg levels in response to 5X K^+ depolarization after blocking activity with *para*^{ts1} and ShiDN^{ts}-pre. Wg levels were normalized by dividing the Wg levels after the 5X K^+ paradigm at restrictive temperature (HS) by the Wg levels after the 5X K^+ paradigm at permissive temperature (RT).
N [#branches quantified; # animals] is (from left to right): (B): [7;4], [12;7], [4;3], [6;4]; (C): [12;8], [13;8], [13;8].Calibration scale is 2.5 μm in A.

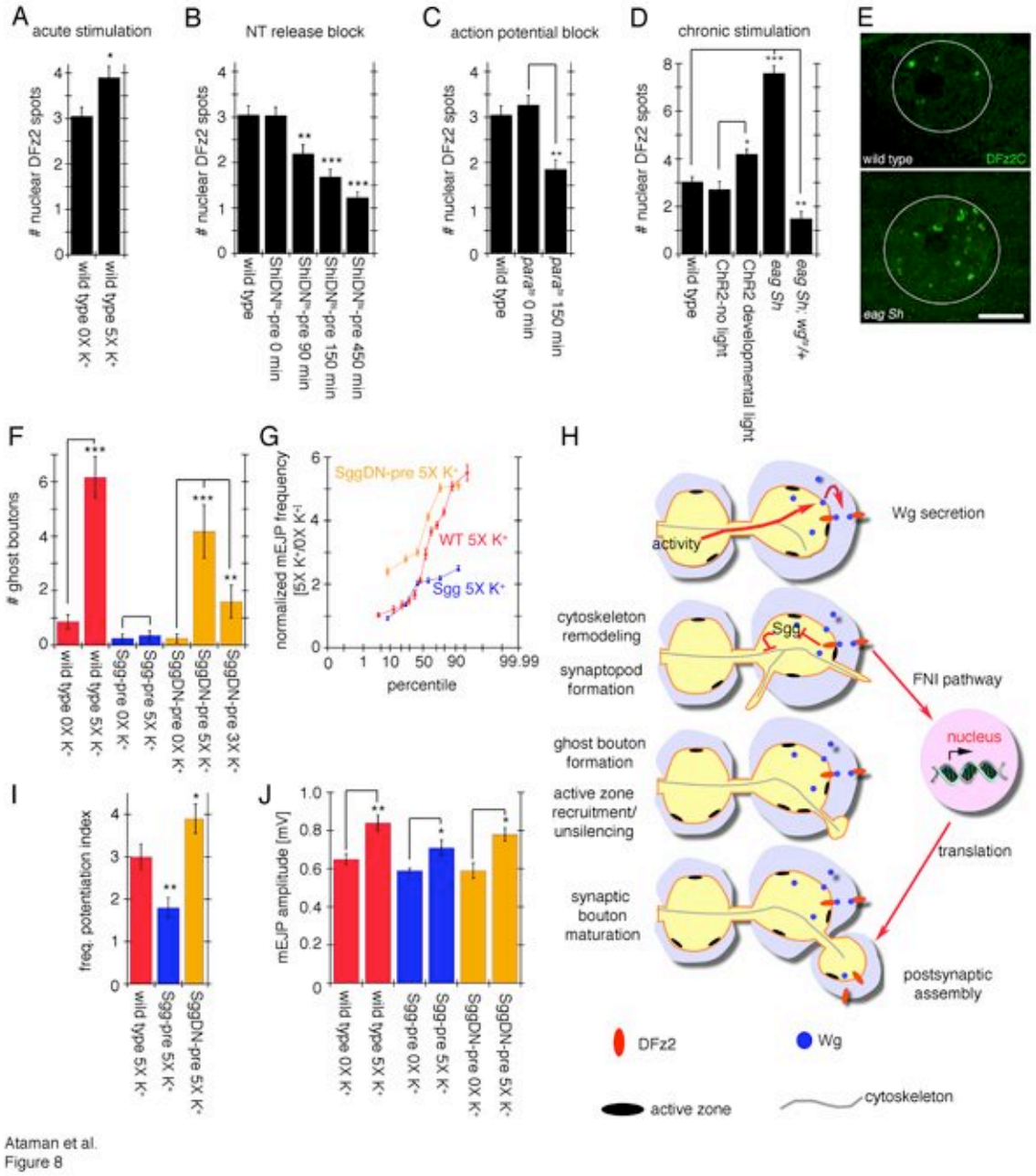

Ataman et al.
Figure 8

Figure 4-8

Figure 4-8. Activity-dependent regulation of postsynaptic DFz2C nuclear import and role of Sgg in rapid activity-dependent changes at the NMJ. (**A-D**) Number of DFz2C nuclear spots in **(A)** wild type after spaced 5X K^+ depolarization, **(B)** larvae expressing $ShiDN^{ts}$ in motorneurons and in which neurotransmitter release was blocked for 90, 150, and 450 min, **(C)** *para*^{ts1} animals in which action potentials were blocked for 150 min, and **(D)** *eag Sh* mutants (chronic hyperexcitability) and larvae expressing ChR2 in motorneurons and stimulated by light with a developmental paradigm (see Methods). (**E**) Nuclear DFz2C immunoreactivity in the postsynaptic muscle nucleus of wild type (top) and *eag Sh* mutants. White circles outline the nucleus. (**F, G, I, J)** Effect of alterations in Sgg activity in ghost bouton number and mEJP potentiation. **(F)** Number of ghost boutons, **(I)** mEJPs frequency potentiation index and (**J**) and mean mEJP amplitude upon spaced 5X K^+ stimulation in controls (red) as well as in animals overexpressing Sgg (blue) and SggDN (orange) in motorneurons. (**G**) shows the normalized probability distribution of mEJP frequencies in the above genotypes. *= $p<0.05$, **= $p<0.001$, ***=$p<0.0001$. Calibration scale in E is 11 μm. **(H)** Proposed model for activity-dependent regulation of synapse formation at the NMJ. Patterned activity induces Wg secretion from presynaptic terminals. Once released, Wg binds to DFz2 receptors localized both pre- and postsynaptically. In the presynaptic cell, Wg transduction leads to the formation of synaptopods and ghost boutons in part through regulation of cytoskeletal dynamics, which involves inhibition of GSK-3ß/Sgg activity. In the postsynaptic cell, Wg activates the

Frizzled Nuclear Import (FNI) pathway and signals the formation/stabilization of synaptic specializations through transcriptional regulation. In (A-D, F) N [# of arbors; #of animals] is (from left to right), (A): [32;6], [36;6]; (B): [36;6], [32;6], [30;5], [24;5], [24;5]; (C): [36;6], [12;4], [18;4]; (D): [36;6], [18;3], [30;5], [18;4], [32;6]; (F): [22;11], [18;9], [8;4], [12;6], [8;4], [14;7], (14;7). In (G, I, J) N [# experimental; #controls animals] is (from left to right): (H, I): [12;6], [6;3], [6;3].

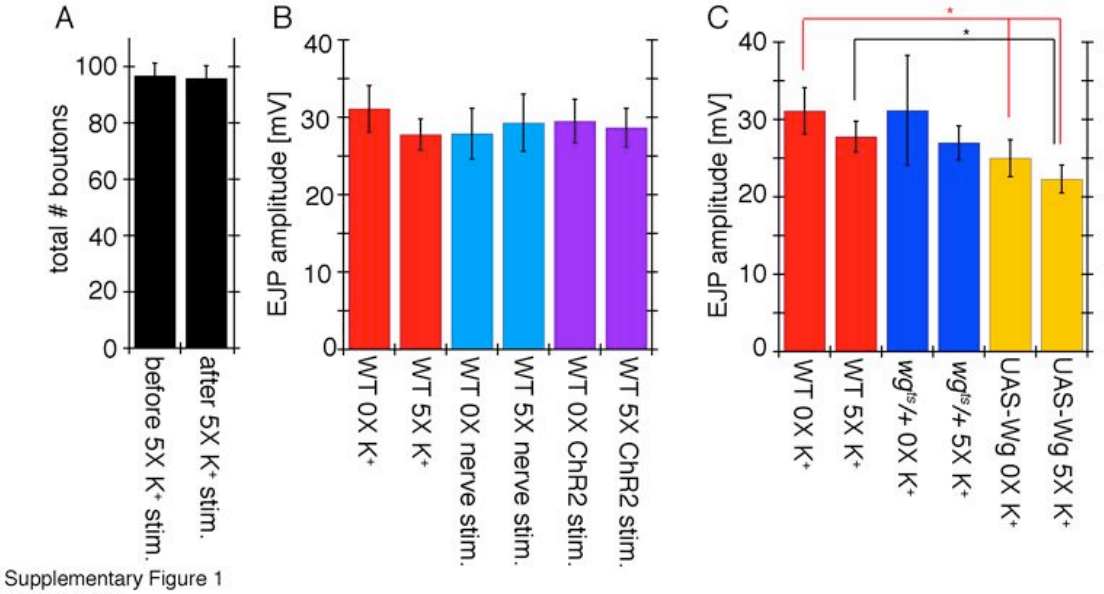

Supplementary Figure 1
Ataman et al.

Supplemental Figure 4-1

Supplemental Figure 4-1. Synaptic bouton number and EJP amplitude does not change upon spaced 5X K^+ depolarization. (**A**) Total number of boutons at muscles 6 and 7 (A3) in the same samples before and after spaced 5X K^+ depolarization. (**B**, **C**) Mean EJP amplitude in (**B**) control and samples stimulated with 5X K^+ depolarization (red), 5X nerve stimulation (light blue), and 5X ChR2 stimulation (purple), and (**C**) wild type (red), wg^{ts}/+ heterozygotes (blue), and larvae expressing UAS-Wg presynaptically, in control and preparations subjected to spaced 5X K^+ stimulation. N [# arbors; # animals] is [13;7] in (A). In (B, C) N [# experimental; #controls animals] is (from left to right): (B): [12;6], [4;5], [13;9] and C: [12;6], [7;7], [8;6].*= $p<0.05$.

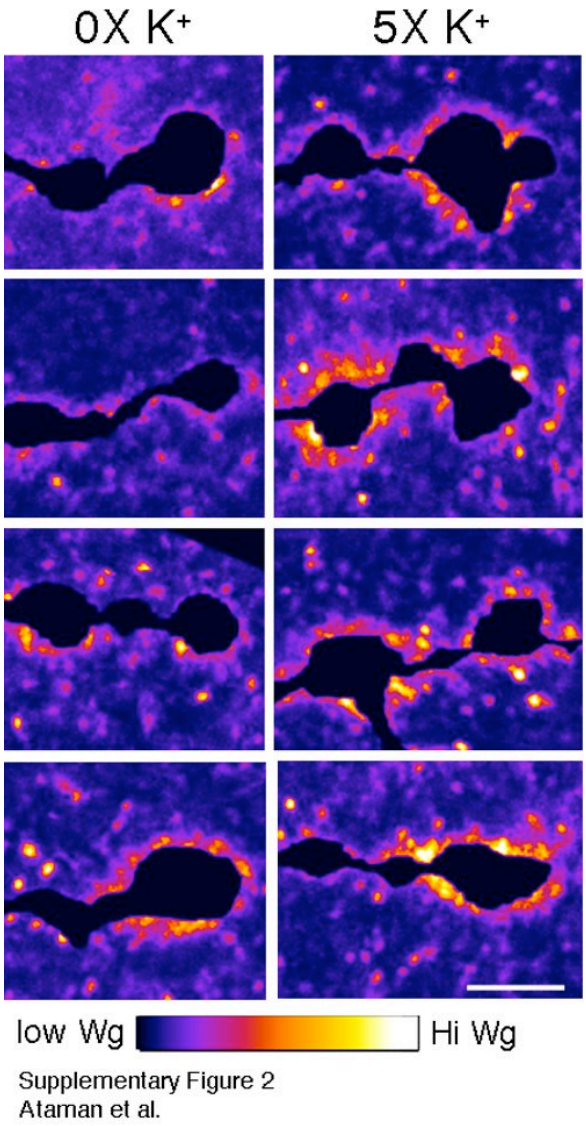

Supplemental Figure 4-2

Supplemental Figure 4-2. Enhanced Wg secretion after spaced 5X K^+ stimulation. Micrographs are pseudocolored intensity heat maps of Wg postsynaptic immunoreactivity in (left column) 0X K^+ control and (right column) spaced 5X K^+ stimulated samples. Each panel shows a representative single confocal slice of a branch at muscle 6 and 7 (A3) from a different animal. The area occupied by HRP (presynaptic compartment) has been removed for clarity. Heat maps were generated with Image J software by using the fire table. Scale of intensities is shown at the bottom of the figure. Calibration bar is 4 μm.

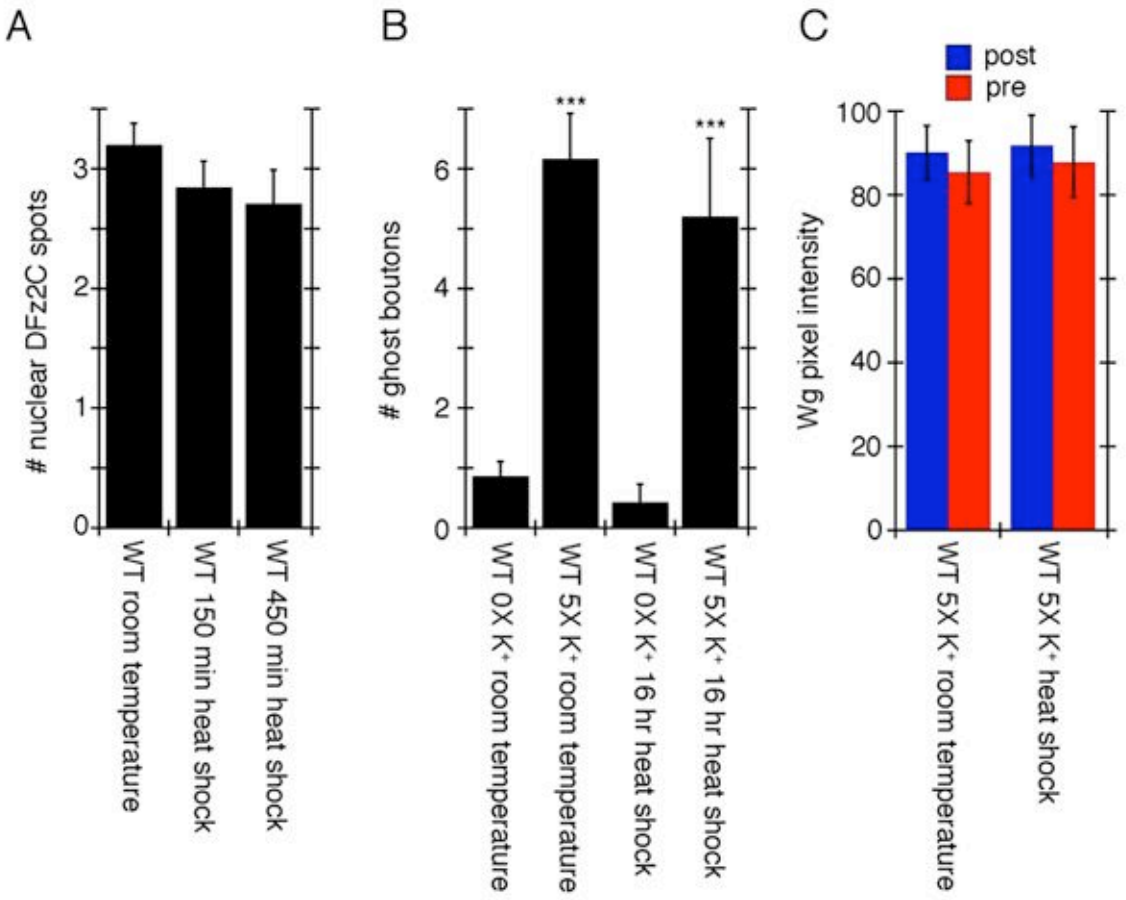

Supplementary Figure 3
Ataman et al.

Supplemental Figure 4-3

Supplemental Figure 4-3. Temperature controls for heat shock paradigms applied to temperature sensitive mutants. (**A**) Number of nuclear DFz2C spots in unstimulated wild type at room temperature and the indicated temperature shifts. (**B**) Number of ghost boutons in controls and in samples subjected to spaced 5X K^+ depolarization at room temperature and upon a temperature shift. (**C**) Wg levels in pre- and postsynaptic compartments in wild type at room temperature and upon a temperature shift. In (A,B) N [# arbors; # animals] is (from left to right): (A): [36;6], [18;4], [18;4]; (B) [22;11], [18;9], [7;4], [11;6]. In (C) N [# branches quantified; # animals] is: [6;4] and [6;4]. *** = $p < 0.0001$.

CHAPTER 5

Final Conclusions and General Discussion

The work presented in this dissertation is focused on the molecular and cellular mechanisms of synaptic plasticity and the elucidation of the role of Wnt/Wg signaling in this process. Our studies showed that patterned activity induces rapid structural and functional modifications at the larval NMJ. Further, this rapid synapse remodeling is determined by the activation of alternative Wnt signaling pathways in the pre- and postsynaptic cells, elicited by activity-dependent Wg release. While secreted Wg activates a divergent canonical pathway that organizes cytoskeletal dynamics through GSK3- β in the presynaptic cell, it simultaneously activates a novel postsynaptic Wg pathway, the Frizzled Nuclear Import (FNI) pathway. In this unconventional Wg pathway, DFz2 is endocytosed from the postsynaptic membrane and transported to the nucleus through interactions with dGRIP, a 7 PDZ domain protein. Upon proteolytic cleavage of the DFz2 receptors at the perinuclear area, the C-terminal fragment of DFz2 is translocated into the nucleus for potential transcriptional regulation of genes involved in synapse development and plasticity.

Activity-dependent synaptic modifications at the larval NMJ

The finding that patterned stimulation of motorneurons results in rapid formation of filopodia and synaptic bouton precursors, challenges the long lasting belief in the field that activity-dependent structural changes at the NMJ occur simply as the result of long-term developmental changes in activity. According to that view, rapid structural synaptic modifications, such as those occurring in dendritic spines, are restricted to central neurons. Here we demonstrate with

three independent methods that patterned activity induces rapid structural changes at the NMJs of live preparations quite similar to those observed in mammalian brain. Thus, these findings highlight a general physiological process underlying synaptic growth and provide the groundwork towards a better understanding of acute synaptic plasticity using the larval NMJ as a model.

Rapid activity dependent synaptic modifications were not only limited to the structural level, a significant potentiation of spontaneous neurotransmitter release was also observed upon patterned activity. Previous studies have implicated spontaneous miniature synaptic potentials (minis) in fundamental synaptic processes such as synapse formation and maturation (Zucker, 2005). Intriguingly, minis were found to affect major aspects of the postsynapse such as glutamate receptor composition, local dendritic protein synthesis (Chung and Kavalali, 2006) and even CaMKII activity (Murphy et al., 1994). These findings support a key role for minis in the regulation of postsynaptic responsiveness to presynaptic signals. Similarly, potentiation of minis in our studies could also be initiating postsynaptic processes that would ultimately stabilize the undifferentiated presynaptic boutons.

New insights into the mechanisms of Wnt signaling at synapses

We have also provided compelling evidence that a bidirectional Wg signaling is downstream of rapid activity-driven synaptic modifications. Previous studies documented that DFz2 receptors are localized in both pre- and postsynaptic membranes, and that Wg is secreted by presynaptic boutons

(Packard et al., 2002). These observations raised the possibility of Wg operating both in an anterograde and an autocrine fashion. In our study, we provided evidence that presynaptically secreted Wnt/Wg actually activates simultaneously alternative transduction pathways in the pre- and postsynaptic cell, a divergent canonical pathway in the presynaptic cell, and the FNI pathway in the postsynaptic cell. This represents a significant advance in understanding how secreted signals can coordinate the development of the different compartments at the synapse. Further, we uncovered a new transduction mechanism in which the Wnt receptor DFz2 was cleaved and translocated into the nucleus. Although the cleavage and nuclear import of transmembrane receptors has been previously demonstrated for other proteins such as Notch and Amyloid Precursor Protein (APP) (Fortini, 2002), this was the first report of a Wnt receptor fragment being imported into the nucleus. These studies highlight the notion that there can be a direct communication between signaling events at the plasma membrane and functions in the nucleus. Notably, a recent study reported that the mammalian Wnt receptors Fzd2, LRP5, Kremen1 and Kremen2, which normally exhibit membrane and cytoplasmic localization in dormant blastocysts, are translocated into the nucleus upon blastocyst activation (Xie et al., 2008). This evidence suggests that Wnt signaling through the nuclear translocation of Wnt receptors, uncovered by our study, is likely a conserved mechanism whose significance in other cell types and organisms remains to be explored.

Our findings demonstrate that cleavage and nuclear import of DFz2 is required for normal synapse development. While we postulate that DFz2 cleavage appears to be constitutive or Wg independent, nuclear import of the DFz2-C fragment appears to be Wg-dependent. However, the exact mechanism by which Wg regulates the nuclear import of a fragment of the receptor that does not directly bind to Wg, DFz2-C, remains to be determined. One possibility is that, upon Wg binding to DFz2, the cytoplasmic region of DFz2 becomes post-translationally modified, thus making the DFz2-C fragment competent for nuclear import. A previous study showed that the phosphorylation of C-terminal serine residues in DFz1 by atypical protein kinase C (aPKC) is critical for DFz1 function during the non-canonical PCP pathway in the *Drosophila* eye (Djiane et al., 2005). These serine residues are also present in the C-terminal of DFz2. Further, aPKC is present in postsynaptic muscles and is a critical regulator of NMJ development (Ruiz-Canada et al., 2004). It would be tempting to speculate that Wg binding to DFz2 could similarly induce the phosphorylation of DFz2-C by aPKC, and that this event might mark DFz2-C for nuclear import. Such a mechanism would be also compatible with the finding that the nuclear import of DFz2-C is an activity dependent process, and that aPKC is a key downstream regulator of long-term plasticity (Drier et al., 2002; Ling et al., 2002). Future cell culture and *in vivo* studies using DFz2 transgenes in which phosphorylation is mimicked or blocked should address this possibility.

Getting a GRIP on Wnt/Wg signaling

In our studies we found that bidirectional Wg signaling is an important pathway required for activity-driven synapse modifications at the NMJ. However, it is unreasonable to suggest that Wg is the only signal that organizes all structural and functional processes during plasticity. It is likely that other known plasticity pathways such as cAMP, CaMKII or TGF-β cooperate with the Wg pathway in orchestrating rapid synapse dynamics. Indeed, previous studies have demonstrated the presence of a retrograde pathway, the TGF-β pathway, which contributes to NMJ plasticity (Marques, 2005). Mutations in genes encoding components of the TGF-β pathway lead to some synaptic phenotypes which are shared by Wg mutants, including a dramatic reduction in bouton outgrowth and detachment of pre- and postsynaptic membranes at the ultrastructural level (Aberle et al., 2002; McCabe et al., 2004; Packard et al., 2002). Therefore, it is possible that the anterograde Wg and the retrograde TGF-β pathways crosstalk during synapse development and plasticity, in the same manner as shown during cell fate determination and differentiation of epithelial cells (Fuentealba et al., 2007). A candidate molecule that could mediate such an interaction between two signaling pathways could be the multi-domain scaffolding protein dGRIP. Members of the GRIP family of proteins have been suggested to associate with a variety of proteins and signaling pathways that regulate synaptic transmission and plasticity in the mammalian brain (Kim and Sheng, 2004). Our study showed that dGRIP is a key component of the anterograde Wg signaling pathway. However, dGRIP exhibits dynamic localization in both pre-and postsynaptic

compartments. In addition, dGRIP has seven PDZ domains that can multimerize and/or potentially interact with synaptic TGF-β pathway members such as Sax and Tkv receptors, which contain type II and type III PDZ binding motifs respectively. Finally, unpublished observations suggest that components of the TGF-β pathway at the NMJ are altered upon dGRIP downregulation (Ataman, B. unpublished). Therefore, dGRIP is in an excellent position to form signaling scaffolds at the synapses, which could regulate a crosstalk between Wg and TGF-β signaling pathways.

Notably, mammalian GRIP, similar to dGRIP in our studies, exhibits close association with vesicular structures and the cytoskeleton (Dong et al., 1999; Wyszynski et al., 1999). In addition, dGRIP and mammalian GRIP homologs share high sequence homology and very similar PDZ domain organization. Thus, it is likely that the synaptic function of GRIP proteins is conserved across species. Given that Wnt signaling is also important for synapse development and plasticity in the mammalian brain it is likely that GRIP might have a similar roles at those synapses.

Activity-dependent gene expression and nuclear DFz2 function

Previous studies have established that long-term plasticity and long term memory is dependent on the regulation of gene expression (Pittenger and Kandel, 2003). In our studies, we showed that Wg signaling is transduced through the nuclear translocation of DFz2-C in the postsynaptic cell in an activity-dependent manner. In addition, we demonstrated that the rapid synaptic

modifications induced by patterned activity required new protein synthesis. An important future goal will be to identify target genes regulated by Wg signaling likely downstream of activity. A genome-wide microarray screen using different Wg and DFz2 mutant alleles would be very informative to identify the transcriptional targets of the nuclear FNI pathway. Analysis of the DFz2-C peptide sequence did not yield any obvious DNA-binding domain, thus DFz2-C likely regulates gene expression through a transcriptional or a chromatin complex.

Remarkably, DFz2-C molecules do not show diffuse localization throughout the nucleus as many known transcription factors do; rather, they form distinct intranuclear subdomains or foci. Previous studies suggested that compartmentalization of the nucleus into distinct domains provides the spatial isolation of nuclear processes such as transcription, RNA processing and splicing (Zimber et al., 2004). In fact, several transcriptional regulators including CREB-binding protein (CBP) are found to be localized in distinct nuclear foci and sites of active transcription (Pombo et al., 1998; von Mikecz et al., 2000). Interestingly, preliminary experiments in the lab showed that a promising nuclear protein, A-type Lamin (LamC), forms intranuclear foci in the postsynaptic nucleus which colocalize with DFz2 foci. In addition, “transcription factories” marked by an antibody against active RNA polymease II were found to be juxtaposed to DFz2-C/LamC foci (Speese S., Barria R., Ataman B. and Budnik V., manuscript in preparation). A-type lamins has been implicated in the regulation of gene expression and nuclear function, and misregulation of lamin function has been

linked to several human diseases (Vlcek and Foisner, 2007). The structural link between DFz2 and Lamin in the postsynaptic nucleus could aid to identify special nuclear/chromosomal regions where specific sets of target genes downstream of the FNI pathway are regulated. Prospective studies involving the identification and characterization of the nuclear function of DFz2-C foci could give us great insights into the molecular components and other potentially converging signaling pathways that are activated by Wg in an activity-dependent manner.

In summary, the studies detailed in this dissertation have addressed fundamental questions regarding the mechanisms of synapse development and plasticity. The identification of a novel signaling pathway, a prominent scaffolding protein involved in this pathway and a molecular mechanism by which the alterations in synaptic activity are translated into structural and functional modifications at the synapse, have significantly advanced our mechanistic understanding of how synaptic architecture and physiology are dynamically regulated. The fruit fly larval NMJ continues to be an exquisite model system for the discovery of genetic and molecular mechanisms underlying the fundamentals of synaptic function. Elucidation of these basic mechanisms may help us to understand complex processes occurring in the brain as well as to establish successful neurological disease models with the hope of developing new treatments.

ACKNOWLEDGEMENTS

I would like to acknowledge the following people with their corresponding contributions to the each chapters.

Chapter II (Nuclear Wg/DFz2 signaling project): Dennis Mathew is the first one who observed nuclear DFz2C spots and initiated the Frizzled Nuclear Import pathway project. I joined him to carry out the critical nuclear import and cleavage assays in S2 cells as well as the synaptic rescue experiments to successfully complete and publish the project. I would like to thank my dear friend Dennis for both being a great example of a researcher and collaborator. I would also like to thank Dr.Susan Cumberledge and her students for sharing DFz2 antibodies and mutants with us.

Chapter III (dGRIP project): I would like to thank James Ashley for generating very critical dGRIP-RNAi and dGRIP-RFP constructs. James has been also extremely helpful during the progression and publication of the dGRIP project with his continuous input and discussions. I would also like to acknowledge Dennis Mathew for teaching me the DFz2 internalization assay and helping me to develop the cellular link between Wg signaling and dGRIP. I would like to thank Dr. Michael Gorczyca for imaging beautiful dGRIP-RFP movies as well as for teaching me live-imaging techniques. I would like to acknowledge the important contribution of David Gorczyca for conducting the Electron Microscopy experiments of dGRIP alleles. I would also like to acknowledge Dr.Stephen

Sigrist and his student Carolin Wichmann for real-time PCR experiments as well as for a constant exchange of ideas and reagents.

Chapter IV (Activity-Dependent Wnt Signaling project): Foremost, I would like to deeply thank James for his very significant contributions during progression and publication of this project. James did all the electrophysiology experiments as well as conducted nerve stimulation and light stimulation paradigms. James also quickly established the live-imaging technique in intact animals to explore the fate of ghost boutons. I am also very grateful to Dr.Michael Gorczyca who first noticed the “synaptopod” structures and conducted a lot of live-imaging which helped me to establish the basis of this project. I would also like to acknowledge Preethi Ramachandran for her hard work during the resubmission of the paper. I would also like to acknowledge Dr.Stephen Sigrist and his student Wernher Fouquet for sharing some of their live-imaging observations with us.

In general, I am grateful for all the great help and support on the various projects from the past and present members of the Budnik lab: Dr. Catalina Ruiz-Canada, Dr. Mary Packard, Dr.Dennis Mathew, Dr. James Ashley, Dr.Michael Gorczyca, David Gorczyca, Stephanie Moeckel-Cole, Marietta Walsh, Dr. Hemachand Tummala, Catherine Luce, Dr. Sean Speese, Ceren Korkut, Yuly Fuentes, Romina Barria, Fransisco Urra . I would also like to thank Dr. Marc Freeman, Dr. Scott Waddell and Dr. Patrick Emery for their continuous encouragement and support throughout my dissertation. I would also like to

thank Brian Bishop and Dawn Merdaa for creating a happy and efficient work environment in the lab. Finally, I would like to express my deep gratitude for the guidance and support of my advisor and dear friend, Dr. Vivian Budnik. All of the above work would not have been successful without her guidance, suggestions and inspiration.

REFERENCES:

Aberle, H., Haghighi, A. P., Fetter, R. D., McCabe, B. D., Magalhaes, T. R., and Goodman, C. S. (2002). wishful thinking Encodes a BMP Type II Receptor that Regulates Synaptic Growth in Drosophila. Neuron *33*, 545-558.

Ahmad-Annuar, A., Ciani, L., Simeonidis, I., Herreros, J., Fredj, N. B., Rosso, S. B., Hall, A., Brickley, S., and Salinas, P. C. (2006). Signaling across the synapse: a role for Wnt and Dishevelled in presynaptic assembly and neurotransmitter release. J Cell Biol *174*, 127-139.

Allen, M. J., Shan, X., Caruccio, P., Froggett, S. J., Moffat, K. G., and Murphey, R. K. (1999). Targeted expression of truncated glued disrupts giant fiber synapse formation in Drosophila. J Neurosci *19*, 9374-9384.

Anderson, M. S., Halpern, M. E., and Keshishian, H. (1988). Identification of the neuropeptide transmitter proctolin in Drosophila larvae: characterization of muscle fiber-specific neuromuscular endings. J Neurosci *8*, 242-255.

Ashley, J., Packard, M., Ataman, B., and Budnik, V. (2005). Fasciclin II signals new synapse formation through amyloid precursor protein and the scaffolding protein dX11/Mint. J Neurosci *25*, 5943-5955.

Ataman, B., Ashley, J., Gorczyca, D., Gorczyca, M., Mathew, D., Wichmann, C., Sigrist, S. J., and Budnik, V. (2006a). Nuclear trafficking of Drosophila Frizzled-2 during synapse development requires the PDZ protein dGRIP. Proc Natl Acad Sci U S A *103*, 7841-7846.

Ataman, B., Budnik, V., and Thomas, U. (2006b). Scaffolding proteins at the Drosophila neuromuscular junction. Int Rev Neurobiol *75*, 181-216.

Atwood, H. L., Govind, C. K., and Wu, C. F. (1993). Differential ultrastructure of synaptic terminals on ventral longitudinal abdominal muscles in Drosophila larvae. J Neurobiol *24*, 1008-1024.

Bailey, C. H., Kandel, E. R., and Si, K. (2004). The persistence of long-term memory: a molecular approach to self-sustaining changes in learning-induced synaptic growth. Neuron *44*, 49-57.

Balice-Gordon, R. J., Chua, C. K., Nelson, C. C., and Lichtman, J. W. (1993). Gradual loss of synaptic cartels precedes axon withdrawal at developing neuromuscular junctions. Neuron *11*, 801-815.

Beaumont, V., Zhong, N., Froemke, R. C., Ball, R. W., and Zucker, R. S. (2002). Temporal synaptic tagging by I(h) activation and actin: involvement in long-term facilitation and cAMP-induced synaptic enhancement. Neuron *33*, 601-613.

Bennett, M. R. (2000). The concept of long term potentiation of transmission at synapses. Prog Neurobiol *60*, 109-137.

Biederer, T., Sara, Y., Mozhayeva, M., Atasoy, D., Liu, X., Kavalali, E. T., and Sudhof, T. C. (2002). SynCAM, a synaptic adhesion molecule that drives synapse assembly. Science *297*, 1525-1531.

Binari, R. C., Staveley, B. E., Johnson, W. A., Godavarti, R., Sasisekharan, R., and Manoukian, A. S. (1997). Genetic evidence that heparin-like glycosaminoglycans are involved in wingless signaling. Development *124*, 2623--2632.

Bladt, F., Tafuri, A., Gelkop, S., Langille, L., and Pawson, T. (2002). Epidermolysis bullosa and embryonic lethality in mice lacking the multi-PDZ domain protein GRIP1. Proc Natl Acad Sci U S A *99*, 6816-6821.

Bliss, T. V., and Lomo, T. (1973). Long-lasting potentiation of synaptic transmission in the dentate area of the anaesthetized rabbit following stimulation of the perforant path. J Physiol *232*, 331-356.

Bourouis, M. (2002). Targeted increase in shaggy activity levels blocks wingless signaling. Genesis *34*, 99-102.

Braithwaite, S. P., Xia, H., and Malenka, R. C. (2002). Differential roles for NSF and GRIP/ABP in AMPA receptor cycling. Proc Natl Acad Sci U S A *99*, 7096-7101.

Brand, A. H., and Perrimon, N. (1993). Targeted gene expression as a means of altering cell fates and generating dominant phenotypes. Development *118*, 401-415.

Broadie, K., and Bate, M. (1993). Innervation directs receptor synthesis and localization in Drosophila embryo synaptogenesis [see comments]. Nature *361*, 350-353.

Broadie, K., Rushton, E., Skoulakis, E. M., and Davis, R. L. (1997). Leonardo, a Drosophila 14-3-3 protein involved in learning, regulates presynaptic function. Neuron *19*, 391-402.

Budnik, V., Koh, Y. H., Guan, B., Hartmann, B., Hough, C., Woods, D., and Gorczyca, M. (1996). Regulation of synapse structure and function by the Drosophila tumor suppressor gene dlg. Neuron *17*, 627-640.

Budnik, V., and Ruiz-Canada, C. (2006). The Fly Neuromuscular Junction: Structure and Function, Volume 75: Second Edition, Academic Press).

Budnik, V., Zhong, Y., and Wu, C. F. (1990). Morphological plasticity of motor axons in Drosophila mutants with altered excitability. J Neurosci *10*, 3754-3768.

Cadigan, K. M., Fish, M. P., Rulifson, E. J., and Nusse, R. (1998). Wingless repression of Drosophila frizzled 2 expression shapes the Wingless morphogen gradient in the wing. Cell *93*, 767--777.

Castellucci, V. F., Frost, W. N., Goelet, P., Montarolo, P. G., Schacher, S., Morgan, J. A., Blumenfeld, H., and Kandel, E. R. (1986). Cell and molecular analysis of long-term sensitization in Aplysia. J Physiol (Paris) *81*, 349-357.

Chang, D. C., and Reppert, S. M. (2003). A novel C-terminal domain of drosophila PERIOD inhibits dCLOCK:CYCLE-mediated transcription. Curr Biol *13*, 758-762.

Chen, C., and Struhl, G. (1999). Wingless transduction by the Frizzled and Frizzled2 proteins of Drosophila. Development *126*, 5441--5452.

Chen, J., Park, C. S., and Tang, S. J. (2006). Activity-dependent synaptic Wnt release regulates hippocampal long term potentiation. J Biol Chem *281*, 11910-11916.

Chklovskii, D. B., Mel, B. W., and Svoboda, K. (2004). Cortical rewiring and information storage. Nature *431*, 782-788.

Chklovskii, D. B., Schikorski, T., and Stevens, C. F. (2002). Wiring optimization in cortical circuits. Neuron *34*, 341-347.

Chung, C., and Kavalali, E. T. (2006). Seeking a function for spontaneous neurotransmission. Nat Neurosci *9*, 989-990.

Ciani, L., Krylova, O., Smalley, M. J., Dale, T. C., and Salinas, P. C. (2004). A divergent canonical WNT-signaling pathway regulates microtubule dynamics: dishevelled signals locally to stabilize microtubules. J Cell Biol *164*, 243-253.

Ciani, L., and Salinas, P. C. (2005). WNTs in the vertebrate nervous system: from patterning to neuronal connectivity. Nat Rev Neurosci *6*, 351-362.

Collins, R. T., Furukawa, T., Tanese, N., and Treisman, J. E. (1999). Osa associates with the Brahma chromatin remodeling complex and promotes the activation of some target genes. Embo J *18*, 7029-7040.

Colman, H., Nabekura, J., and Lichtman, J. W. (1997). Alterations in synaptic strength preceding axon withdrawal. Science *275*, 356-361.

Contractor, A., Rogers, C., Maron, C., Henkemeyer, M., Swanson, G. T., and Heinemann, S. F. (2002). Trans-synaptic Eph receptor-ephrin signaling in hippocampal mossy fiber LTP. Science *296*, 1864-1869.

Corpet, F. (1988). Multiple sequence alignment with hierarchical clustering. Nucleic Acids Res *16*, 10881-10890.

Couso, J. P., Bishop, S. A., and Martinez Arias, A. (1994). The wingless signalling pathway and the patterning of the wing margin in Drosophila. Development *120*, 621-636.

Crossley, C. A. (1978). The morphology and development of the Drosophila muscular system. In The Genetics and Biology of Drosophila, Ashburner, and Wright, eds. (New York, Academic Press).

DasGupta, R., Boutros, M., and Perrimon, N. (2005). Drosophila Wnt/Fz pathways. Sci STKE *2005*, cm5.

Davis, G. W., DiAntonio, A., Petersen, S. A., and Goodman, C. S. (1998). Postsynaptic PKA controls quantal size and reveals a retrograde signal that regulates presynaptic transmitter release in Drosophila. Neuron *20*, 305-315.

Davis, G. W., Schuster, C. M., and Goodman, C. S. (1996). Genetic dissection of structural and functional components of synaptic plasticity. III. CREB is necessary for presynaptic functional plasticity [see comments]. Neuron *17*, 669-679.

De Ferrari, G. V., and Moon, R. T. (2006). The ups and downs of Wnt signaling in prevalent neurological disorders. Oncogene *25*, 7545-7553.

Debski, E. A., and Cline, H. T. (2002). Activity-dependent mapping in the retinotectal projection. Curr Opin Neurobiol *12*, 93-99.

DeFelipe, J. (2002). Sesquicentenary of the birthday of Santiago Ramon y Cajal, the father of modern neuroscience. Trends Neurosci *25*, 481-484.

Del Castillo, J., and Katz, B. (1954). Quantal components of the end-plate potential. J Physiol *124*, 560-573.

Del Rio, T., and Feller, M. B. (2006). Early retinal activity and visual circuit development. Neuron *52*, 221-222.

Djiane, A., Yogev, S., and Mlodzik, M. (2005). The apical determinants aPKC and dPatj regulate Frizzled-dependent planar cell polarity in the Drosophila eye. Cell *121*, 621-631.

Dong, H., O'Brien, R. J., Fung, E. T., Lanahan, A. A., Worley, P. F., and Huganir, R. L. (1997). GRIP: a synaptic PDZ domain-containing protein that interacts with AMPA receptors. Nature *386*, 279-284.

Dong, H., Zhang, P., Liao, D., and Huganir, R. L. (1999). Characterization, expression, and distribution of GRIP protein. Ann N Y Acad Sci *868*, 535-540.

Drier, E. A., Tello, M. K., Cowan, M., Wu, P., Blace, N., Sacktor, T. C., and Yin, J. C. (2002). Memory enhancement and formation by atypical PKM activity in Drosophila melanogaster. Nat Neurosci *5*, 316-324.

Dunaevsky, A., and Mason, C. A. (2003). Spine motility: a means towards an end? Trends Neurosci *26*, 155-160.

Eaton, B. A., and Davis, G. W. (2005). LIM Kinase1 controls synaptic stability downstream of the type II BMP receptor. Neuron *47*, 695-708.

Eaton, B. A., Fetter, R. D., and Davis, G. W. (2002). Dynactin is necessary for synapse stabilization. Neuron *34*, 729-741.

Eickholt, B. J., Walsh, F. S., and Doherty, P. (2002). An inactive pool of GSK-3 at the leading edge of growth cones is implicated in Semaphorin 3A signaling. J Cell Biol *157*, 211-217.

Engert, F., and Bonhoeffer, T. (1999). Dendritic spine changes associated with hippocampal long-term synaptic plasticity. Nature *399*, 66-70.

Eric R. Kandel, J. H. S., Thomas M. Jessell (2000). Principles of Neural Science, McGraw-Hill Professional).

Faeder, I. R., and Salpeter, M. M. (1970). Glutamate uptake by a stimulated insect nerve muscle preparation. J Cell Biol *46*, 300-307.

Feng, Y., Ueda, A., and Wu, C. F. (2004). A modified minimal hemolymph-like solution, HL3.1, for physiological recordings at the neuromuscular junctions of normal and mutant Drosophila larvae. J Neurogenet *18*, 377-402.

Fortini, M. E. (2002). Gamma-secretase-mediated proteolysis in cell-surface-receptor signalling. Nat Rev Mol Cell Biol *3*, 673-684.

Franco, B., Bogdanik, L., Bobinnec, Y., Debec, A., Bockaert, J., Parmentier, M. L., and Grau, Y. (2004). Shaggy, the homolog of glycogen synthase kinase 3, controls neuromuscular junction growth in Drosophila. J Neurosci *24*, 6573-6577.

Fuentealba, L. C., Eivers, E., Ikeda, A., Hurtado, C., Kuroda, H., Pera, E. M., and De Robertis, E. M. (2007). Integrating patterning signals: Wnt/GSK3 regulates the duration of the BMP/Smad1 signal. Cell *131*, 980-993.

Gogel, S., Wakefield, S., Tear, G., Klambt, C., and Gordon-Weeks, P. R. (2006). The Drosophila microtubule associated protein Futsch is phosphorylated by Shaggy/Zeste-white 3 at an homologous GSK3beta phosphorylation site in MAP1B. Mol Cell Neurosci *33*, 188-199.

Goold, R. G., and Gordon-Weeks, P. R. (2004). Glycogen synthase kinase 3beta and the regulation of axon growth. Biochem Soc Trans *32*, 809-811.

Gorczyca, D., Ashley, J., Speese, S., Gherbesi, N., Thomas, U., Gundelfinger, E., Gramates, L. S., and Budnik, V. (2007). Postsynaptic membrane addition depends on the Discs-Large-interacting t-SNARE Gtaxin. J Neurosci *27*, 1033-1044.

Gorczyca, M., Augart, C., and Budnik, V. (1993). Insulin-like receptor and insulin-like peptide are localized at neuromuscular junctions in Drosophila. J Neurosci *13*, 3692-3704.

Gramates, L. S., and Budnik, V. (1999). Assembly and maturation of the Drosophila larval neuromuscular junction. Int Rev Neurobiol *43*, 93-117.

Grieder, N. C., de Cuevas, M., and Spradling, A. C. (2000). The fusome organizes the microtubule network during oocyte differentiation in Drosophila. Development *127*, 4253-4264.

Griffith, L. C., and Budnik, V. (2006). Plasticity and second messengers during synapse development. Int Rev Neurobiol *75*, 237-265.

Guan, B., Hartmann, B., Kho, Y. H., Gorczyca, M., and Budnik, V. (1996). The Drosophila tumor suppressor gene, dlg, is involved in structural plasticity at a glutamatergic synapse. Curr Biol *6*, 695-706.

Hall, A. C., Lucas, F. R., and Salinas, P. C. (2000). Axonal remodeling and synaptic differentiation in the cerebellum is regulated by WNT-7a signaling. Cell *100*, 525-535.

Hebb, D. O. (1949). Organization of behavior (New York, John wiley and Sons, Inc.).

Hirbec, H., Francis, J. C., Lauri, S. E., Braithwaite, S. P., Coussen, F., Mulle, C., Dev, K. K., Coutinho, V., Meyer, G., Isaac, J. T.*, et al.* (2003). Rapid and differential regulation of AMPA and kainate receptors at hippocampal mossy fibre synapses by PICK1 and GRIP. Neuron *37*, 625-638.

Hoogenraad, C. C., Milstein, A. D., Ethell, I. M., Henkemeyer, M., and Sheng, M. (2005). GRIP1 controls dendrite morphogenesis by regulating EphB receptor trafficking. Nat Neurosci *8*, 906-915.

Huberman, A. D. (2007). Mechanisms of eye-specific visual circuit development. Curr Opin Neurobiol *17*, 73-80.

James, T. C., Eissenberg, J. C., Craig, C., Dietrich, V., Hobson, A., and Elgin, S. C. (1989). Distribution patterns of HP1, a heterochromatin-associated nonhistone chromosomal protein of Drosophila. Eur J Cell Biol *50*, 170-180.

Jan, L. Y., and Jan, Y. N. (1976). L-glutamate as an excitatory transmitter at the Drosophila larval neuromuscular junction. J Physiol (Lond) *262*, 215-236.

Jan, L. Y., and Jan, Y. N. (1982). Antibodies to horseradish peroxidase as specific neuronal markers in Drosophila and in grasshopper embryos. Proc Natl Acad Sci U S A *79*, 2700-2704.

Jia, X. X., Gorczyca, M., and Budnik, V. (1993a). Ultrastructure of neuromuscular junctions in Drosophila: comparison of wild type and mutants with increased excitability. J Neurobiol *24*, 1025-1044.

Jia, X. X., Gorczyca, M., and Budnik, V. (1993b). Ultrastructure of neuromuscular junctions in Drosophila: comparison of wild type and mutants with increased excitability [published erratum appears in J Neurobiol 1994 Jul;25(7):893-5]. J Neurobiol *24*, 1025-1044.

Johansen, J., Halpern, M. E., and Keshishian, H. (1989). Axonal guidance and the development of muscle fiber-specific innervation in Drosophila embryos. J Neurosci *9*, 4318-4332.

Kalidas, S., and Smith, D. P. (2002). Novel genomic cDNA hybrids produce effective RNA interference in adult Drosophila. Neuron *33*, 177-184.

Kalil, K., and Dent, E. W. (2005). Touch and go: guidance cues signal to the growth cone cytoskeleton. Curr Opin Neurobiol *15*, 521-526.

Kandel, E. R. (2001). The molecular biology of memory storage: a dialogue between genes and synapses. Science *294*, 1030-1038.

Keshishian, H., Broadie, K., Chiba, A., and Bate, M. (1996). The drosophila neuromuscular junction: a model system for studying synaptic development and function. Annu Rev Neurosci *19*, 545-575.

Keshishian, H., and Chiba, A. (1993). Neuromuscular development in Drosophila: insights from single neurons and single genes. Trends Neurosci *16*, 278-283.

Keshishian, H., Chiba, A., Chang, T. N., Halfon, M. S., Harkins, E. W., Jarecki, J., Wang, L., Anderson, M., Cash, S., Halpern, M. E., and et al. (1993). Cellular mechanisms governing synaptic development in Drosophila melanogaster. J Neurobiol *24*, 757-787.

Kim, E., and Sheng, M. (2004). PDZ domain proteins of synapses. Nat Rev Neurosci *5*, 771-781.

Kitamoto, T. (2001). Conditional modification of behavior in Drosophila by targeted expression of a temperature-sensitive shibire allele in defined neurons. J Neurobiol *47*, 81-92.

Kittel, R. J., Hallermann, S., Thomsen, S., Wichmann, C., Sigrist, S. J., and Heckmann, M. (2006a). Active zone assembly and synaptic release. Biochem Soc Trans *34*, 939-941.

Kittel, R. J., Wichmann, C., Rasse, T. M., Fouquet, W., Schmidt, M., Schmid, A., Wagh, D. A., Pawlu, C., Kellner, R. R., Willig, K. I.*, et al.* (2006b). Bruchpilot promotes active zone assembly, Ca2+ channel clustering, and vesicle release. Science *312*, 1051-1054.

Koenig, J. H., and Ikeda, K. (1989). Disappearance and reformation of synaptic vesicle membrane upon transmitter release observed under reversible blockage of membrane retrieval. J Neurosci *9*, 3844-3860.

Kogan, J. H., Frankland, P. W., Blendy, J. A., Coblentz, J., Marowitz, Z., Schutz, G., and Silva, A. J. (1997). Spaced training induces normal long-term memory in CREB mutant mice. Curr Biol *7*, 1-11.

Koh, Y. H., Popova, E., Thomas, U., Griffith, L. C., and Budnik, V. (1999). Regulation of DLG localization at synapses by CaMKII-dependent phosphorylation. Cell *98*, 353-363.

Krylova, O., Herreros, J., Cleverley, K. E., Ehler, E., Henriquez, J. P., Hughes, S. M., and Salinas, P. C. (2002). WNT-3, expressed by motoneurons, regulates terminal arborization of neurotrophin-3-responsive spinal sensory neurons. Neuron *35*, 1043-1056.

Lammich, S., Kojro, E., Postina, R., Gilbert, S., Pfeiffer, R., Jasionowski, M., Haass, C., and Fahrenholz, F. (1999). Constitutive and regulated alpha-secretase cleavage of Alzheimer's amyloid precursor protein by a disintegrin metalloprotease. Proc Natl Acad Sci U S A *96*, 3922-3927.

Lee, T., and Luo, L. (1999). Mosaic analysis with a repressible cell marker for studies of gene function in neuronal morphogenesis. Neuron *22*, 451-461.

Ling, D. S., Benardo, L. S., Serrano, P. A., Blace, N., Kelly, M. T., Crary, J. F., and Sacktor, T. C. (2002). Protein kinase Mzeta is necessary and sufficient for LTP maintenance. Nat Neurosci *5*, 295-296.

Liu, S. J., and Cull-Candy, S. G. (2005). Subunit interaction with PICK and GRIP controls Ca(2+) permeability of AMPARs at cerebellar synapses. Nat Neurosci *8*, 768-775. Epub 2005 May 2015.

Lo, Y. J., Wang, T., and Poo, M. M. (1991). Repetitive impulse activity potentiates spontaneous acetylcholine secretion at developing neuromuscular synapses. J Physiol (Paris) *85*, 71-78.

Lu, B. (2003). BDNF and activity-dependent synaptic modulation. Learn Mem *10*, 86-98.

Lucas, F. R., Goold, R. G., Gordon-Weeks, P. R., and Salinas, P. C. (1998). Inhibition of GSK-3beta leading to the loss of phosphorylated MAP-1B is an early event in axonal remodelling induced by WNT-7a or lithium. J Cell Sci *111*, 1351-1361.

Macleod, G. T., Hegstrom-Wojtowicz, M., Charlton, M. P., and Atwood, H. L. (2002). Fast calcium signals in Drosophila motor neuron terminals. J Neurophysiol *88*, 2659-2663.

Malenka, R. C., and Nicoll, R. A. (1999). Long-term potentiation--a decade of progress? Science *285*, 1870-1874.

Maletic-Savatic, M., Malinow, R., and Svoboda, K. (1999). Rapid dendritic morphogenesis in CA1 hippocampal dendrites induced by synaptic activity. Science *283*, 1923-1927.

Marques, G. (2005). Morphogens and synaptogenesis in Drosophila. J Neurobiol *64*, 417-434.

Marques, G., Bao, H., Haerry, T. E., Shimell, M. J., Duchek, P., Zhang, B., and O'Connor, M. B. (2002). The Drosophila BMP Type II Receptor Wishful Thinking Regulates Neuromuscular Synapse Morphology and Function. Neuron *33*, 529-543.

Marques, G., Haerry, T. E., Crotty, M. L., Xue, M., Zhang, B., and O'Connor, M. B. (2003). Retrograde Gbb signaling through the Bmp type 2 receptor Wishful Thinking regulates systemic FMRFa expression in Drosophila. Development *130*, 5457-5470.

Marrus, S. B., Portman, S. L., Allen, M. J., Moffat, K. G., and DiAntonio, A. (2004). Differential localization of glutamate receptor subunits at the Drosophila neuromuscular junction. J Neurosci *24*, 1406-1415.

Mathew, D., Ataman, B., Chen, J., Zhang, Y., Cumberledge, S., and Budnik, V. (2005). Wingless signaling at synapses is through cleavage and nuclear import of receptor DFrizzled2. Science *310*, 1344-1347.

Mathew, D., Popescu, A., and Budnik, V. (2003). Drosophila amphiphysin functions during synaptic Fasciclin II membrane cycling. J Neurosci *23*, 10710-10716.

Mauelshagen, J., Sherff, C. M., and Carew, T. J. (1998). Differential induction of long-term synaptic facilitation by spaced and massed applications of serotonin at sensory neuron synapses of Aplysia californica. Learn Mem *5*, 246-256.

McCabe, B. D., Hom, S., Aberle, H., Fetter, R. D., Marques, G., Haerry, T. E., Wan, H., O'Connor, M. B., Goodman, C. S., and Haghighi, A. P. (2004). Highwire regulates presynaptic BMP signaling essential for synaptic growth. Neuron *41*, 891-905.

McHugh, T. J., Blum, K. I., Tsien, J. Z., Tonegawa, S., and Wilson, M. A. (1996). Impaired hippocampal representation of space in CA1-specific NMDAR1 knockout mice. Cell *87*, 1339-1349.

Michael Ashburner, K. G. G., R.Scott Hawley (2005). Drosophila: A Laboratory Handbook, Cold Spring Harbor Laboratory Press).

Moline, M. M., Southern, C., and Bejsovec, A. (1999). Directionality of wingless protein transport influences epidermal patterning in the Drosophila embryo. Development *126*, 4375-4384.

Monastirioti, M., Gorczyca, M., Rapus, J., Eckert, M., White, K., and Budnik, V. (1995). Octopamine immunoreactivity in the fruit fly Drosophila melanogaster. J Comp Neurol *356*, 275-287.

Montarolo, P. G., Goelet, P., Castellucci, V. F., Morgan, J., Kandel, E. R., and Schacher, S. (1986). A critical period for macromolecular synthesis in long-term heterosynaptic facilitation in Aplysia. Science *234*, 1249-1254.

Moon, R. T., Bowerman, B., Boutros, M., and Perrimon, N. (2002). The promise and perils of Wnt signaling through beta-catenin. Science *296*, 1644-1646.

Morris, R. G., Anderson, E., Lynch, G. S., and Baudry, M. (1986). Selective impairment of learning and blockade of long-term potentiation by an N-methyl-D-aspartate receptor antagonist, AP5. Nature *319*, 774-776.

Mosca, T. J., Carrillo, R. A., White, B. H., and Keshishian, H. (2005). Dissection of synaptic excitability phenotypes by using a dominant-negative Shaker K+ channel subunit. Proc Natl Acad Sci U S A *102*, 3477-3482.

Murphy, T. H., Blatter, L. A., Bhat, R. V., Fiore, R. S., Wier, W. G., and Baraban, J. M. (1994). Differential regulation of calcium/calmodulin-dependent protein kinase II and p42 MAP kinase activity by synaptic transmission. J Neurosci *14*, 1320-1331.

Nagel, G., Ollig, D., Fuhrmann, M., Kateriya, S., Musti, A. M., Bamberg, E., and Hegemann, P. (2002). Channelrhodopsin-1: a light-gated proton channel in green algae. Science *296*, 2395-2398.

Nagerl, U. V., Eberhorn, N., Cambridge, S. B., and Bonhoeffer, T. (2004). Bidirectional activity-dependent morphological plasticity in hippocampal neurons. Neuron *44*, 759-767.

Niell, C. M., Meyer, M. P., and Smith, S. J. (2004). In vivo imaging of synapse formation on a growing dendritic arbor. Nat Neurosci *7*, 254-260.

Nusslein-Volhard, C., Kluding, H., and Jurgens, G. (1985). Genes affecting the segmental subdivision of the Drosophila embryo. Cold Spring Harb Symp Quant Biol *50*, 145-154.

Osten, P., Khatri, L., Perez, J. L., Kohr, G., Giese, G., Daly, C., Schulz, T. W., Wensky, A., Lee, L. M., and Ziff, E. B. (2000). Mutagenesis reveals a role for ABP/GRIP binding to GluR2 in synaptic surface accumulation of the AMPA receptor. Neuron *27*, 313-325.

Packard, M., Koo, E. S., Gorczyca, M., Sharpe, J., Cumberledge, S., and Budnik, V. (2002). The Drosophila wnt, wingless, provides an essential signal for pre- and postsynaptic differentiation. Cell *111*, 319-330.

Packard, M., Mathew, D., and Budnik, V. (2003). Wnts and TGF beta in synaptogenesis: old friends signalling at new places. Nat Rev Neurosci *4*, 113-120.

Pan, D., and Rubin, G. M. (1997). Kuzbanian controls proteolytic processing of Notch and mediates lateral inhibition during Drosophila and vertebrate neurogenesis. Cell *90*, 271-280.

Petersen, S. A., Fetter, R. D., Noordermeer, J. N., Goodman, C. S., and DiAntonio, A. (1997). Genetic analysis of glutamate receptors in Drosophila reveals a retrograde signal regulating presynaptic transmitter release. Neuron *19*, 1237-1248.

Pittenger, C., and Kandel, E. R. (2003). In search of general mechanisms for long-lasting plasticity: Aplysia and the hippocampus. Philos Trans R Soc Lond B Biol Sci *358*, 757-763.

Pombo, A., Cuello, P., Schul, W., Yoon, J. B., Roeder, R. G., Cook, P. R., and Murphy, S. (1998). Regional and temporal specialization in the nucleus: a transcriptionally-active nuclear domain rich in PTF, Oct1 and PIKA antigens associates with specific chromosomes early in the cell cycle. Embo J *17*, 1768-1778.

Prokop, A., Landgraf, M., Rushton, E., Broadie, K., and Bate, M. (1996). Presynaptic development at the Drosophila neuromuscular junction: assembly and localization of presynaptic active zones. Neuron *17*, 617-626.

Ramón y Cajal, S. (1904). La textura del sistema nerviosa del hombre y los vertebrados. (Madrid, Moya).

Rasse, T. M., Fouquet, W., Schmid, A., Kittel, R. J., Mertel, S., Sigrist, C. B., Schmidt, M., Guzman, A., Merino, C., Qin, G.*, et al.* (2005). Glutamate receptor dynamics organizing synapse formation in vivo. Nat Neurosci *8*, 898-905.

Reichsman, F., Smith, L., and Cumberledge, S. (1996). Glycosaminoglycans can modulate extracellular localization of the wingless
protein and promote signal transduction. J Cell Biol 1996 Nov;135(3):819-27 *135*, 819-827.

Roche, J. P., Packard, M. C., Moeckel-Cole, S., and Budnik, V. (2002). Regulation of synaptic plasticity and synaptic vesicle dynamics by the PDZ protein Scribble. J Neurosci *22*, 6471-6479.

Rohrbough, J., Grotewiel, M. S., Davis, R. L., and Broadie, K. (2000). Integrin-mediated regulation of synaptic morphology, transmission, and plasticity. J Neurosci *20*, 6868-6878.

Rosso, S. B., Sussman, D., Wynshaw-Boris, A., and Salinas, P. C. (2005). Wnt signaling through Dishevelled, Rac and JNK regulates dendritic development. Nat Neurosci *8*, 34-42. Epub 2004 Dec 2019.

Ruiz-Canada, C., Ashley, J., Moeckel-Cole, S., Drier, E., Yin, J., and Budnik, V. (2004). New Synaptic Bouton Formation Is Disrupted by Misregulation of Microtubule Stability in aPKC Mutants. Neuron *42*, 567-580.

Ruiz-Canada, C., and Budnik, V. (2006). Introduction on the use of the Drosophila embryonic/larval neuromuscular junction as a model system to study synapse development and function, and a brief summary of pathfinding and target recognition. Int Rev Neurobiol *75*, 1-31.

Ryder, E., Blows, F., Ashburner, M., Bautista-Llacer, R., Coulson, D., Drummond, J., Webster, J., Gubb, D., Gunton, N., Johnson, G.*, et al.* (2004). The DrosDel collection: a set of P-element insertions for generating custom chromosomal aberrations in Drosophila melanogaster. Genetics *167*, 797-813.

Schroll, C., Riemensperger, T., Bucher, D., Ehmer, J., Voller, T., Erbguth, K., Gerber, B., Hendel, T., Nagel, G., Buchner, E., and Fiala, A. (2006). Light-induced activation of distinct modulatory neurons triggers appetitive or aversive learning in Drosophila larvae. Curr Biol *16*, 1741-1747.

Schuster, C. M. (2006). Experience-dependent potentiation of larval neuromuscular synapses. Int Rev Neurobiol *75*, 307-322.

Schuster, C. M., Davis, G. W., Fetter, R. D., and Goodman, C. S. (1996a). Genetic dissection of structural and functional components of synaptic plasticity. I. Fasciclin II controls synaptic stabilization and growth. Neuron *17*, 641-654.

Schuster, C. M., Davis, G. W., Fetter, R. D., and Goodman, C. S. (1996b). Genetic dissection of structural and functional components of synaptic plasticity. II. Fasciclin II controls presynaptic structural plasticity. Neuron *17*, 655-667.

Seals, D. F., and Courtneidge, S. A. (2003). The ADAMs family of metalloproteases: multidomain proteins with multiple functions. Genes Dev *17*, 7-30.

Setou, M., Seog, D. H., Tanaka, Y., Kanai, Y., Takei, Y., Kawagishi, M., and Hirokawa, N. (2002). Glutamate-receptor-interacting protein GRIP1 directly steers kinesin to dendrites. Nature *417*, 83-87.

Seung, H. S. (2000). Half a century of Hebb. Nat Neurosci *3 Suppl*, 1166.
Shakiryanova, D., Tully, A., Hewes, R. S., Deitcher, D. L., and Levitan, E. S. (2005). Activity-dependent liberation of synaptic neuropeptide vesicles. Nat Neurosci *8*, 173-178.

Shakiryanova, D., Tully, A., and Levitan, E. S. (2006). Activity-dependent synaptic capture of transiting peptidergic vesicles. Nat Neurosci *9*, 896-900.
Sigrist, S. J., Reiff, D. F., Thiel, P. R., Steinert, J. R., and Schuster, C. M. (2003). Experience-dependent strengthening of Drosophila neuromuscular junctions. J Neurosci *23*, 6546-6556.

Sigrist, S. J., Thiel, P. R., Reiff, D. F., Lachance, P. E., Lasko, P., and Schuster, C. M. (2000). Postsynaptic translation affects the efficacy and morphology of neuromuscular junctions. Nature *405*, 1062-1065.

Sisson, J. C., Field, C., Ventura, R., Royou, A., and Sullivan, W. (2000). Lava lamp, a novel peripheral golgi protein, is required for Drosophila melanogaster cellularization. J Cell Biol *151*, 905-918.

Speese, S. D., and Budnik, V. (2007). Wnts: up-and-coming at the synapse. Trends Neurosci *30*, 268-275.

Stahnisch, F. W., and Nitsch, R. (2002). Santiago Ramon y Cajal's concept of neuronal plasticity: the ambiguity lives on. Trends Neurosci *25*, 589-591.

Steinert, J. R., Kuromi, H., Hellwig, A., Knirr, M., Wyatt, A. W., Kidokoro, Y., and Schuster, C. M. (2006). Experience-dependent formation and recruitment of large vesicles from reserve pool. Neuron *50*, 723-733.

Stepanyants, A., Hof, P. R., and Chklovskii, D. B. (2002). Geometry and structural plasticity of synaptic connectivity. Neuron *34*, 275-288.

Stewart, B. A., Atwood, H. L., Renger, J. J., Wang, J., and Wu, C. F. (1994). Improved stability of Drosophila larval neuromuscular preparations in haemolymph-like physiological solutions. J Comp Physiol [A] *175*, 179-191.

Swan, L. E., Wichmann, C., Prange, U., Schmid, A., Schmidt, M., Schwarz, T., Ponimaskin, E., Madeo, F., Vorbruggen, G., and Sigrist, S. J. (2004). A glutamate receptor-interacting protein homolog organizes muscle guidance in Drosophila. Genes Dev *18*, 223-237. Epub 2004 Jan 2016.

Sweatt, J. D. (1999). Toward a molecular explanation for long-term potentiation. Learn Mem *6*, 399-416.

Takamiya, K., Kostourou, V., Adams, S., Jadeja, S., Chalepakis, G., Scambler, P. J., Huganir, R. L., and Adams, R. H. (2004). A direct functional link between the multi-PDZ domain protein GRIP1 and the Fraser syndrome protein Fras1. Nat Genet *36*, 172-177.

Tang, Y. P., Wang, H., Feng, R., Kyin, M., and Tsien, J. Z. (2001). Differential effects of enrichment on learning and memory function in NR2B transgenic mice. Neuropharmacology *41*, 779-790.

Tejedor, F. J., Bokhari, A., Rogero, O., Gorczyca, M., Zhang, J., Kim, E., Sheng, M., and Budnik, V. (1997). Essential role for dlg in synaptic clustering of Shaker K+ channels in vivo. J Neurosci *17*, 152-159.

Toni, N., Buchs, P. A., Nikonenko, I., Bron, C. R., and Muller, D. (1999). LTP promotes formation of multiple spine synapses between a single axon terminal and a dendrite. Nature *402*, 421-425.

Torroja, L., Packard, M., Gorczyca, M., White, K., and Budnik, V. (1999). The Drosophila beta-amyloid precursor protein homolog promotes synapse differentiation at the neuromuscular junction. J Neurosci *19*, 7793-7803.

Tortorella, M. D., Burn, T. C., Pratta, M. A., Abbaszade, I., Hollis, J. M., Liu, R., Rosenfeld, S. A., Copeland, R. A., Decicco, C. P., Wynn, R.*, et al.* (1999). Purification and cloning of aggrecanase-1: a member of the ADAMTS family of proteins. Science *284*, 1664-1666.

Treisman, J. E., Luk, A., Rubin, G. M., and Heberlein, U. (1997). eyelid antagonizes wingless signaling during Drosophila development and has homology to the Bright family of DNA-binding proteins. Genes Dev *11*, 1949-1962.

Tully, T., Preat, T., Boynton, S. C., and Del Vecchio, M. (1994). Genetic dissection of consolidated memory in Drosophila. Cell *79*, 35-47.

van den Heuvel, M., Harryman-Samos, C., Klingensmith, J., Perrimon, N., and Nusse, R. (1993). Mutations in the segment polarity genes wingless and porcupine impair secretion of the wingless protein [published erratum appears in EMBO J 1994 Jun 15;13(12):2950]. Embo J *12*, 5293-5302.

Vlcek, S., and Foisner, R. (2007). Lamins and lamin-associated proteins in aging and disease. Curr Opin Cell Biol *19*, 298-304.

von Mikecz, A., Zhang, S., Montminy, M., Tan, E. M., and Hemmerich, P. (2000). CREB-binding protein (CBP)/p300 and RNA polymerase II colocalize in transcriptionally active domains in the nucleus. J Cell Biol *150*, 265-273.

Wagh, D. A., Rasse, T. M., Asan, E., Hofbauer, A., Schwenkert, I., Durrbeck, H., Buchner, S., Dabauvalle, M. C., Schmidt, M., Qin, G.*, et al.* (2006). Bruchpilot, a protein with homology to ELKS/CAST, is required for structural integrity and function of synaptic active zones in Drosophila. Neuron *49*, 833-844.

Walsh, M. K., and Lichtman, J. W. (2003). In vivo time-lapse imaging of synaptic takeover associated with naturally occurring synapse elimination. Neuron *37*, 67-73.

Wayman, G. A., Impey, S., Marks, D., Saneyoshi, T., Grant, W. F., Derkach, V., and Soderling, T. R. (2006). Activity-dependent dendritic arborization mediated by CaM-kinase I activation and enhanced CREB-dependent transcription of Wnt-2. Neuron *50*, 897-909.

Whitlock, J. R., Heynen, A. J., Shuler, M. G., and Bear, M. F. (2006). Learning induces long-term potentiation in the hippocampus. Science *313*, 1093-1097.

Wu, C. F., and Ganetzky, B. (1980). Genetic alteration of nerve membrane excitability in temperature-sensitive paralytic mutants of Drosophila melanogaster. Nature *286*, 814-816.

Wu, G. Y., Deisseroth, K., and Tsien, R. W. (2001). Spaced stimuli stabilize MAPK pathway activation and its effects on dendritic morphology. Nat Neurosci *4*, 151-158.

Wucherpfennig, T., Wilsch-Brauninger, M., and Gonzalez-Gaitan, M. (2003). Role of Drosophila Rab5 during endosomal trafficking at the synapse and evoked neurotransmitter release. J Cell Biol *161*, 609-624.

Wyatt, R. M., and Balice-Gordon, R. J. (2003). Activity-dependent elimination of neuromuscular synapses. J Neurocytol *32*, 777-794.

Wyszynski, M., Kim, E., Dunah, A. W., Passafaro, M., Valtschanoff, J. G., Serra-Pages, C., Streuli, M., Weinberg, R. J., and Sheng, M. (2002). Interaction between GRIP and liprin-alpha/SYD2 is required for AMPA receptor targeting. Neuron *34*, 39-52.

Wyszynski, M., Valtschanoff, J. G., Naisbitt, S., Dunah, A. W., Kim, E., Standaert, D. G., Weinberg, R., and Sheng, M. (1999). Association of AMPA receptors with a subset of glutamate receptor-interacting protein in vivo. J Neurosci *19*, 6528-6537.

Xie, H., Tranguch, S., Jia, X., Zhang, H., Das, S. K., Dey, S. K., Kuo, C. J., and Wang, H. (2008). Inactivation of nuclear Wnt-{beta}-catenin signaling limits blastocyst competency for implantation. Development *135*, 717-727.

Yao, J., Qi, J., and Chen, G. (2006). Actin-dependent activation of presynaptic silent synapses contributes to long-term synaptic plasticity in developing hippocampal neurons. J Neurosci *26*, 8137-8147.

Ye, B., Liao, D., Zhang, X., Zhang, P., Dong, H., and Huganir, R. L. (2000). GRASP-1: a neuronal RasGEF associated with the AMPA receptor/GRIP complex. Neuron *26*, 603-617.

Yin, J. C., Wallach, J. S., Del Vecchio, M., Wilder, E. L., Zhou, H., Quinn, W. G., and Tully, T. (1994). Induction of a dominant negative CREB transgene specifically blocks long-term memory in Drosophila. Cell *79*, 49-58.

Yoshihara, M., Adolfsen, B., Galle, K. T., and Littleton, J. T. (2005). Retrograde signaling by Syt 4 induces presynaptic release and synapse-specific growth. Science *310*, 858-863.

Yu, D., Akalal, D. B., and Davis, R. L. (2006). Drosophila alpha/beta mushroom body neurons form a branch-specific, long-term cellular memory trace after spaced olfactory conditioning. Neuron *52*, 845-855.

Yu, X., and Malenka, R. C. (2003). Beta-catenin is critical for dendritic morphogenesis. Nat Neurosci *6*, 1169-1177.

Yuste, R., and Bonhoeffer, T. (2004). Genesis of dendritic spines: insights from ultrastructural and imaging studies. Nat Rev Neurosci *5*, 24-34.

Zhang, J., and Carthew, R. W. (1998). Interactions between Wingless and DFz2 during Drosophila wing development. Development *125*, 3075-3085.

Zhong, Y., Budnik, V., and Wu, C. F. (1992). Synaptic plasticity in Drosophila memory and hyperexcitable mutants: role of cAMP cascade. J Neurosci *12*, 644-651.

Zhong, Y., and Pena, L. A. (1995). A novel synaptic transmission mediated by a PACAP-like neuropeptide in Drosophila. Neuron *14*, 527-536.

Zhong, Y., and Wu, C. F. (1991). Altered synaptic plasticity in Drosophila memory mutants with a defective cyclic AMP cascade. Science *251*, 198-201.

Zimber, A., Nguyen, Q. D., and Gespach, C. (2004). Nuclear bodies and compartments: functional roles and cellular signalling in health and disease. Cell Signal *16*, 1085-1104.

Zinsmaier, K. E., Eberle, K. K., Buchner, E., Walter, N., and Benzer, S. (1994). Paralysis and early death in cysteine string protein mutants of Drosophila. Science *263*, 977-980.

Zito, K., Parnas, D., Fetter, R. D., Isacoff, E. Y., and Goodman, C. S. (1999). Watching a synapse grow: noninvasive confocal imaging of synaptic growth in Drosophila. Neuron *22*, 719-729.

Zucker, R. S. (2005). Minis: whence and wherefore? Neuron *45*, 482-484.